THE UV PHOTOELECTRON SPECTROSCOPY OF TRANSIENTS. AN EXPERIMENTAL AND COMPUTATIONAL INVESTIGATION OF ELECTRONIC STRUCTURE AND REACTION MECHANISMS

By

TOM BAJOREK, B.Sc.

A thesis

Submitted to the School of Graduate Studies

In Partial Fulfillment of the Requirements for the Degree

Doctor of Philosophy

McMaster University

UV PHOTOELECTRON SPECTROSCOPY OF TRANSIENTS

DOCTOR OF PHILOSOPHY (2003)
(Chemistry)

McMaster University
Hamilton, Ontario

TITLE: THE UV PHOTOELECTRON SPECTROSCOPY OF TRANSIENTS. AN EXPERIMENTAL AND COMPUTATIONAL INVESTIGATION OF ELECTRONIC STRUCTURE AND REACTION MECHANISMS

AUTHOR: Tom Bajorek, B.Sc. (McMaster University)

SUPERVISOR: Professor Nick H. Werstiuk

NUMBER OF PAGES: xvi, 156

Abstract

A test study of the vacuum thermolysis of phenyldiazoethane has shown the ability to generate a diazo compound from the respective sodium salt. It has also illustrated the utility of using a CW CO_2 laser as a directed heat source to thermolize a diazo compound and record the PE spectrum of the pyrolysate. The spectrum of styrene was successfully recorded upon the thermolysis of phenydiazoethane in the source chamber of the PE spectrometer.

Photoelectron spectra of possible precursors to the elusive cycloheptatetraene were recorded. Thermolyses of these precursors were performed in the source chamber of the PE spectrometer and PE spectra of their thermolysates were recorded. Calculations of ionization potentials and simulation of partial PE spectra of possible products of the thermolysis were employed in order to attempt to assign the observed experimental ionization potential bands. Although a clear PE spectrum of cycloheptatetraene could not be obtained, the thermolysis experiment has shown IP bands belonging to fulvenallene, which is the lowest energy isomer on the C_7H_6 potential energy surface. A PE spectrum of bicyclo[3.2.0]hepta-1,3,6-triene was recorded and its ionization potentials were assigned relative to calculated values. Although this triene is considered as a key intermediate on the C_7H_6 potential energy surface it was not detected in the pyrolysis of 2-diazobicyclo[3.2.0]hepta-3,6-diene.

Thermolysis of bicyclo[3.2.0]hept-6-en-2-one has made it possible to record a PE spectrum of a transient cyclohepta-2(*Z*),4(*E*)-dien-1-one. PE spectra of both ketones were

recorded for the first time. The thermolysis has also illustrated that the ring opening of the cyclobutene moiety follows the conrotatory path in accord with the Woodward – Hoffmann rules despite the small size of the ring adjoined to the cyclobutene. A PE spectroscopic, thermolysis and computational investigation of *N,N*-bicyclo[3.2.0]hepta-3,6-dien-1-amine has illustrated the ability of *E,Z,Z* transient isomer to rearrange through a *trans-cis* isomerisation to yield a thermodynamically more stable product.

An investigation of 7-substituted cycloheptatrienes has shown that most cycloheptatrienes favor the substituents in the *equatorial* position. The only compound that has been identified with PE spectroscopy to prefer the substituent in the *axial* position was the methylthiocycloheptatriene.

Acknowledgments

I would like to take this opportunity to thank the people who influenced my life during the time of my graduate studies. Foremost I would like to thank my supervisor and mentor Dr. Nick Werstiuk for taking me under his wing. His constant support, guidance and personal attention were invaluable in the course of my studies. I would also like to thank my supervisory committee members, Dr. Willie Leigh and Dr. John Warkentin for helpful discussions and advice about my research.

I also wish to extend my thanks to Dr. Heidi Muchall, a former member of the NHW group for her help and advice during the first two years of my graduate work.

I would also like to express my gratitude to members of the WJL group who were always willing to help with photochemistry and my friends both past and present: Sarah, Bernie, Randy, Neil, John, Lisa, Barbara and Paul.

Finally and most importantly I would like to thank my family: Mom, Dad and my sister Margaret. Thank you for believing in me. Without your support I would not be where I am today. Thank you.

To my parents: Ludwika and Stanisław

and in the memory of all my grandparents

"Bardzo w to wierzę że wszystko można mieć,
By życie bajką było wystarczy tylko chcieć."

Anonymous

Table of Contents

List of Figures

List of Tables

List of Schemes

Chapter 1

Introduction

The studies described in this thesis are based on UV photoelectron spectroscopy experiments combined with *ab inito* calculations of transient and stable molecules. Thus the following introduction presents general aspects of photoelectron spectroscopy (Chapter 1.1) and computational chemistry (Chapter 1.2). A description of the unique photoelectron instrument used in these studies is presented in Chapter 2. Since in large part this thesis deals with transient species the introduction is also intended to provide background information on these types of molecules (Chapter 1.3). The scope of this thesis is also extended to possible transients which can be generated upon thermal ring-opening of a cyclobutene moiety (Chapter 4). Therefore the introduction also presents background information on the ring opening of cyclobutene (Chapter 1.4) and the possible transients which can be generated in this fashion. Lastly, photoelectron spectroscopy may also be used to probe the conformational properties of stable molecules such as 7-substituted cycloheptatrienes, thus Chapter 1.5 deals with this aspect.

1.1 Ultraviolet photoelectron spectroscopy

Ultraviolet photoelectron spectroscopy is an experimental technique that allows the study of the electronic structure of stable molecules, transient species and ions. A photoelectron spectrometer measures the kinetic energy E_k of photoelectrons that are ejected from a molecule by monochromatic radiation such as He(I) photons with an energy of 21.22 eV, generated by a He direct current (DC) discharge lamp. The measured E_k allows the determination of ionization energies E_I and intensities. The process that allows ejection of electrons from a molecule is called the photoelectric effect or photoionization (eqn. 1.1).

$$M + h\nu \longrightarrow M^{+\bullet} + e^{-} \qquad [1.1]$$

Ultraviolet photoionization involves the interaction of photons ($h\nu$) with a molecule (M) in order to eject electrons from their outer shell, thereby generating a radical cation ($M^{+\bullet}$) and an electron (e^-). Therefore the ejected electrons are called photoelectrons. The photons of the monochromatic radiation have an energy $h\nu$, while the electrons held within the molecule by the ionization energy possess kinetic energy E_k when ejected from the molecule. For the process of ionization to occur the energy of the photons must be greater than the ionization energy of the molecule. The measurement of the kinetic energy directly determines the ionization energy of the photoelectrons, according to the law of conservation of energy (eqn. 1.2).

$$E_k = h\nu - E_i \qquad [1.2]$$

Electrons occupying different energy levels within a molecule are expected to have different ionization energies. These energy levels correspond to different molecular orbitals of the molecule. The ejection of electrons from the orbitals and the measurement of their kinetic energy provides information about the geometries and vibrational frequencies of the radical cations, and the bonding and localization properties of the molecular orbitals.[1]

In ultraviolet photoelectron spectroscopy, UV radiation is used to eject electrons from a molecule in the gas phase, thereby allowing the study of valence molecular orbitals. The molecules are bombarded with photons in the target chamber, also called the source chamber, at pressure of ca. 10^{-3} Torr. The dislodged electrons are sorted according to their kinetic energies by an electron analyzer, and a photoelectron spectrum is obtained by plotting the number of ejected electrons (counts from an electron multiplier) on the y-axis against their kinetic energy on the x-axis.

Ultraviolet photoelectron spectroscopy is a tool for studying the electronic structure of stable molecules and transient species. The most outstanding feature of photoelectron spectroscopy is its ability to single out individual molecular orbitals, when combined with *ab initio* calculations of molecular orbital eigenvalues (orbital energies) and eigenvectors (orbital coefficients). This joint method gives information about the electronic structure and bonding of molecules that is provided by no other experimental technique.[2,3]

1.2 Computational chemistry and photoelectron spectroscopy

The great advances in computer technology in the last decade have allowed for a wider use of computers in our society. It also made it possible for advances in computational chemistry. The term computational chemistry is used to describe the application of theoretical or quantum chemistry to chemical problems encountered in everyday research environments with the use of computers which perform the task of quantum calculations with the use of an appropriate computer program. Computational chemistry is applied in such fields as pharmaceuticals for drug design. It is also used in chemical dynamics, organic and inorganic chemistry for prediction of chemical processes and molecular properties. With faster computers and their larger storage capacities computational chemists are able to apply larger basis sets using more accurate theoretical procedures. A basis set provides a way of representing molecular orbitals within a molecule mathematically and it can be interpreted as restricting each electron to a particular region of space. Exact molecular orbitals are represented more accurately with larger basis sets, which impose fewer constraints on the electrons.

A theoretical procedure is the method used to calculate molecular properties or chemical processes. These procedures correspond to different approximation methods also known as different levels of theory. The more accurate the level of theory, and the larger the basis set, the more computationally expensive the calculation will be. The most commonly applied levels of theory are the Hartree-Fock Self-Consistent Field (HF)

method,[4] and the Becke3LYP[5] method, which is a Becke-style 3–parameter Density Functional Theory using the Lee-Yang-Parr correlation functional.[6]

The basis sets that are used in conjunction with the different levels of theory range from the minimal basis set STO-3G which employs Slater-type orbitals and three primitive gaussians, hence the abbreviation 3G. Thus, this basis set approximates Slater orbitals with guassian functions. Another rather small basis set is the 3-21G split-valence basis set. A split-valence basis set is one which has two or more sizes of basis functions for each valence orbital. The 3-21G basis set is an example of a double split-valence basis set. Another example of a double split-valence basis set is the larger basis set 6-31G. Basis sets are made larger by increasing the number of basis functions per atom. There also exist basis sets that are Triple split-valence basis sets such as the 6-311G basis set. In split-valence basis sets the orbitals are allowed to change in size but not in shape. To allow for the orbitals to change shape polarization functions are introduced to the basis set which adds orbitals with angular momentum. For example in the 6-31G* basis set also written as 6-31G(d), d functions are added to heavy atoms. Hydrogens may also be assigned p functions. An example of such a basis set is 6-31G(d,p) also designated as 6-31G**. To allow the orbitals to occupy a larger region of space, a basis set may be assigned diffuse functions, which are large-size versions of the s- and p-type functions. An example of a basis set which has both polarized function and diffuse functions on the heavy atoms is the 6-31+G(d) basis set. The plus signifies the addition of diffuse functions to heavy atoms. A second plus sign indicates that diffuse functions are also added to H atoms. In systems where the electrons are far away from the nucleus, such as

molecules with lone pairs, anions and systems with significant negative charge, it is important to include diffuse functions to increase the size of the functions.[7]

1.2.1 Method for calculating vertical ionization potentials

A method for ordering the energies of molecular orbitals can be provided by the calculations of equilibrium molecular geometries and their molecular orbital eigenvalues within the limits of Koopmans' theorem (eqn. 1.3),[1,8] which states that the ionization potential is approximately equal to the orbital energy.

$$IP_v \cong -\varepsilon^{SCF} \qquad [1.3]$$

The interpretation of a photoelectron spectrum involves *ab initio* molecular orbital calculations at an appropriate level of theory (eg. Becke3LYP), and a sufficient basis set such as 6-31+G(d). These calculations provide eigenvectors ϕ (MO wave functions) and eigenvalues ε (MO energies). The eigenvalues are the binding energies of the electrons in specific MOs. The experimental vertical ionization energies (IP_v) are approximately equal to the negative of the eigenvalues ($-\varepsilon^{SCF}$) which are obtained from a Self-Consistent-Field (SCF) calculation, as stated in Koopmans' theorem.

There exists another, recently developed[9,10] and successfully applied,[11,12,13] computational method for predicting of ionization energies or ionization potentials (IPs). Although this method has been reported for the prediction of the first vertical and adiabatic IPs of carbenes, it may be applied to other molecules. The Becke3LYP level of theory was shown to provide results which were in good agreement with experimental

values. The molecule M, and its radical cation $M^{+\bullet}$, have the same geometry at IP_v. The geometries of the molecule M and its radical cation $M^{+\bullet}$ may differ at adiabatic ionization potential (IP_a), which corresponds to a transition from the electronic, vibrational and rotational ground state of the molecule to the lowest vibrational and rotational levels of an electronic state of the radical cation.[1] So calculating the energy of the radical cation without optimizing its geometry, (a single point calculation), and then subtracting the calculated energy of the optimized ground state molecule, yields the first vertical ionization potential. In order to obtain the adiabatic ionization potential (IP_a), the energy of the optimized ground state molecule (E(M)) must be subtracted from the energy of the geometry optimized radical cation ($E(M^{+\bullet})$) (eqn. 1.4).

$$IP = E(M^{+\cdot}) - E(M) \qquad [1.4]$$

Simulating PE spectra is an important practice in photoelectron spectroscopic studies of stable molecules and transient species generated by gas phase vacuum pyrolysis reactions. PE spectral simulations involve the calculation of the first vertical ionization potential (IP_v), and the eigenvalues or ε (orbital energies). By anchoring the calculated orbital energies to the calculated first vertical ionization potential (IP_v), a good approximation of the ionization potentials can be obtained. A simulation is run specifying the calculated IPs, width at half hight, lowest and highest IP, and the number of IPs, in a simulation program called PESPEC.[14]

1.2.2 Calculations and reaction mechanisms

Computational chemistry is also widely applied in the study of reaction mechanisms and potential energy surfaces. Through the use of calculations one can gain greater knowledge and understanding of chemical processes and chemical rearrangements. Transition state calculations are applied to find the first order saddle point which is a transition state. The stationary point found by a transition state calculation is characterized as a true transition state if a frequency calculation on this geometry shows one imaginary frequency. Therefore one looks for a single negative frequency and a single negative eigenvalue, as well as visualizing the exaggerated normal mode corresponding to the imaginary frequency. If the displacement that composes the normal mode tends to lead in the direction of the expected structures that the transition state may connect then it is the true transition state. It is possible that a transition state calculation may yield a single imaginary frequency but the normal mode does not correspond to the expected mode connecting the products and reactants. This is because a saddle point always connects two minima on the potential energy surface, but these minima may not necessarily correspond to the desired products and reactants. Therefore it is necessary to confirm transition state calculations not only with a frequency calculation but also by visualization of the normal mode corresponding to the imaginary frequency. In cases where it is very difficult to assess the validity of the transition state visually, an Intrinsic Reaction Coordinate (IRC) calculation must be performed. In this type of calculation the transition state is evaluated through the optimization of a number

of geometries or points that lie on the reaction coordinate connecting the products and reactants. A certain number of points along the coordinate are evaluated starting from the transition state toward the products and from the transitions state toward the reactants. Thus, in this way the reactants and products are determined explicitly.

A comparison of the energies of the optimized equilibrium geometry and the energy of the transition state gives the energy barrier for the reaction. In some cases where two reaction pathways are possible, the energy barriers for the processes should be compared in order to predict which process has a lower energy barrier. The energy barriers may also be compared for different temperatures. A frequency calculation which yields a temperature correction to the total energy is performed with a specified temperature. The calculation is performed at several temperatures for the ground state geometry and the transition state and comparison of the thermally corrected energies yields a thermally corrected energy barriers.

1.3 Transients and reactive intermediates

The word transient means "lasting only a short time or existing briefly or temporarily".[15] A molecule which is termed a transient is a compound that cannot be isolated and stored using conventional methods. A transient is also a reactive intermediate. Such species are studied using special techniques such as Ar matrix isolation IR spectroscopy, laser flash photolysis, photoelectron spectroscopy as well as chemical methods where the transient is trapped using another chemical compound. One

type of a transient or reactive intermediate that is extensively studied is a carbene.[16] Another type of transient of great interest to experimentalists and computational chemists is a strained cyclic allene. A transient may also be a strained cyclic diene, which may be generated from a thermal electrocyclic ring opening reaction of a bicyclic cyclobutene.

1.3.1 Carbenes

A carbene is an uncharged intermediate that contains a divalent carbon atom with a total of four valence electrons. Two of the four valence electrons are bonding and two are non-bonding. The two nonbonding electrons of the divalent carbon may reside either in the σ, sp^2 hybridized orbital or in each of the *p* and σ orbitals. When both electrons are located in the σ orbital with antiparallel spins, the intermediate is a ground state singlet carbene. If the two electrons occupy each of the *p* and σ orbitals with parallel spins, the carbene is a ground state triplet. In both cases the geometry of the carbene is a bent molecule.[16,17] In a singlet carbene the angle is smaller than in a triplet carbene.[16,17] The simplest possible carbene is a methylene which is shown in Figure 1 as an example of a singlet and triplet carbene.

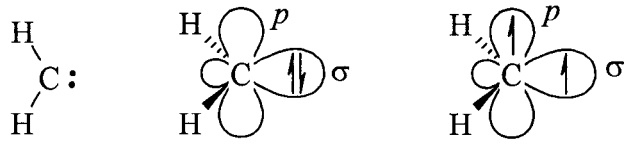

singlet triplet

Figure 1. Schematic representation of singlet and triplet carbene (methylene).

Carbenes may be generated by α-elimination of halomethylenes,[18,19,20] or by the Simmons-Smith reaction which is a source of methylene (CH_2).[21] Carbenes may also be generated from diazo compounds (**1**) and diazirines (**2**) by photochemical or thermal decomposition.[22,23] Tosylhydrazones (**3**) are also an invaluable source of carbenes.[24] Examples of the generic reactions are shown in Eqn. 1.5.

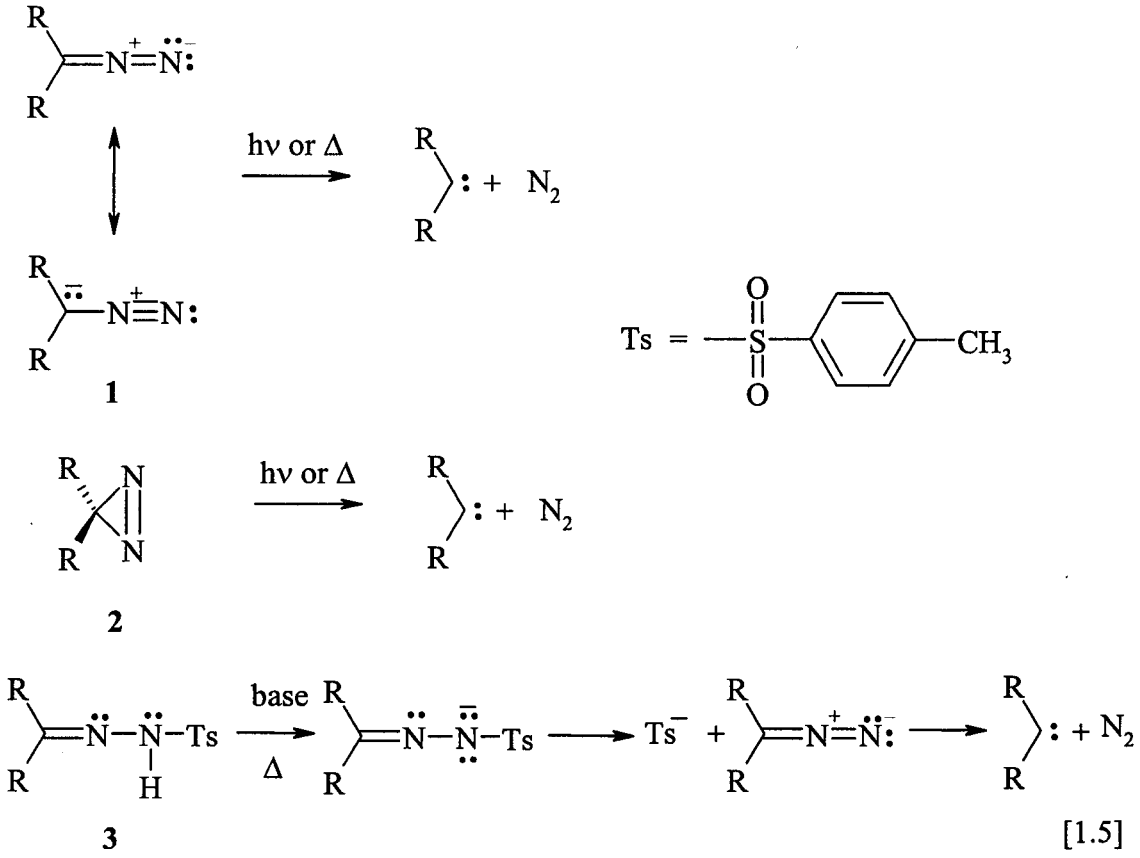

[1.5]

Carbenes undergo four characteristic reactions: insertion, where the carbene inserts into a sigma bond; addition, where the carbene adds across a C–X multiple bond to yield a 3-membered ring; dimerization, where two carbenes react together to yield an alkene; and rearrangement. The reaction schemes are summarized in Table 1.

Table 1. Fundamental Reactions of Carbenes.[17]

Insertion	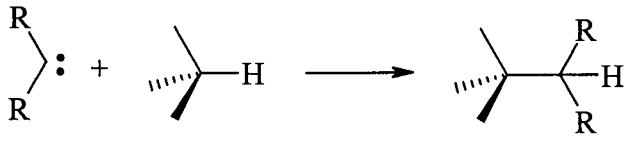
	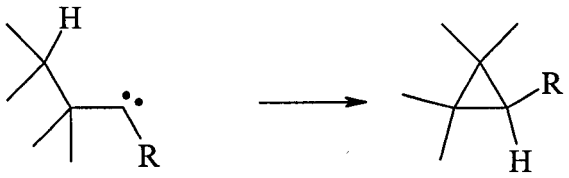
Addition	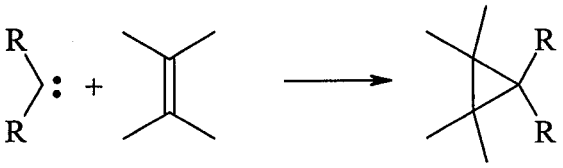
Dimerization	
Rearrangement	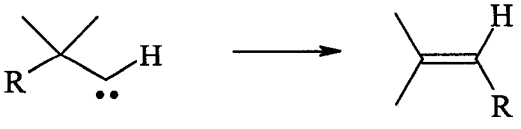

Carbenes can be studied by experimental methods such as UV photoelectron spectroscopy to explore their electronic structure and bonding. An example of such a photoelectron spectroscopic study is the investigation of 2,2-dimethoxy-5,5-dimethyl-Δ^3-1,3,4-oxadiazoline.[10] In this thermolysis study the authors reported the photoelectron spectrum of dimethoxycarbene after the subtraction of the PE spectra of other thermolysis products such as acetone, tetramethoxyethylene and dimethyl oxalate. Stable carbenes have also been studied with UV PES.[9,25] The study of such stable carbenes as shown in Figure 2 was also used to establish an inexpensive calculational method for predicting vertical ionization potentials.[9]

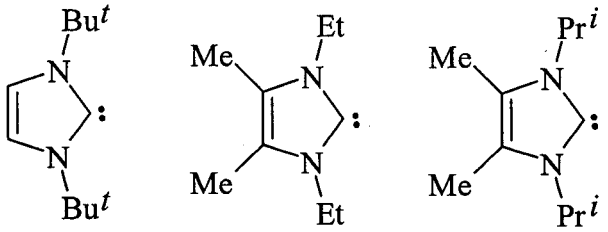

Figure 2. Stable carbenes.

1.3.2 Strained cyclic cumulenes

A cumulene is a hydrocarbon chain with two or more double bonds connected in sequence, sharing common atoms. The smallest cumulene is allene, 1,2-propadiene (**4**).

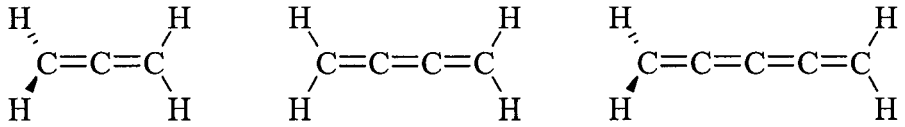

4 **5** **6**

Figure 3. Straight chain cumulenes **4**, **5**, and **6**.

The next two compounds in this homologous series of hydrocarbons are 1,2,3-butatriene (**5**) and 1,2,3,4-pentatetraene (**6**) as shown in Figure 3.

These acyclic cumulenes all have linear equilibrium geometries. The arrangement of the four attached substituents alternates between planar and orthogonal geometries with D_{2h} and D_{2d} symmetries, respectively. Although many allenes dimerize easily and cumulenes such as **5** and **6** polymerize when not in dilute solutions, the unsubstituted cumulenes are not considered to be highly reactive.[26]

The introduction of strain to cumulenic molecules in the form of a cyclic geometry introduces higher reactivity. The smaller the ring incorporating the allene the higher the reactivity. As early as 1936, attempts to synthesize a strained cumulene have been reported. Favorski claimed that compound **7** is obtained from a reaction of 1-bromo-2-chlorocycloheptene with sodium in ether.[27]

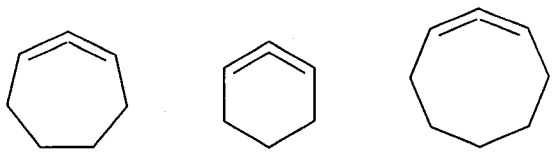

7 **8** **9**

Figure 4. Cyclic allenes.

Although the report of Favorski was incorrect, it was not until the 1940s when Domnin reported unsuccessful attempts to isolate 1,2-cyclohexadiene (**8**).[28] About 20 years later the first successful syntheses of 1,2-cycloheptadiene (**7**) and 1,2-cyclooctadiene (**9**) were reported by Ball and Landor.[29]

Up to this day there is continued interest in the chemistry of strained cyclic cumulenes. One example that has received considerable attention both from the experimental and computational point of view is 1,2,4,6-cycloheptatetraene (**10**).

1.3.3 Cycloheptatetraene and Cycloheptatrienylidene

1,2,4,6-Cycloheptatetraene (**10**) is thought to be the key intermediate on the C_7H_6 potential energy surface. [30] Along with its carbene isomer cycloheptatrienylidene (**11**), it has been studied extensively over the past 30 years.[26] Thus **10** may be the best studied cyclic cumulene. Recent computational studies implicate singlet **11** as the transition state for the interconversion of two chiral cyclic allenes **10**, as opposed to it being a discrete intermediate in the racemization process (Figure 5).[31,32,33]

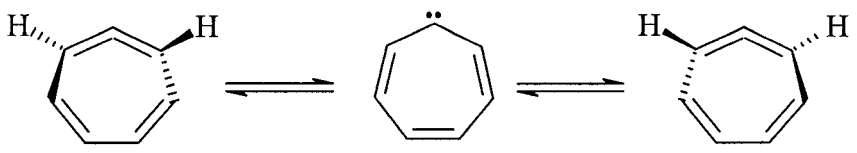

10 **11** **10**

Figure 5. Racemization of cycloheptatetraene.

A number of precursors have been employed to prepare the transient **10** directly. In an elegant Ar matrix isolation / IR spectroscopy experiment, Chapman and coworkers have reported an IR spectrum that they assign to matrix-isolated **10**.[30] The precursors employed in their studies range from the widely studied phenyldiazirine (**12**) and phenydiazomethane (**13**), which are thought to generate **10** by rearrangement of phenylcarbene (**14**)[34], to such precursors as 7-acetoxynorbornadiene (**15**), 8-diazobicyclo[2.2.2]hepta-3,6-dien-7-one (**16**) and 2-diazobicyclo[3.2.0]hepta-3,6-diene (**17**).[35] The proposed photochemical and thermal reactions of these precursors are shown in Scheme 1.

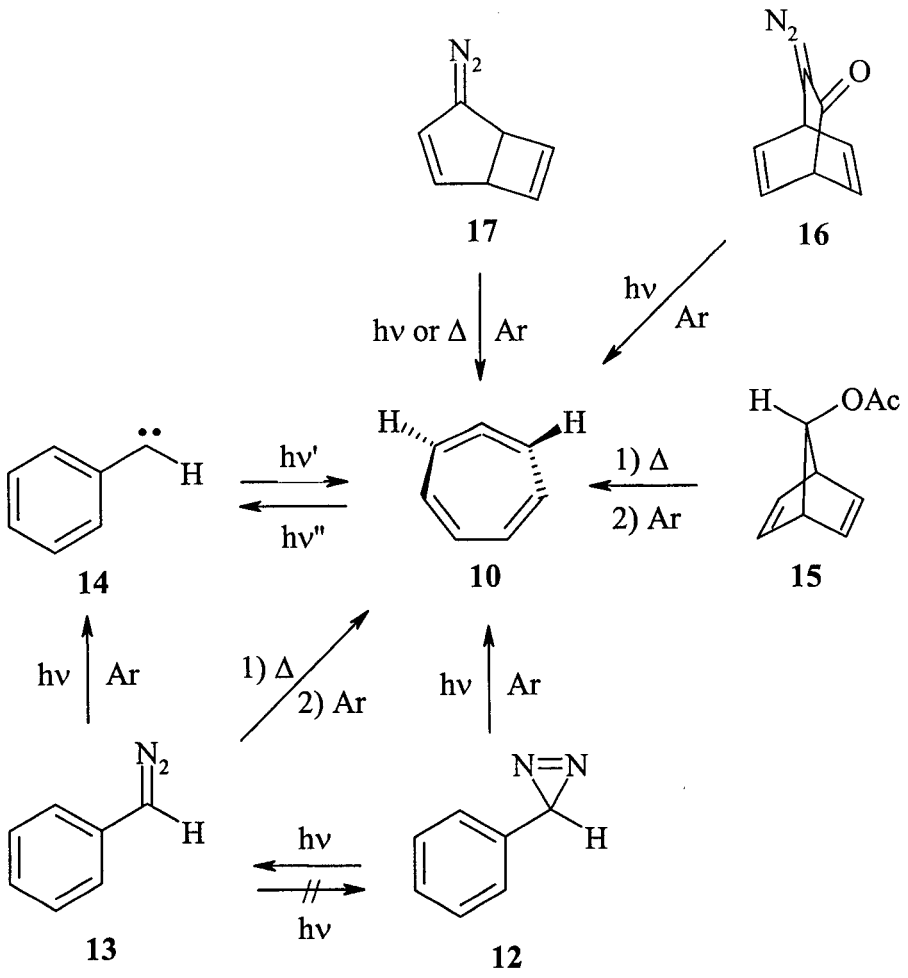

Scheme 1. Precursors of 1,2,4,6-cycloheptatetraene (**10**).[30]

In these experiments the authors have either generated the transient **10** first by thermolysis or photolysis of the precursors followed by codeposition of the products in an Ar matrix or by codepositing the precursor itself in an Ar matrix and then photolysing or raising the temperature of the matrix. Perhaps the most studied precursor of **10** is phenyldiazomethane (**13**) which upon photolysis and thermolysis generates phenylcarbene (**14**) whose rearrangement has been under investigation for the past three

decades.[36,37] It has been reported that upon flash vacuum pyrolysis at 590°C, the isomerization of **14** involves cycloheptatrienylidene (**11**) and bicyclo[3.2.0]hepta-1,3,6-triene (**18**) to yield fulvenallene (**20**).[38] This study was also performed using a [1-^{13}C]phenyldiazomethane at 900°C where the label was completely scrambled in the product **20**. The authors suggested that the diradical species **19** is also involved in the rearrangement. The proposed path of the rearrangement is shown in Scheme 2.

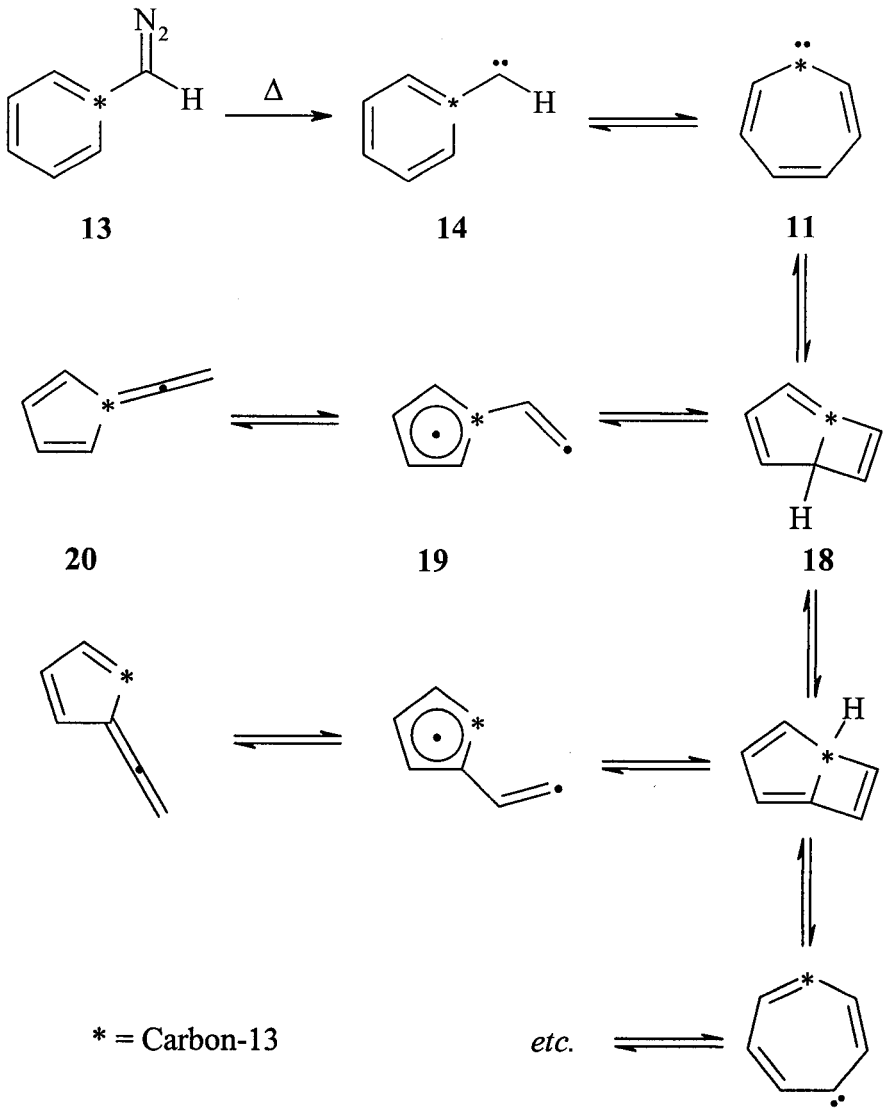

Scheme 2. Phenyl carbene rearrangement.

In earlier ^{13}C-labeling studies, Jones and coworkers considered a path for the conversion of phenylcarbene (**14**) to cycloheptatrienylidene (**11**) which involves bicyclo[4.1.0]hepta-2,4,6-triene (**21**).[39,40]

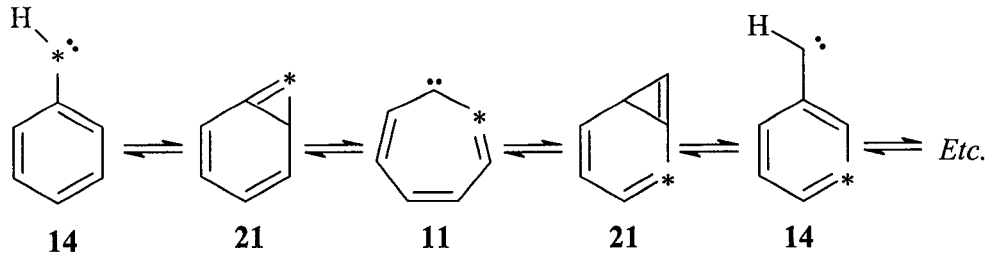

Scheme 3. Equilibrium of phenylcarbene and cycloheptatetraene.

The authors of this work stated that it was suprising that fulvenallene was not observed in these experiments.[39] Chapman and coworkers also considered the intermediacy of **21** in their study of arylcarbene rearrangements.[30] Although there is no direct evidence for the formation of **21**, product studies have been reported characterizing **21** and its related precursors.[41,42,43] Direct evidence for the existence of analogous intermediates in the rearrangement of naphthylcarbene has been provided by studies on benzannelated derivatives.[44,45,46,47,48,49] Chapman and coworkers proposed in their reports that 1,2,4,6-cycloheptatetraene (**10**), rather than cycloheptatrienylidene (**11**), is the key intermediate on the C_7H_6 potential energy surface, and reported the IR spectrum of **10** in support of their proposal.[30,34] More recently, the full UV/VIS and IR spectra of both phenylcarbene (**14**) and cycloheptatetraene (**10**) have been reported, with spectral assignments based on *ab initio* calculations.[50] NMR studies on **13**, **14**, and **10** incarcerated in a hemicarcerand have also been recently reported.[51,52] Therefore the interest in the rearrangements of phenylcarbene and the characterization of cycloheptatetraene remains high.

A number of computational studies of **10**, **11** and **14** as well as the C_7H_6 potential energy surface have been reported in the literature.[31,32,33,53,54,55,56] A list of the optimized

isomers on the C_7H_6 potential energy surface has been compiled along with an outline of the potential energy surface of the interconverting isomers using high level *ab initio* calculations.[31] High level calculations have also been performed on the interconversions of **18**.[33] Computational results on the substituent effects in the interconversions of **14**, **10**, and **21** at the Becke3LYP level of theory have also been recently reported.[56]

1.4 The ring opening of cyclobutene

A pericyclic reaction is a process that involves a change in bonding relationship that takes place as a continuous concerted reorganization of electrons.[57] Five types of pericyclic reactions are most commonly encountered in chemistry: cycloadditions, electrocyclic reactions, sigmatropic rearrangements, cheletropic reactions and group transfer reactions. The cycloaddition reaction is one where a ring is formed by the addition of two or more molecules which transfer electrons from π bonds to new σ bonds.[58] An electrocyclic reaction is one where a ring opening or closing occurs within a single molecule.[59] The σ bonds are converted to π bonds and vice versa in such a reaction.[17] The migration of a σ-bond (a substituent) to a new site over a conjugated π system is characteristic of a sigmatropic rearrangement reaction.[59] The transfer of a group from one molecule to another is described as a group transfer reaction.[17] A cheletropic reaction is a variation of a cycloaddition reaction where on one of the components new bonds are made to the same single atom.[59]

The prototypical example of an electrocyclic reaction is the interconversion of cyclobutene (**22**) and butadiene (**23**) (eqn. 1.6).

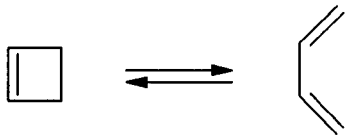

[1.6]

22 **23**

This ring opening may occur via two different processes: a disrotatory process where the substituents of the breaking σ bond are rotating in opposite directions, and a conrotatory process where the substituents are rotating in the same direction. The terms disrotatory and conrotatory were introduced by Woodward and Hoffmann.[60]

1.4.1 The Woodward-Hoffmann rules

The Woodward-Hoffmann rules are a set of theoretical rules developed by Woodward and Hoffman to predict the course and stereochemistry of pericyclic reactions on the basis of conservation of orbital symmetry.[61] The concept of conservation of orbital symmetry may be used to predict the stereochemistry of such reactions as the electrocyclic ring opening of cyclobutene.

1.4.2 Electrocyclic ring opening of cyclobutenes and orbital symmetry

The electrocyclic ring opening of cyclobutene is a 4 electron process that involves the conversion of one σ- and one π-bond to two conjugated π-bonds in the product. It and the reverse reaction are most often used to illustrate the application of the Woodward-Hoffman rules. The process can occur in two stereochemically distinct ways, which are termed conrotatory (in which the σ-bond cleaves with rotation of the two carbonds in the same direction) and disrotatory (in which the σ-bond cleaves with rotation of the two carbons in the opposite direction). In each case the symmetry of the participating orbitals in the reactant must be conserved in those of the product and at all stages in between. The conrotatory process preserves C_2 symmetry while the disrotatory path preserves σ_v symmetry. Using the molecular orbitals (MOs) for the reactant (cyclobutene) and the product (butadiene) a molecular orbital correlation diagram may be constructed to illustrate the preferred stereochemistry of the reaction. Four orbitals in cyclobutene and butadiene are viewed as participating in the reaction: the σ, π, π^* and σ^* orbitals of cyclobutene and π_1, π_2, π_3^* and π_4^* orbitals of butadiene. Based on the two symmetry elements involved in the two processes, the molecular orbitals in reactant and product are either assigned as symmetric (S) or antisymmetric (A). The symmetry-allowed path may be located by matching the two S and two A orbitals of the reactant and product. The orbital correlation diagram for the conrotatory ring opening of cyclobutene is illustrated in Figure 6 and the orbital correlation diagram for the disrotatory path is shown in Figure 7.

Since the controtatory process links the ground electronic state of cyclobutene to the ground state of butadiene it is predicted to be the preferred pathway upon thermal activation and thus it is termed "thermally allowed". The disrotatory path generates a doubly excited state of the butadiene from the ground state of cyclobutene and is thus thermally forbidden (Figure 7).

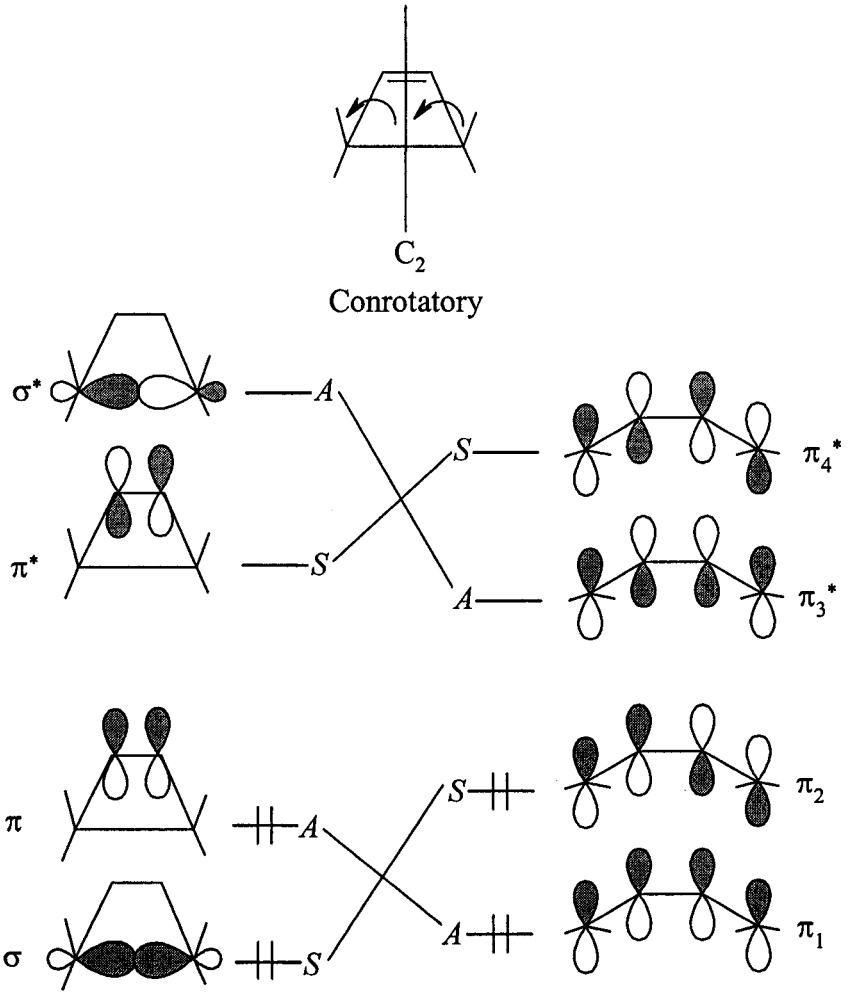

Figure 6. Orbital correlation diagram for conrotatory ring opening of cyclobutene.

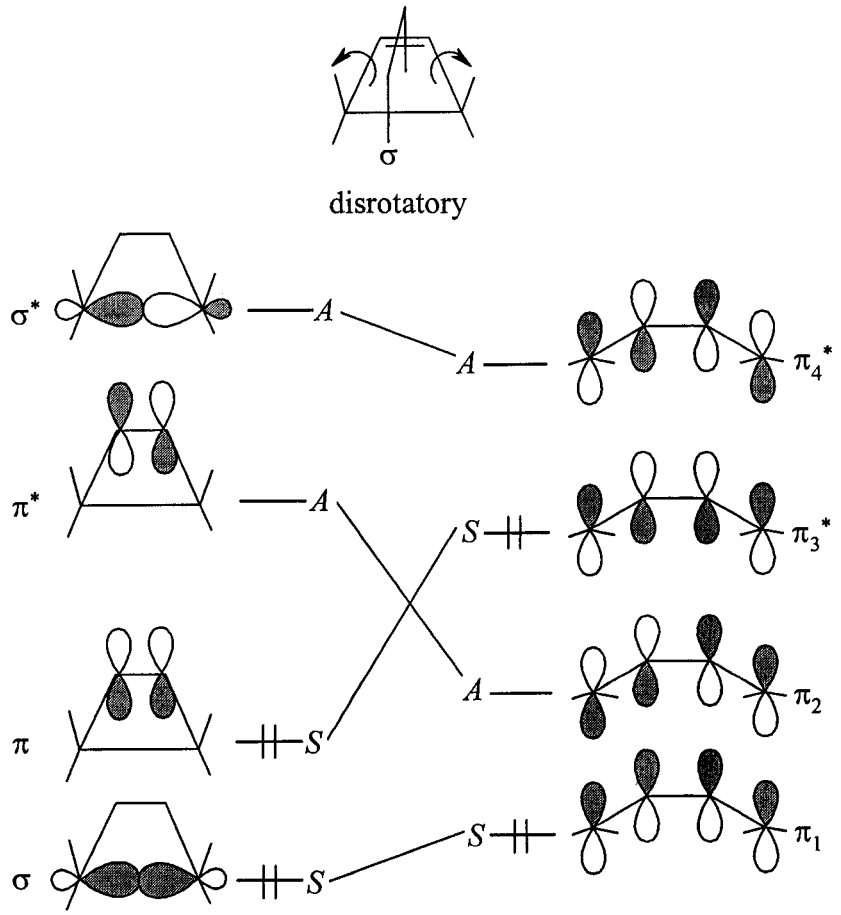

Figure 7. Orbital correlation diagram for disrotatory ring opening of cyclobutene.

There are two conrotatory pathways and two disrotatory ones, and each of them can lead to different products as shown in Figure 8. The electrocyclic ring opening of 3,4-substituted cyclobutene could yield four possible products (eqn. 1.7).

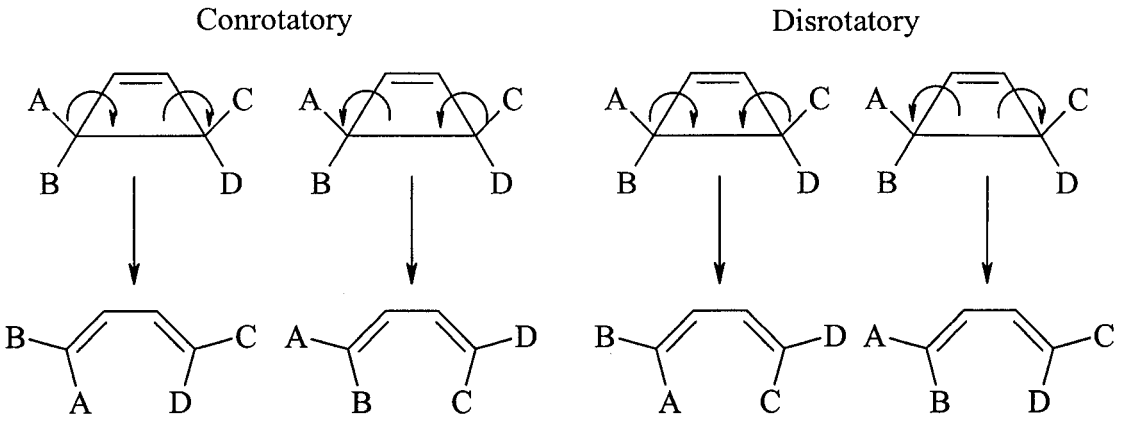

Figure 8. Possible products of a cyclobutene ring opening.

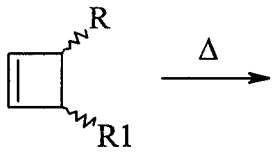

$$RCH{=}\underset{H}{C}{-}\underset{H}{C}{=}CHR_1 \qquad [1.7]$$

E,Z-, E,E-, Z,Z-, or Z,E- isomers

For example, if both substituents at C3 and C4 are the same and possess the *cis* stereochemistry then the product of conrotatory ring opening will only be the *E,Z*-2,4-hexadiene as for *cis*-3,4-dimethylcyclobutene (**24**) (eqn. 1.8).[62] This is because the two conrotatory pathways are degenerate when the substituents at C3 and C4 are identical. If on the other hand the same two substituents have *trans* stereochemistry as in *trans*-3,4-dimethylcyclobutene (**25**), then conrotatory ring opening can give the *E,E*-2,4-hexadiene (eqn. 1.9)[63] and *Z,Z*-2,4-hexadiene. Only the *E,E*-isomer is observed experimentally, so the reaction is stereospecific.

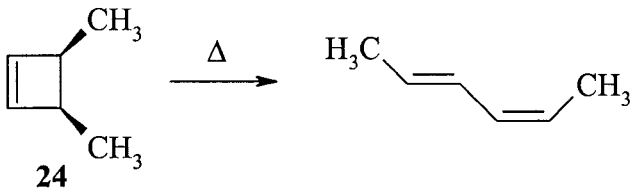

24 [1.8]

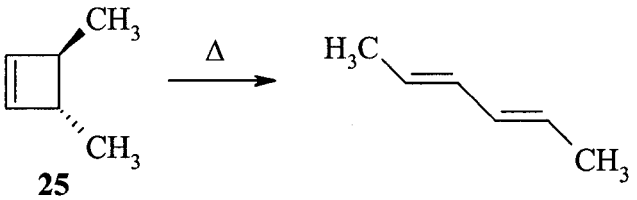

25 [1.9]

In similar experiments with *cis*-1,2,3,4-dimethylcyclobutene (**26**) it was found that the sole product of thermal ring-opening reaction was *E,Z*-3,4-dimethylhexa-2,4-diene (eqn. 1.10), while for the ring-opening of *trans*-1,2,3,4-dimethylcyclobutene (**27**) it was shown that the product was *E,E*-3,4-dimethylhexa-2,4-diene (eqn. 1.11).[64]

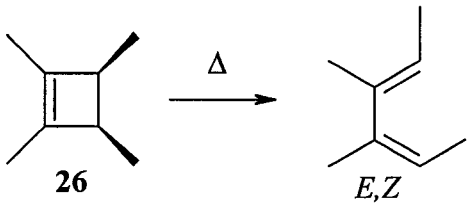

26 *E,Z* [1.10]

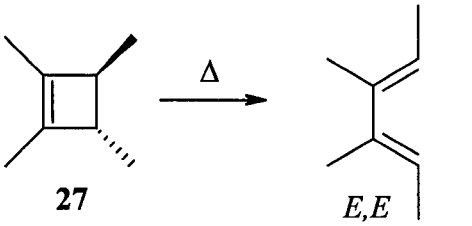

27 *E,E* [1.11]

The above examples illustrate that the thermal ring opening proceeds as symmetry selection rules predict. They also illustrate the stereospecificity or "torquoselectivity" of this type of electrocyclic reaction.

1.4.3 Torquoselectivity and the Ground-State Ring Opening of Cyclobutenes

Although Woodward-Hoffmann rules of conservation of orbital symmetry predict that there are two possible orbital-symmetry-allowed conrotatory processes available for the ring-opening, there exists a preferential direction for the rotation of the substituents at the C3 and C4 position. This preferential direction of rotation of the substituent was illustrated in Eqns. 1.8-1.11 in the preceding section. Experiments with 3-methylcyclobutene (**28**), which upon the ring opening gave only *trans*-1,3-pentadiene (eqn. 1.12) also have shown stereoselectivity.[65]

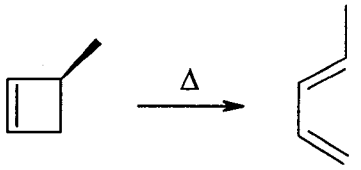

28 [1.12]

The rationale for this stereospecificity, where the substituents rotate outward, was attributed to the minimization of steric effects in the electrocyclic transition state. [66] In 1984 it was shown that electronic effects rather than steric effects were dominant in the determination of stereochemical and kinetic behaviour of 3-substituted cyclobutenes.[67,68] The stereoselectivity of the cyclobutene ring openings has been accounted for with the use of a comprehensive electronic theory based on the computational results of Rondan, Kirmse and Houk.[68,69] The authors have invented the term "torquoselectivity" to describe this type of observed stereoselective conrotation, or the preferential direction of rotation of the breaking σ bond in the transition state. The theory has been recently summarized.[66]

Since in a conrotatory electrocyclic ring opening there are two possible orbital symmetry allowed paths there may be four possible isomers of the diene obtained upon the ring opening (Figure 9).

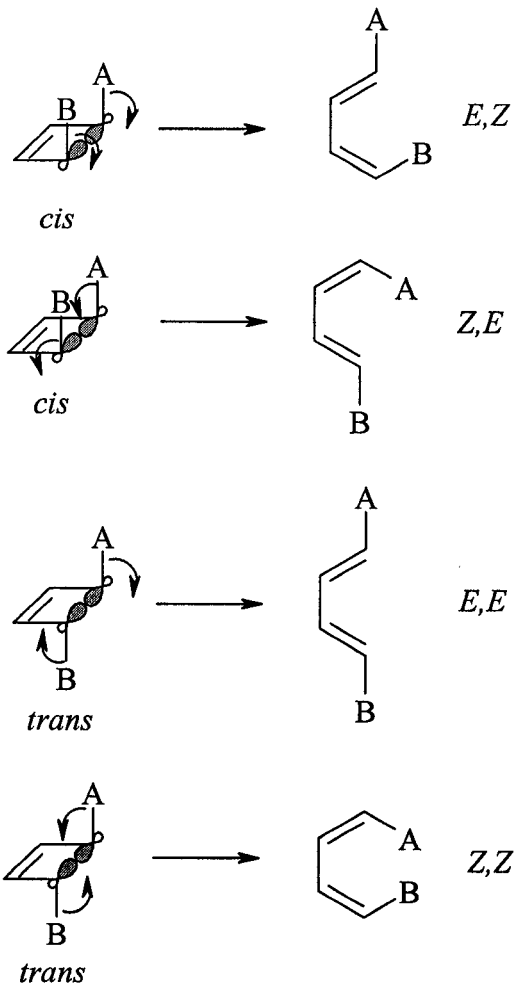

Figure 9. Four possible products of a conrotatory ring opening of disubstituted cyclobutene.

The rotation of the substituents in the *cis* disubstituted cyclobutene upon the breaking of the σ bond will produce an *E,Z* diene. Upon the breaking of the σ bond in a *trans* disubstituted cyclobutene the product may either be a *Z,Z*, or *E,E* diene, depending

on the direction of rotation of the substituents. In the case of a *cis* disubstituted cyclobutene one of the substituents is rotating "outward" and the other is rotating "inward". Outward signifies the rotation of the substituent away from the ring and inward describes the rotation of the substituent toward the ring. In the case of a *trans* disubstituted cyclobutene, the substituents both rotate either inward or outward.

Computational results have shown that upon inward rotation of an electron donor substituent a filled orbital of the donor substituent overlaps with the transition state HOMO of the cyclobutene transition state.[66] A destabilizing four electron interaction is the result of this overlap, thus the activation energy for the inward rotation of a donor substituent is significantly increased.[66] There is less overlap of these orbitals in the outward rotation of a donor substituent which results in less repulsion. There is also an overlap of the donor orbital of the substituent with the LUMO of the transition state. This results in lowering of the activation energy for the outward rotation of a donor substituent. The overlap of the substituent orbital with the transition state LUMO upon an inward rotation is minimal which results in little stabilizing interaction (Figure 10).[66]

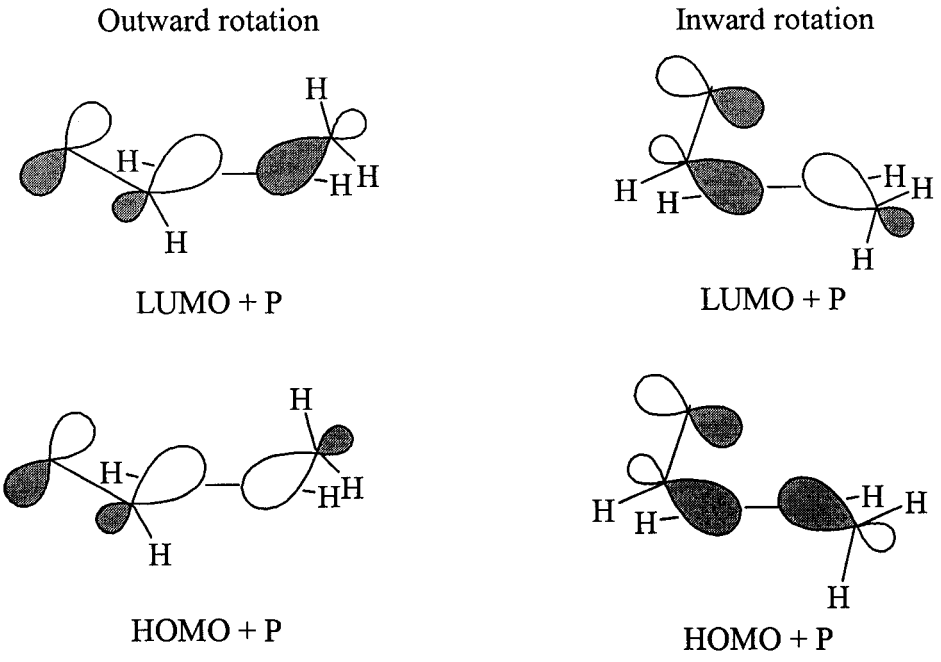

Figure 10. Schematic representation of transition state HOMO and LUMO for outward and inward conrotation.[66]

In the case of inward conrotation of electron acceptor substituents a low-lying vacant orbital overlaps with the HOMO of the transition state. The transition state is stabilized by this two-electron interaction which is especially large for the inward conrotation. This significantly lowers the activation energy for this process. Upon the outward rotation of electron acceptor substituents the overlap with the HOMO of the transition state is smaller resulting in a smaller stabilizing effect.[66]

Based on the combination of both experimental and computational results the authors of the torquoselectivity theory have provided an answer to the problem of which electrocyclic pathway of the cyclobutene ring opening will occur. Out of the four possible outcomes of the ring opening, orbital symmetry rules out the two disrotatory processes.

The stereoselective principle of torquoselectivity favours the rotation of an electron acceptor inward and an electron donor outward (Figure 11).[66]

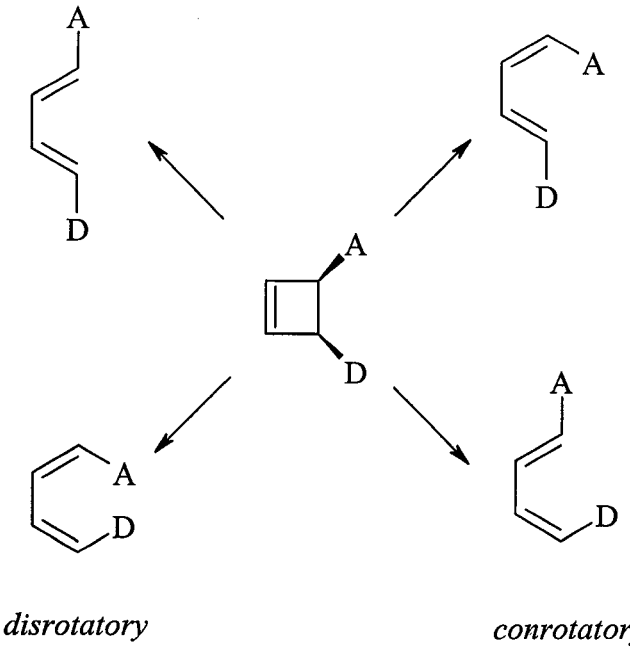

Figure 11. Electron donor and acceptors in conrotatory and disrotatory ring opening of cyclobutene.

One of the examples for the validity of the torquoselectivity theory was provided by computational and experimental results for the ring-opening of 3-formylcyclobutene.[70]

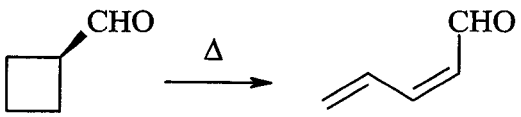

[1.13]

It was shown computationally that the formyl group, being an electron acceptor, prefers the inward rotation to yield *Z*-2,4-pentadienal (Eqn. 1.13), which was predicted to be 3.1 kcal mol^{-1} less stable than the *E*-isomer.[70] It was also shown experimentally that this reaction yields exclusively the *Z* product in >98% yield.[70]

The theory is also supported by experiments on the thermal ring-opening of 3-methoxy-3-*tert*-butylcyclobutene, which have shown that the bulkier *tert*-butyl substituent exclusively rotates inward (Eqn. 1.14).[71] This has illustrated that the electronic effect of the methoxy group forces the bulky *tert*-butyl group to rotate inward.

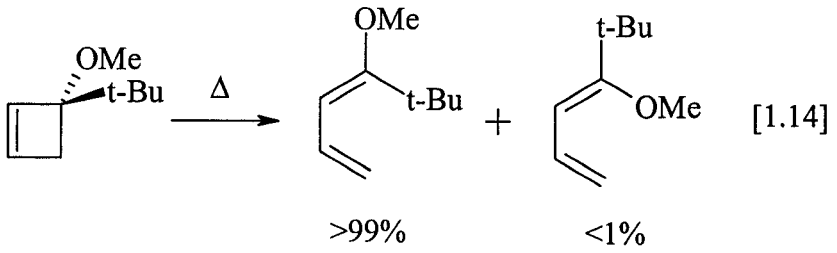

[1.14]

The predictive principal of torquoselectivity theory has also been shown to be applicable to electrocyclic reactions other than the thermal cyclobutene ring opening. It has been applied in such reactions as electrocyclic ring openings of aziridines and oxiranes,[72] the cyclization of pentadienyl cation,[73,74,75,76] the hexatriene-cyclohexadiene interconversion,[77] the octatetraene-cyclooctatriene interconversions,[78] and the ring opening of cyclobutenones.[79]

1.4.5 Strained transient molecules from cyclobutenes.

An additional constraint may be introduced to the cyclobutene ring opening in the form of a syn-cycloalkyl ring joining C3 and C4. In such a case conrotatory ring opening will have to overcome a higher energy barrier in order to accommodate the *trans* double bond in the cyclic diene product. Since the thermal conrotatory process of a *cis* disubstituted cyclobutene will generate an *E,Z* product, the *trans* double contained in a

cyclic molecular system will render the molecule highly strained and such a molecule may be a transient species. The degree of strain in the products will depend on the size of the ring which joins C3 and C4 of the cyclobutene moiety.

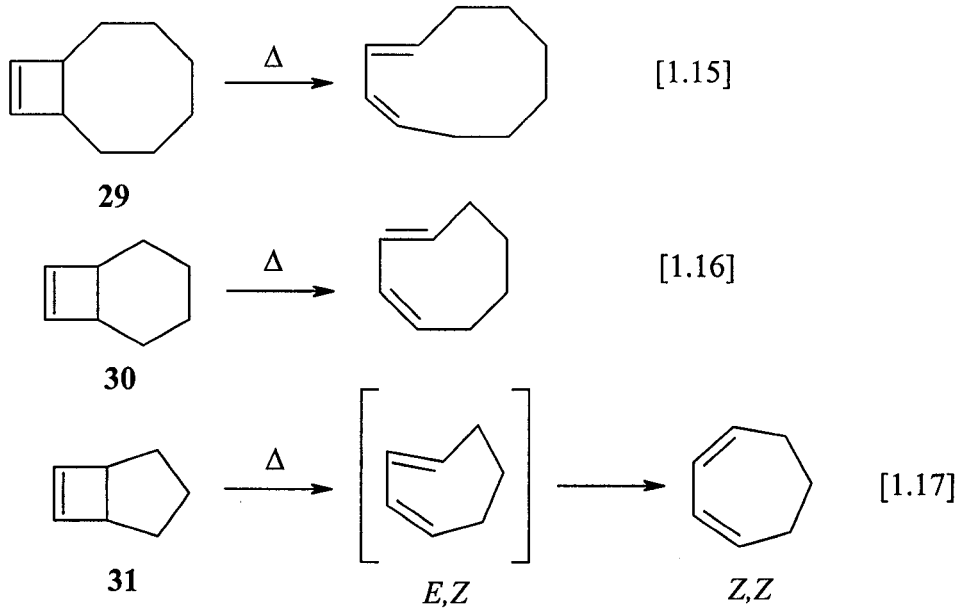

The thermolysis of *cis*-bicyclo[6.2.0]deca-9-ene (**29**) generates *E,Z*-cyclodeca-1,3-diene (eqn. 1.15).[80] The second ring joining the saturated carbons of the cyclobutene moiety is large enough to accommodated the *trans* double bond in the new cyclic diene. Similarly the thermolysis of *cis*-bicyclo[4.2.0]oct-7-ene (**30**) gives *E,Z*-cycloocta-1,3-diene (eqn. 1.16).[81] On the other hand the thermolysis of bicyclo[3.2.0]hept-6-ene (**31**) yields only *Z,Z*-cyclohepta-1,3-diene (eqn. 1.17).[64] The process involves an initial conrotatory ring opening to give a strained *E,Z* intermediate which isomerizes to the *Z,Z* product.[82] The *E*- to *Z*-isomerizaton was confirmed by a deuterium labeling study,[83] which has ruled out the possibility of a 1,5-H shift that has been postulated earlier.[84,85]

E,Z-1,3-Cycloheptadiene is known to have a lifetime of only 7.1 minutes in fluid solution at -78°C, and decays by competing *E,Z* isomerization and ring closure to regenerate **31**.[86]

1.5 Conformational analysis with photoelectron spectroscopy

Ultraviolet photoelectron spectroscopy is an invaluable experimental tool for studying molecular electronic structure. It may be used to study transient as well as stable compounds. The combination of *ab initio* calculation and PES may also be applied in the studies of molecular conformational properties, as for example in the case of tetrahydrotetrazines,[12] phenyl and pyridinyl diazoketones and diazoesters,[13] dimethoxycarbene,[10] as well as in the studies of the conformational behavior and electronic structure of silylketenes.[87] The utility of photoelectron spectroscopy as a tool for the study of conformational properties has been well documented in an excellent review by Brown and Jorgensen.[88]

1.5.1 7-Substituted cycloheptatrienes

1,3,5-Cycloheptatriene was also known earlier as "tropylidene". It was first isolated by Ladenburg in 1883,[89] and ever since has been under experimental and more recently, computational investigation.[90] A number of substituted cycloheptatrienes has been prepared and their photochemical and thermal behavior has been studied. Ter Borg and coworkers have studied the photoisomerizations of 1-substituted cycloheptatrienes

with such substituents as cyano, phenyl, methyl, thiomethyl, methoxy, and dimethylamino.[91] The authors have found that the presence of substituents can change the ratio of competing photochemical pathways by several orders of magnitude. The processes involved in the photochemical isomerizations are the 1,7-hydrogen shift[92,93,94] and valence tautomerization, which is a cyclization to bicyclo[3.2.0]hepta-2,6-diene.[95] In analogous experiments the authors have studied the thermal isomerization of these compounds with the substituents originally in the 7-position, also finding that the presence of difference substituents plays a major role in defining the equilibrium compositions of mono-substituted cycloheptatrienes.[96] The thermal chemistry of cycloheptatrienes involves the 1,5 hydrogen shift. The authors have discovered an interesting finding in the thermal isomerization of dimethylamino substituted cycloheptatriene where the only isomer present at equilibrium was the 1-substituted dimethylamino cycloheptatriene.

The parent 1,3,5-cycloheptatriene has a non-planar boat conformation as has been established experimentally from electron diffraction[97] and microwave[98] studies and by *ab initio* calculations.[99,100] Cycloheptatriene is also in rapid equilibrium with norcaradiene, even at room temperature. Norcaradiene has been implicated to be 4 to 6.5 kcal mol^{-1} less stable than cycloheptatriene.[101] The boat-shaped conformation of cycloheptatriene has also been demonstrated by Jensen and Smith[102] and Anet[103] who have shown that it is associated with a degenerate ring-inversion equilibrium. Low temperature ^1H NMR experiments were used to measure the free energy barrier of the ring-inversion in cycloheptatriene. In $CBrF_3$ as the solvent the free energy barrier was found to be 5.7 kcal

mol^{-1},[102] and in CF_2Cl_2 it was measured to be 6.3 kcal mol^{-1}.[103] It has also been shown by Jensen and Smith in experiments with 7-*d*-cycloheptatriene that it shows an *equatorial* preference for the deuterium.[102,104]

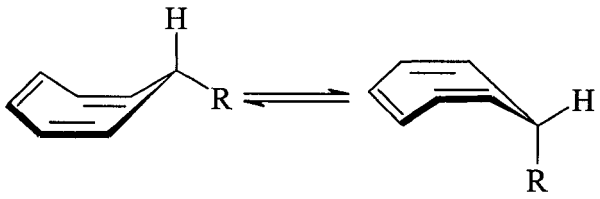

Figure 12. Ring inversion of cycloheptatriene.

It has been shown computationally that the 7-methoxy-1,3,5-cycloheptatriene also adopts the boat conformation and shows a preference for the methoxy group to be in the *equatorial* position.[100] Early semiempirical (MNDO) studies of 7-methyl- and 7-silyl-1,3,5-cycloheptatriene indicated that these substituents prefer the *axial* conformation.[99] The ring-inversion conformerization of the two boat conformations of 7-substituted cycloheptatrienes has been proposed to occur through a planar transition state.[99,100]

1.6 Objectives

This study was undertaken in order to explore the C_7H_6 potential energy surface with the intent to study possible transient species with PE spectroscopy. It has been reported in the literature that 1,2,4,6-cycloheptatetraene (**10**) is the key intermediate on the C_7H_6 potential energy surface and that it rearranges to fulvenallene via a transient triene. The main objective of this study was to thermolyze a suitable precursor of **10**, record the thermolysis PE spectrum and assign the IP's to potential C_7H_6 isomers. The objective was also to identify the transient triene through thermolysis and PE spectroscopy of an *N*-oxide precursor to bicyclo[3.2.0]hepta-1,3,6-triene (**18**). This was designed to illustrate whether the triene is observable in the themolysis PE spectrum of the precursor for **10**.

The objectives of this study were also extended to the investigation of the thermal cyclobutene ring opening. The impetus for this study was a proposed mechanism that emerged from the thermolysis and computational study of a diazodiene precursor for **10**. The study of thermal cyclobutene ring opening was aimed at identifying transient dienes which may be generated upon the thermolysis of bicyclic cyclobutenes. The thermal ring opening was also studied computationally with the intent of predicting the preferred direction of rotation of the breaking sigma bond and correlating the computational results to the experimental findings.

Chapter 2

HeI Ultraviolet Photoelectron Spectrometer

2.1 General

The ultraviolet photoelectron spectrometer employed in the studies described in this thesis is a locally built instrument.[105] A schematic diagram of the photoelectron spectrometer used in this work is shown in Figure 13. The instrument consists of seven major components: the vacuum system which maintains the proper pressure in the source of the spectrometer, a set of Helmholtz coils which provide magnetic shielding of the instrument, a source chamber where the introduced sample is ionized, the ionization radiation source, the electron kinetic energy analyzer which measures the kinetic energy of the ejected photoelectrons, and a detection, amplification and recording system which allows for the graphical display of the results of the experiment. The spectrometer is interfaced with a CW CO_2 infrared laser, which is used as a directed heat source for thermolysis studies.

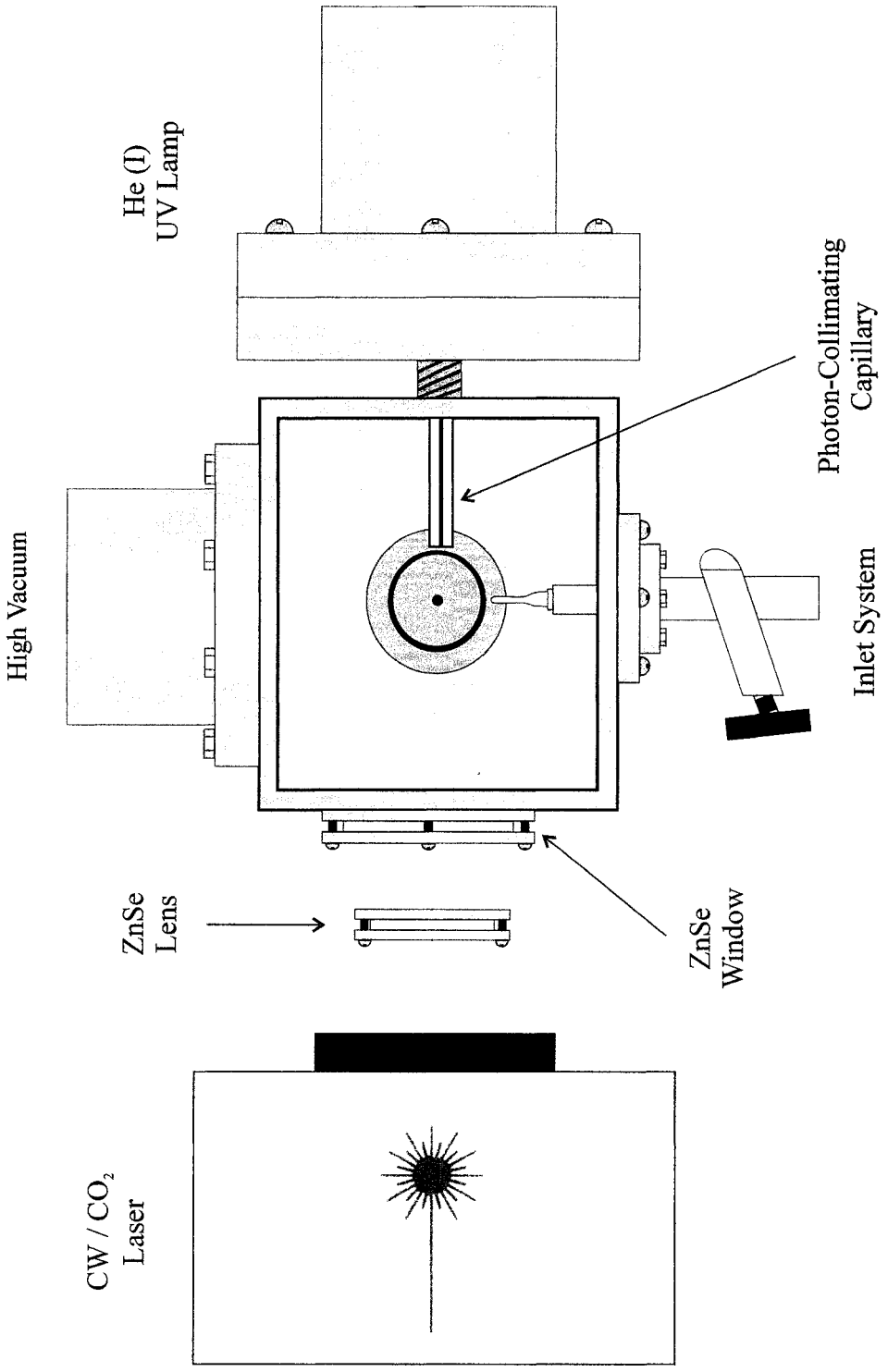

Figure 13. Schematic representation of UV PES instrumental setup.

2.2 Instrumental setup

2.2.1 Vacuum system

The instrument operates at a pressure of 10^{-4} Torr. During a photoelectron spectroscopy experiment the pressure in the source chamber is maintained between 10^{-3} Torr and below 10^{-2} Torr. An automatic triggering system is employed in the spectrometer system to shut off the high voltage to the electron multiplier and the ionization source in case the pressure in the source chamber should rise above 2×10^{-2} Torr. Three rotary pumps and two oil diffusion pumps supply the vacuum. The first rotary pump is a backing pump for the operation of the diffusion pumps. The second and third rotary pumps are connected to the He(I) DC discharge lamp and the inlet system, respectively. Two diffusion pumps connected to the instrument supply the high vacuum. A large diffusion pump is situated beside the instrument and provides the ability of fast pumping for the evacuation of the source chamber. It is connected to the instrument with a high vacuum valve. The second, smaller diffusion pump is located directly below the source chamber of the photoelectron spectrometer and maintains the high vacuum throughout the instrument.

2.2.2 Magnetic shielding

The instrument is magnetically shielded to eliminate stray magnetic fields, which influence the trajectory of the ejected photoelectrons. The field of the analyzer should determine the trajectory of the photoelectrons exclusively. All components of the instrument are constructed from nonferromagnetic materials such as aluminum, stainless steel and brass. The source chamber as well as the He(I) DC discharge lamp are constructed from aluminum. The housing of the electron multiplier is constructed from brass while the inlet system is constructed from stainless steel. Three pairs of Helmholtz coils surround the instrument, providing magnetic shielding. The coils are arranged perpendicular to each other and are connected to a power supply with variable resistance. The voltages in the coils are adjusted in order to achieve near zero field in the vicinity of the source chamber and analyzer.

2.2.3 Source chamber

The gaseous molecules that are being ionized are confined within an aluminum housing known as the collision chamber. It is constructed from half-inch thick aluminum plates that are welded together in a form of a cube. An Einzel lens composed of three elements is fitted inside the source chamber. Each element is made from brass and is connected to its own individual variable electrical potential, used to focus and transport the electrons from the point of ionization to the entrance of the energy analyzer. A

hemispherical electron kinetic energy analyzer is attached to the bottom plate of the collision chamber. One of the walls of the source chamber is fitted with a circular ZnSe window to allow the IR laser radiation to enter the chamber during pyrolysis experiments. The wall opposite the ZnSe window has a half-inch, threaded opening which accommodates the attachment of the He(I) DC discharge lamp. A high vacuum connection and an inlet system connection are placed on the other two walls of the source chamber. The top of the source chamber is fitted with a quadrupole.

2.2.4 Ionization source

Electrons from a sample in the gas phase are ejected using monochromatic radiation provided by a direct-current discharge of helium gas. The rare gas enters the DC discharge lamp through a 1-mm diameter glass discharge capillary. A second collimating glass capillary, which allows the flow of the photons into the ionization chamber, is aligned end-to-end with the discharge capillary at a distance of 1- to 2-mm. The lamp operates at a voltage of 1.5 kV and a current of 30 mA. A rotary pump is connected to a pumping port in the He I DC discharge lamp in order to pump out excess gas. The energy of the photons generated by the discharge is 21.22 eV. This allows for the ionization of valence shell electrons in most molecules.

The body of the lamp is constructed from aluminum and the lamp is air cooled with a fan during its operation.

Table 2. Ionization energies and principle resonance lines for He I.[1]

Gas	Resonance Line		Ionization Energy	
	(Å)	(eV)	(Å)	(eV)
He I	584.3340	21.2175 (100)[a]	500.259	24.5868
	537.0296	23.0865 (2)		
	522.02128	23.7415 (0.5)		

a – relative intensities

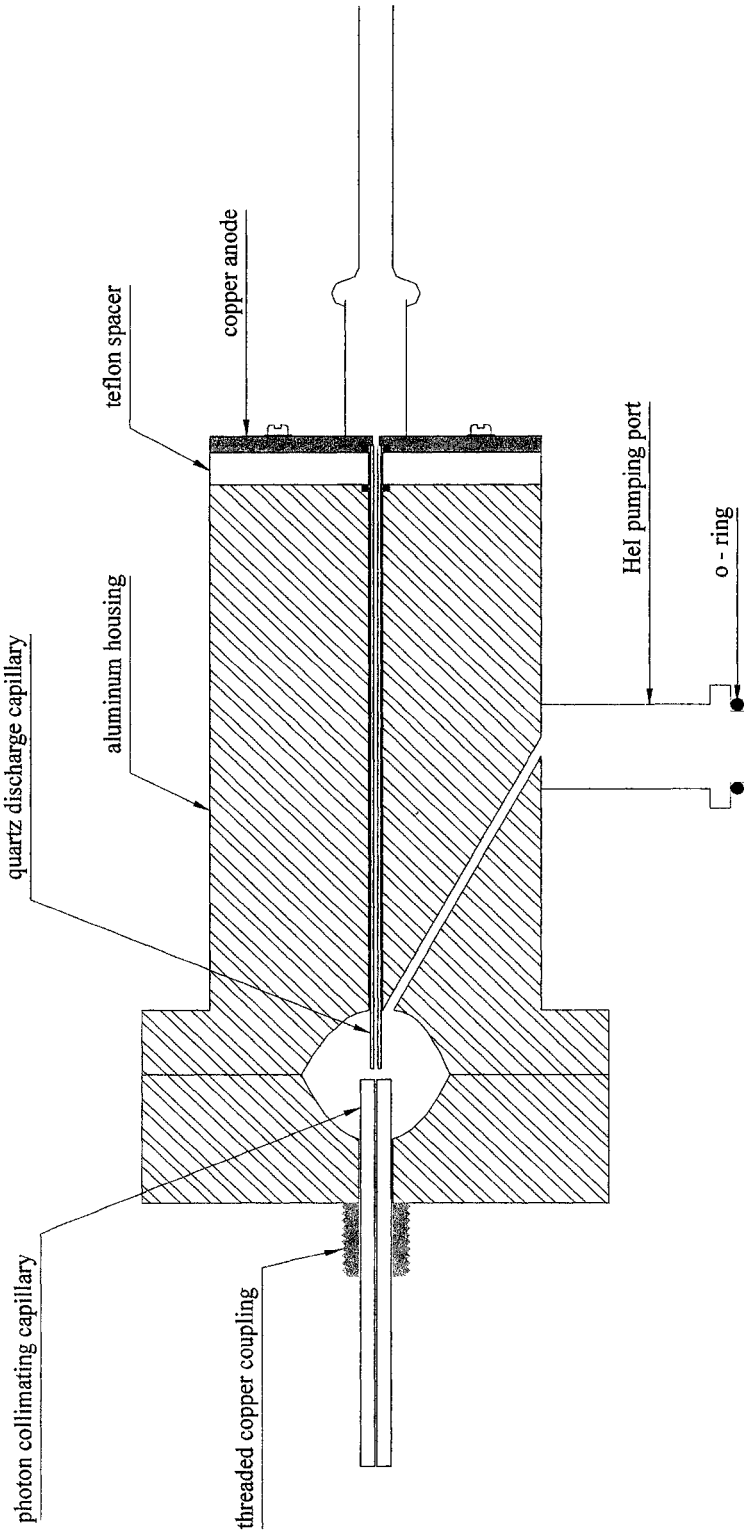

Figure 14. HeI DC discharge lamp.

2.2.5 Electron kinetic energy analyzer

This UV photoelectron spectrometer employs hemispherical plates as the electron kinetic energy analyzer. Both the top and the bottom plates of the analyzer are directly attached to the bottom of the ionization chamber. The two hemispherical plates are separated from each other by a distance of 10 cm. and are coated with carbon-black to prevent charging. In the analyzer the ejected photoelectrons are sorted according to their kinetic energies. The photoelectrons enter the analyzer through a small slit in the bottom of the ionization chamber after passing through a number of focusing lenses. A voltage is applied to the two hemispherical plates of the analyzer and the photoelectrons are focused into a beam which exits the analyzer through a tiny slit less than 1-mm in diameter leading to the electron multiplier (channeltron).

2.2.6 Detection and recording system

The electron flux from the analyzer is detected using an electron channel multiplier (the "channeltron"). A focused electron beam from the analyzer enters the channeltron through a slit and the electrons impinge on its surface. The channeltron is a spiral tube coated internally with a high-resistance material. High voltage is applied across the channeltron and the electrons entering the multiplier are accelerated through repeated cycles. A cascade of secondary electrons is generated when the photoelectrons come into collision with the walls of the channel electron multiplier tube. The device

itself is located outside the ionization chamber in a separate compartment constructed from brass. A constant vacuum of 10^{-4} Torr is maintained in this compartment. The electrons then travel to an amplifier connected to a count-meter. The spectrum is obtained by scanning voltages using an Apple II computer equipped with an analog-to-digital computer board (Cyborg). The spectrum is plotted on an HP 7015 X Y recorder.

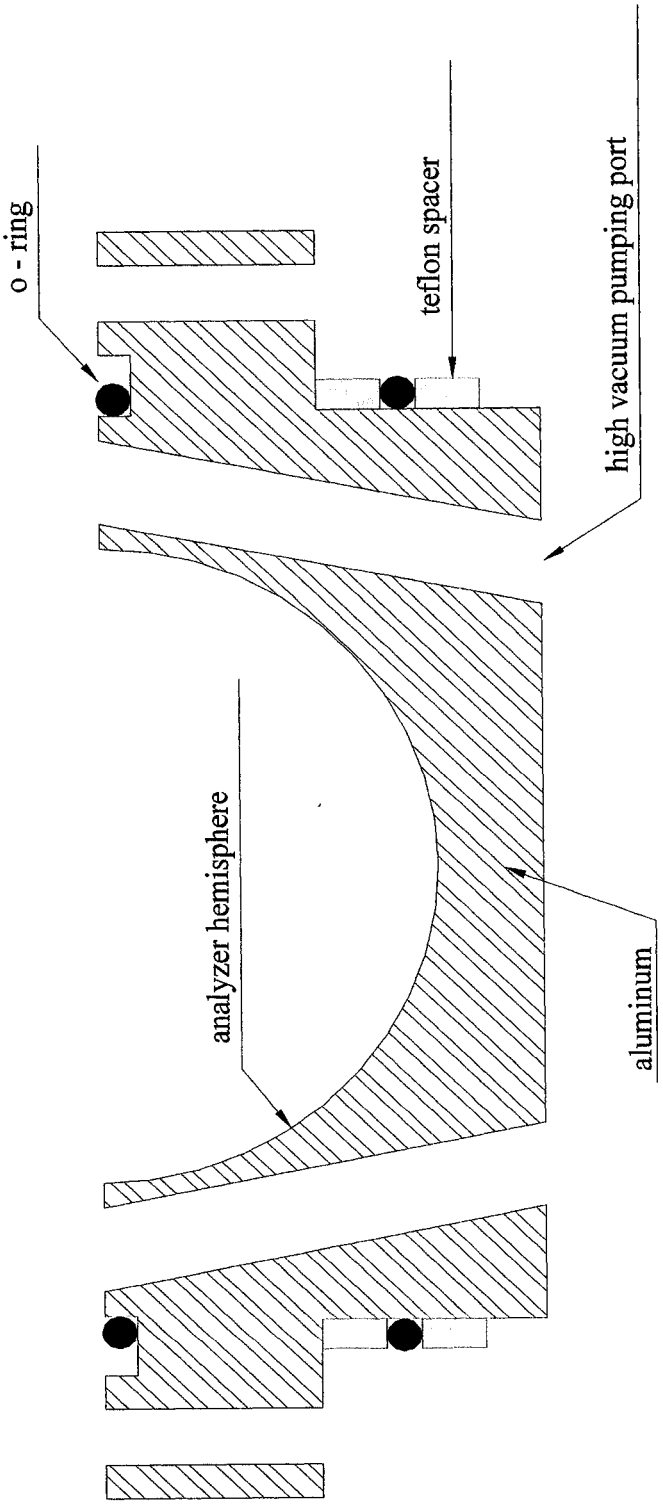

Figure 15. Cross section of the bottom hemisphere of the electron analyzer.

2.2.7 Directed heat source

Thermolysis experiments are performed directly in the source chamber of the ultraviolet photolelectron spectrometer with the use of a tunable continuous wave carbon dioxide laser as a directed heat source. The beam of the laser is focused on the tip of a quartz nozzle protruding from the probe inserted into the source chamber. The laser has been calibrated using a closed-tip quartz probe fitted with a thermocouple. A beam-chopper is used to control the laser power. The calibration values are shown in Table 3.

Table 3. Temperature and laser setting calibration.

Laser setting	Temperature °C
4844	29
4807	31
4790	342
4784	396
4780	534
4780 w/ chopper	374
4771	615
4771 w/ chopper	423
4754	702
4754 w/ chopper	540

Chapter 3

Cycloheptatetraene: UV PE Spectroscopy and Thermolysis

3.1 Background

1,2,4,6-Cycloheptatetraene (**10**) is a strained transient allene on the C_7H_6 potential energy surface. A number of precursors have been employed in order to generate **10** and explore the chemistry of it and its isomers.[30] The C_7H_6 potential energy surface has been the subject of many theoretical and experimental investigations during the past two decades mainly owing to the fact that the isomers, which reside on this potential energy surface are all interconnected through high-energy processes.[31] Wentrup and coworkers have shown through ^{13}C labeling studies that phenylcarbene isomerizes to fulvenallene (**20**) at high temperature.[38]

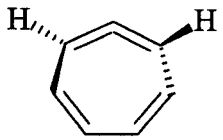

10

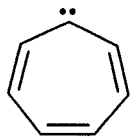

11

The ^{13}C label was completely scrambled in the isolated product. Cycloheptatrienylidene (**11**) was initially implicated as the transient intermediate involved in the rearrangement along with bicyclo[3.2.0]hepta-1,3,6-triene (**18**).[38]

3.2 Validation of the PES and thermolysis experiment

The validity of the UV photoelectron spectroscopic experiments combined with direct thermolysis in the source chamber of the UV photoelectron spectrometer was confirmed by a test experiment involving the thermolysis of phenyldiazoethane (**35**). It was important to confirm the possibility of generating a diazo compound from the sodium salt of a tosylhydrazone, external to the source, under the specific operating conditions of the PE spectrometer. The sodium salt of acetophenone tosylhydrazone (**34**) was used as the precursor for the thermal generation of **35**. The salt was thermolyzed in a sample container attached to the probe outside the source chamber of the spectrometer and a PE spectrum of the resultint diazo compound was recorded. Thermolysis of the diazo compound was then performed inside the source chamber of the spectrometer with the use of the IR laser beam focused on the tip of the quartz nozzle of the probe. The ionization potentials of **35** and styrene (**37**) have previously been reported, [106,107] thus allowing the thermolysis spectra obtained in this experiment to be assigned.

3.2.1 Synthesis of acetophenone tosylhydrazone sodium salt (32).

A solution of acetophenone (**32**) in methanol was treated with *p*-toluenesulfonhydrazide affording acetophenone tosylhydrazone (**33**). A solution of **33** in dichloromethane was treated with sodium hydride and allowed to stir over two hours, yielding the acetophenone tosylhydrazone sodium salt (**34**) after workup (Eqn. 3.1)

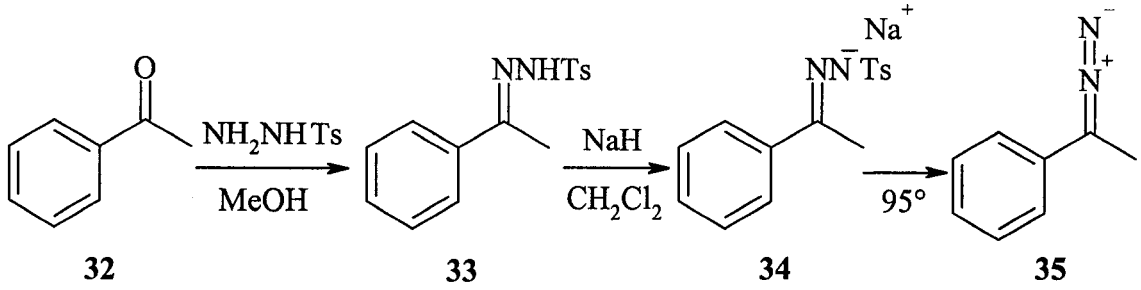

32 **33** **34** **35**

[3.1]

3.2.2 Photoelectron Spectroscopy and Thermolysis of Phenyldiazoethane (35)

Thermolysis of the sodium salt at 95°C afforded phenyldiazoethane (**35**), which was identified by its photoelectron spectrum (Figure 16a). The observed ionization potentials were in agreement with previously reported values as well as with the Becke3LYP/6-31+G(d) calculated vertical ionization potentials (Table 4).[106] The calculated IPs were obtained by the computational method previously reported in the litarature,[9] and described in the introduction (Chapter 1.2.1). Thermolysis of the diazo compound **35** using the CW CO_2 IR laser generated styrene (**37**) as the sole product.

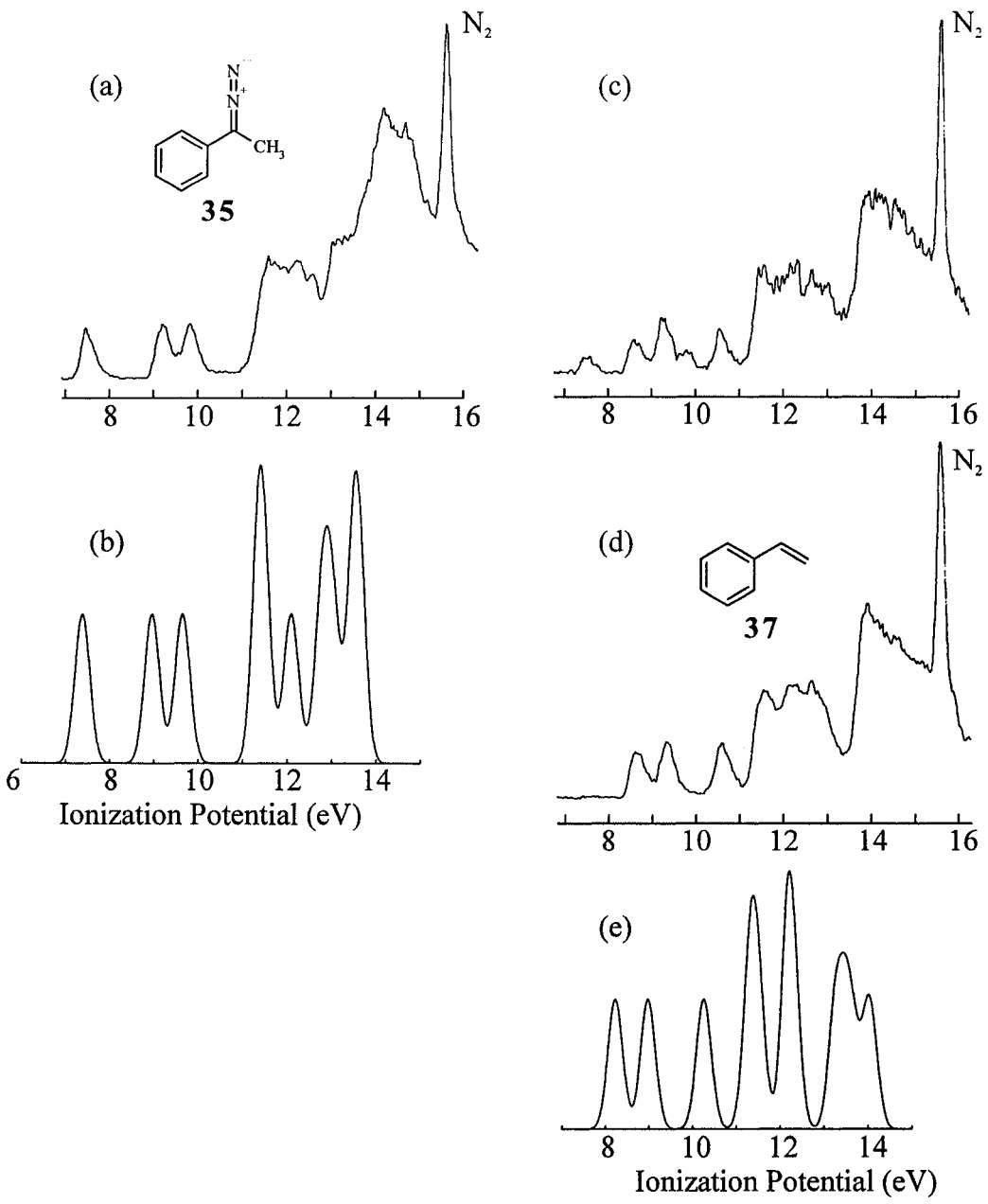

Figure 16. Experimental UV photoelectron spectra of: (a) **35**, (c) partial thermolysis of **35**, and (d) complete thermolysis of **35**. Calculated partial UV PE spectra of: (b) **35** and (e) **37**.

Table 4. Experimental, calculated Becke3LYP/6-31+G(d) and literature vertical ionization potentials of **35** and **37**.

		Ionization Potential		
		eV		
	Exp.	7.46	9.22	9.85
35	B3LYP	7.38	8.96	9.65
	Lit.[106]	7.41	9.19	9.85
	Exp.	8.63	9.36	10.65
37	B3LYP	8.23	8.98	10.26
	Lit.[107]	8.65	9.25	10.53

The intermediate in this reaction is thought to be carbene **36**, which rapidly undergoes a 1,2-hydrogen shift to yield stryrene (Eqn. 3.2).

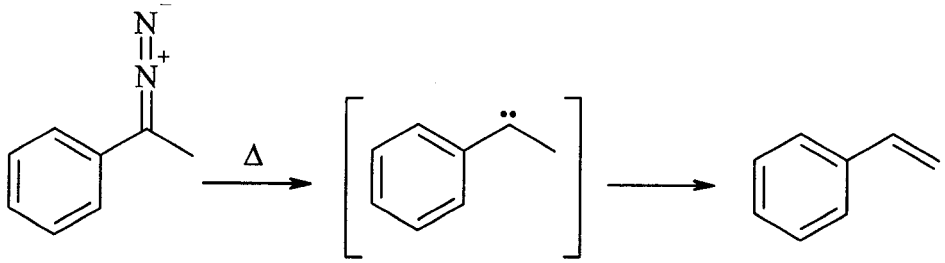

35 **36** **37** [3.2]

The photoelectron spectra of the diazo compound and styrene differ considerably, allowing the ionization potentials of the two compounds to be assigned in straight forward fashion.

Figure 16 shows the experimental and simulated partial PE spectra of **35** and **37**. The PE spectrum of **37** was obtained upon the thermolysis of **35** in the source chamber of the PE spectrometer and was identical to a previously published spectrum.[107] The

spectrum of **35** (Figure 16a) shows three distinct IP bands. Upon partial thermolysis of **35** the PE spectrum changes and IP bands of both **35** and **37** are visible (Figure 16c). A complete thermolysis was achieved by increasing the laser power and the resultant PE spectrum is that of **37** as shown in Figure 16d. The simulated partial PE spectrum of **35** is shown in Figure 16b and illustrates an excellent agreement between experiment and theory. Similarly, the simulated partial PE spectrum of **37** also shows excellent agreement with the experimental spectrum as illustrated in Figure 16e.

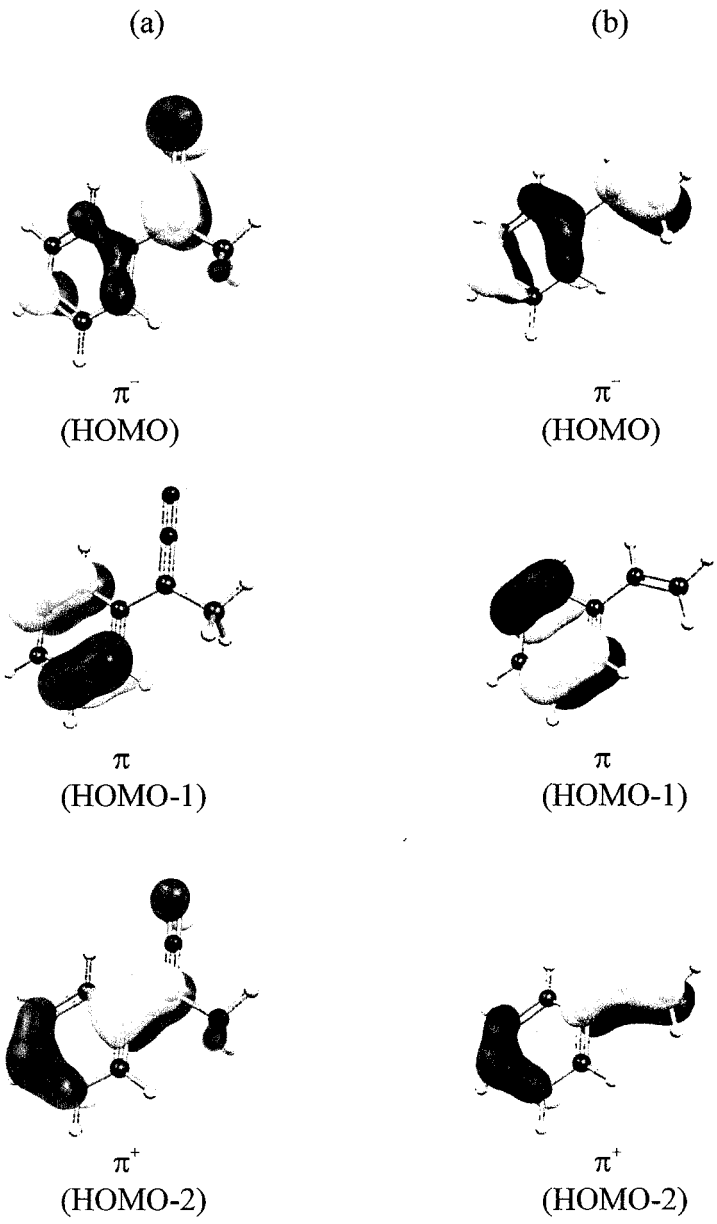

Figure 17. B3LYP molecular orbitals of: (a) **35**, HOMO–HOMO-2 and (b) **37**, HOMO–HOMO-2.

Figure 17 illustrates the calculated molecular orbitals which can be correlated to the different ionization energies giving rise to the photoelectron spectra shown in Figure 16. The molecular orbitals in column (a) are those of phenydiazoethane (**35**). They are the

π orbitals which give rise to the first three ionization potential bands shown in Figure 16a. The highest occupied molecular orbital (HOMO) has a π^- character which denotes the antibonding contribution of orbital coefficients between the diazo group and the phenyl ring. HOMO-2 is a π orbital with the orbital coefficients located on the phenyl ring with no contribution from the diazo group. HOMO-3 has a π^+ character with bonding orbital coefficient contributions of the diazo group and the phenyl ring. Column (b) illustrates the Becke3LYP molecular orbitals of styrene (**37**). Similarly, these three π orbitals give rise to the first three bands in the photoelectron spectrum of **37** shown in Figure 16d. The HOMO is a π^- orbital, HOMO-1 is a π orbital and HOMO-2 is a π^+ orbital.

3.2.3 Computations and simulated photoelectron (PE) spectra

The experiment of the thermolysis of phenydiazoethane (**35**) proved to be an excellent test for the application of *ab initio* calculations for the study of reaction mechanisms, electronic structure and bonding, computation of ionization potentials and simulation of PE spectra. In many cases the PE spectra of certain compounds are not available in the literature for comparison. Therefore it is important to apply computational chemistry to predict the ionization potentials and simulate spectra of such compounds, especially in the case of transients.

Although the experimental ionization potentials of both **35** and **37** are known,[106,107] applying computations at the Becke3LYP/6-31+G(d) level of theory to compare their IPs has proven to be an effective method for the assignment of their spectra and the study of their electronic structure. It has also been shown in previous PES studies that there is an excellent correlation between the theoretically predicted ionization potentials and those obtained experimentally.[9,10,11,13]

The calculations applied in this test study of **35** have also confirmed that they are an excellent tool for the analysis of the potential energy surface. The energy barriers for the extrusion of nitrogen from **35** and the subsequent 1,2–hydrogen shift in the initially generated carbene **36** were calculated to be 35.4 kcal mol^{-1} and 10.6 kcal mol^{-1} respectively. The total and relative energies of **35-39** and the transition states are listed in Table 5.

Table 5. Becke3LYP total and relative energies of **35–39** and **TS1–TS3**.

	E_T (hartrees)	ZPVE correction	Relative Energy (kcal mol^{-1})
35	-419.133 821	0.143 108	0.0
35ts	-419.077 402	0.138 740	35.4
36	-309.557 871	0.130 188	0.0
TS1	-309.541 040	0.128 006	10.6
37	-309.661 274	0.133 518	-64.9
TS2	-309.532 570	0.129 810	15.9
38	-309.555 214	0.131 151	0.0
TS3	-309.552 260	0.130 027	1.9
39	-309.576 443	0.131 476	-13.3

Calculations were also carried out on a hypothetical rearrangement of **36**, where the carbene inserts into an ortho C-H bond in the phenyl ring to generate 7-methylbicyclo[4.1.0]hepta-2,4,6-triene (**38**). This transient cannot be detected under our experimental conditions but it can be studied computationally. The calculated two-dimensional slice of the potential energy surface is shown in Scheme 4.

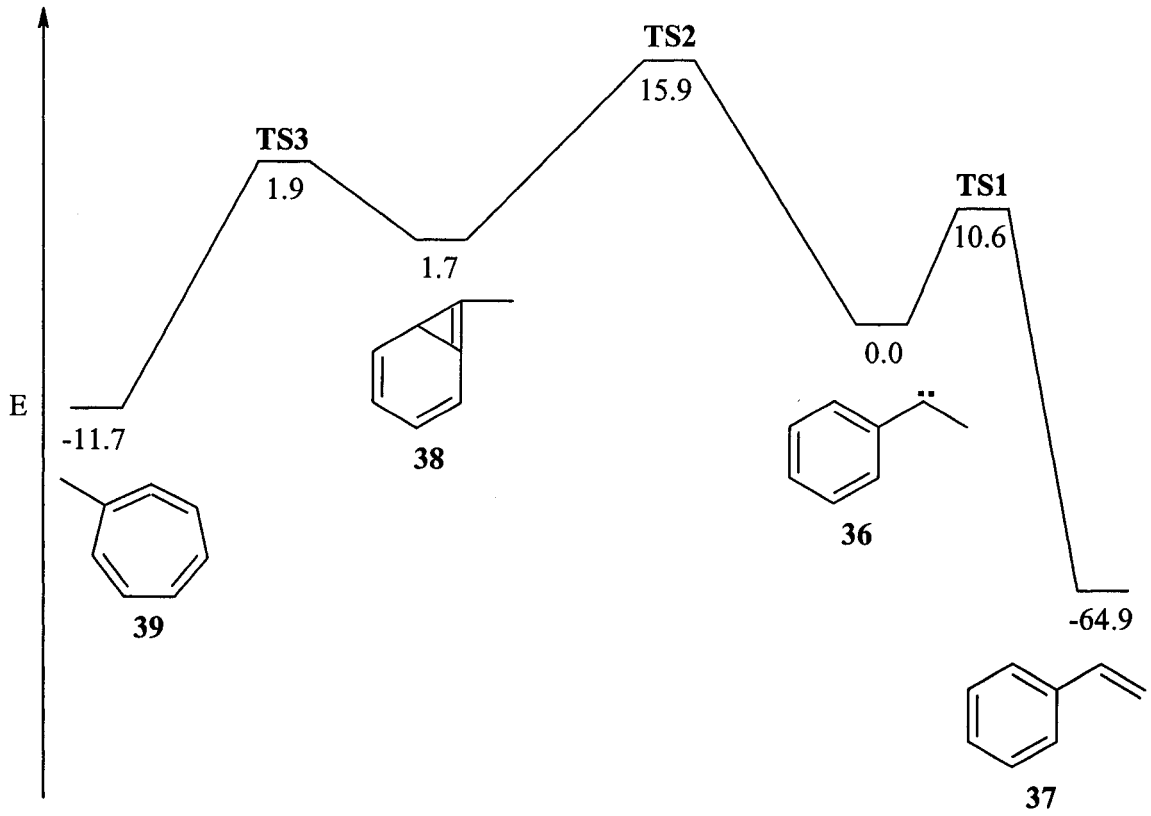

Scheme 4. 2-Dimensional slice of the PE surface for the rearrangement of **36**.

TS1 denotes the transition state for the 1,2-hydrogen shift from **36** to **37**. **TS2** represents the transition state for the carbene insertion in the reaction of **36** to form **38**. **TS3** is the transition state for the ring opening of **38** to yield **39**. Table 4 lists the

Becke3LYP/6-31G(d) total energies and the relative energies associated with the processes described above. The energy barrier for the generation of this species was found to be 15.9 kcal mol^{-1}, which is 5.3 kcal mol^{-1} higher in energy than the 1,2–hydrogen shift leading to **37**. Therefore carbene **36** favors the 1,2-hydrogen shift where the aromaticity of the phenyl ring is conserved.

The transition states for both the hydrogen shift and the C-H insertion were found and confirmed by frequency calculations. Both transition states possess a single negative eigenvalue and a single negative frequency. Upon inspection of these imaginary frequencies it was found that both correspond to the appropriate molecular motion. In the case of the 1,2–hydrogen shift the vibration resembles the movement of one of the hydrogens from the terminal methyl group toward the carbene center. In the case of the hypothetical C-H insertion, the vibration corresponds to the movement of the carbene center toward C2 in the phenyl ring. Although the hypothetical rearrangement does not occur, the ability to use calculations to study this kind of process is invaluable in the investigations of other transients and processes that may be involved in their generation. The rearrangement of **38** to **39** may also be studied computationally. The calculated energy barrier for this process was found to be 1.9 kcal mol^{-1}.

3.2.4 Summary of the thermolysis test experiment

It has been demonstrated that a diazo compound can be generated from the corresponding tosylhydrazone sodium salt directly in the probe of the photoelectron

spectrometer. The photoelectron spectrum of phenydiazoethane (**35**) was recorded and the ionization potentials agree well with literature and calculated values. The photoelectron spectrum of styrene was generated upon thermolysis of **35** directly in the source chamber of the spectrometer, confirming the utility and application of the CW CO_2 laser as a directed heat source.

3.3 Results and discussion

3.3.1 Synthesis of benzaldehyde tosylhydrazone sodium salt (40)

A solution of benzaldehyde (**41**) in methanol was treated with *p*-toluenesulfonhydrazide resulting in the formation of benzaldehyde tosylhydrazone (**42**). The tosylhydrazone was treated with sodium hydride in dichloromethane to yield the corresponding sodium salt **40**.

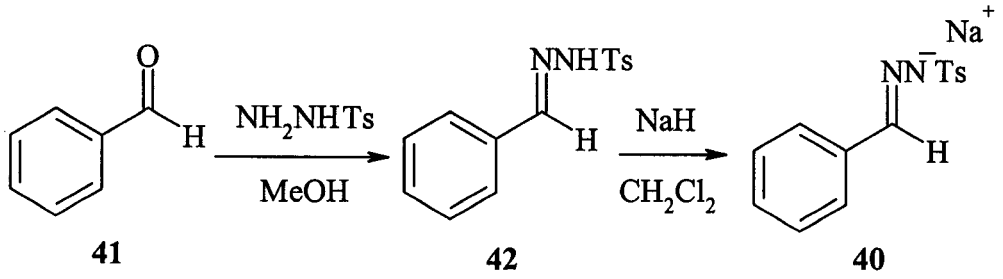

41 **42** **40** [3.3]

3.3.2 Photoelectron spectra and thermolysis of phenydiazomethane

Thermolysis of the sodium salt of benzaldehyde tosylhydrazone in a sample tube attached to the probe of the PE spectrometer yielded the PE spectrum of phenyldiazomethane (**13**), which is shown in Figure 18a along with the simulated PE spectrum calculated on the basis of Becke3LYP/6-31+G(d) calculations.

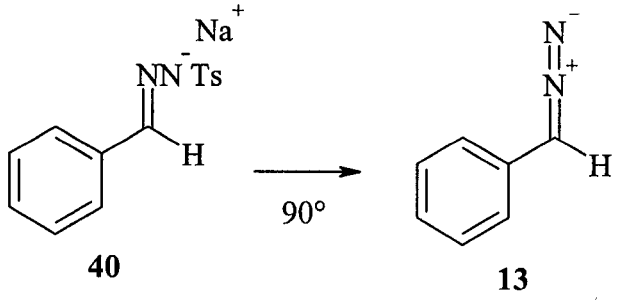

40 **13** [3.4]

The ionization potentials were compared to those previously reported in the literature as well as to calculated values.[106] There is excellent agreement between the experimental and calculated values confirming the authenticity of the PE spectrum. The first three ionization potential bands occur at 7.89 eV, 9.40 eV and 10.16 eV. The calculated IPs are at 7.64 eV, 9.08 eV and 9.96 eV. The literature values are at 7.88 eV, 9.36 eV and 10.24 eV.[106]

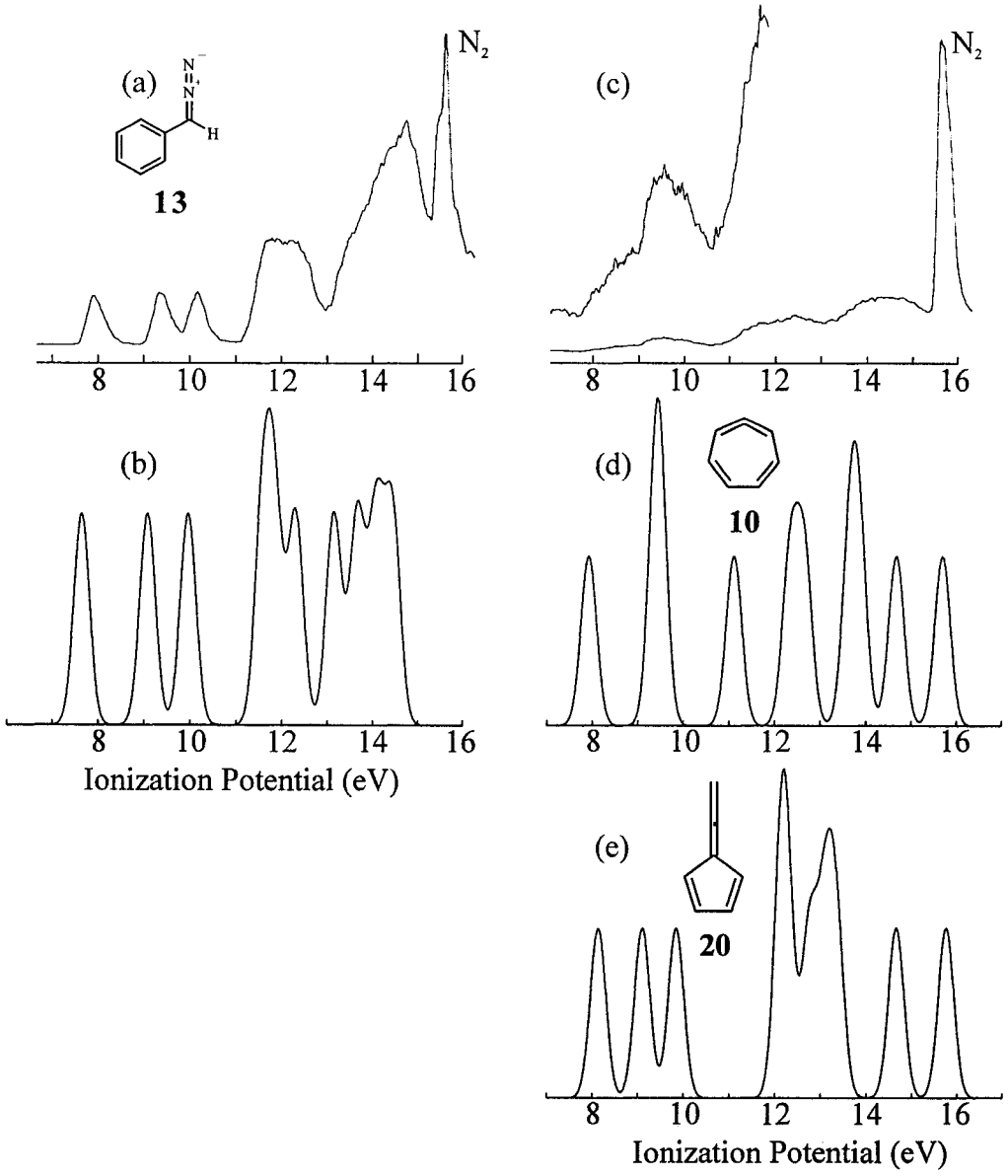

Figure 18. Experimental UV PE spectra of: (a) **13** and (c) upon thermolysis of **13**. Partial simulated PE spectra of: (b) **13**, (d) **10** and (e) **20**.

Table 6. Experimental, calculated (Becke3LYP/6-31+G(d)) and literature IPs of **13**, **20**, and **10**.

		Ionization Potential			
		eV			
13	Exp.	7.89	9.40	10.16	
	B3LYP	7.64	9.08	9.96	
	Lit.[106]	7.88	9.36	10.24	
10	B3LYP	7.92	9.39	9.48	11.11
20	Lit.[108]	8.29	9.14	10.15	
	B3LYP	8.13	9.10	9.84	

The experimental, calculated and literature IPs are listed in Table 6. The first three IP bands of **13** as illustrated in Figure 18a may be assigned to the three π MOs shown in Figure 19. They are similar to the corresponding orbitals of **35** discussed in the previous section. The HOMO has antibonding π^- character. HOMO-1 is a benzenoid π orbital and HOMO-2 has a bonding character between the diazo moiety and the phenyl ring and is assigned as π^+. The simulated partial PE spectrum of **13** correlates well with the experimental PE spectrum (Figure 18a, 18b), both spectra showing three well separated first three ionization potential bands.

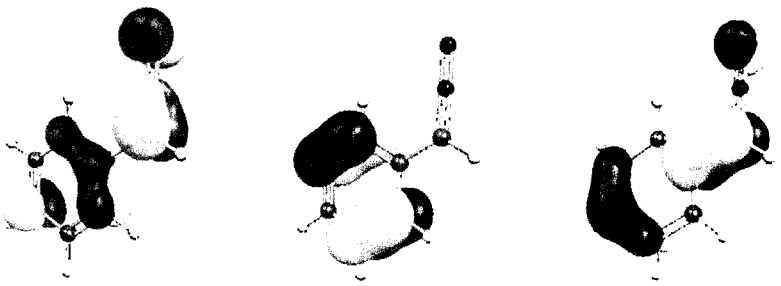

Figure 19. Becke3LYP molecular orbitals of **13**, HOMO–HOMO-2.

Upon thermolysis of **13** in the source chamber of the spectrometer with the use of the IR laser, the original spectrum changed completely. The second IP band in the thermolysis spectrum (Figure 18c) appears as a very broad band in the place where the second and third IP bands of **13** used to reside. This indicates that a thermal reaction is taking place at the tip of the quartz nozzle of the probe while it is being heated. It is possible that the thermolysis spectrum contains bands of fulvenallene (**20**), which has been shown to be a product of the thermolysis of **13** as indicated in the report of Wentrup.[38] The simulated partial PE spectra of **10** and **20** are shown in Figure 18d and 18e respectively. It must also be pointed out that the calculated ionization potentials of **13**, **10**, and **20** have similar values, which makes their identification very difficult. The structures of these molecules are also shown in Figure 18.

3.3.3 2-Diazobicyclo[3.2.0]hepta-3,6-diene (17)

A compound that has also proven to be a good precursor to **10** is 2-diazobicyclo[3.2.0]hepta-3,6-diene (**17**). It has been reported in the literature that the thermolysis or photolysis of the diazodiene generates **10**.[30,35]

3.3.4 Synthesis of 2-diazobicyclo[3.2.0]hepta-3,6-diene (17)

The route to the diazodiene is a ten step synthetic process. The diazodiene is generated in the last step by thermolysis of a tosylhydrazone sodium salt (**52**). The first step of the synthesis involves a [2+2] photochemical cycloaddition of a mixture of *cis* and *trans* 1,2–dichloroethylene (**44**) to 2–cyclopentenone (**43**). This reaction gives a mixture of isomers of 6,7-dichlorobicyclo[3.2.0]hepta-2-one (**45**). This bicyclic dichloroketone is protected with ethylene glycol and the ketal **46** is reacted with sodium in liquid ammonia to eliminate the chlorines to form a cyclobutene moiety in the unsaturated ketal **47**. Ketal **47** is then deprotected to form bicyclo[3.2.0]hept-6-en-2-one (**48**) which in turn is reacted with methyl benzenesulfinate.[109] The sulfinate is synthesized in a one pot reaction according to Equation 3.5.

$$(C_6H_5S)_2 + 3Pb(OAc)_4 + 4CH_3OH \longrightarrow 2C_6H_5S(O)OCH_3 + 3Pb(OAc)_2 + 4AcOH + 2AcOCH_3 \qquad [3.5]$$

This reaction yields an isomeric mixture of 3-(phenylsulfinyl)bicyclo[3.2.0]hept–6-en-2-ones (**50**). The phenylsulfinylenone **50** is then treated with *p*-toluenesulfonhydrazide to yield the corresponding phenylsulfinyl tosylhydrazone (**51**). This product is then refluxed in acetonitrile to introduce a double bond in the 5-membered ring yielding bicyclo[3.2.0]hepta-3,6-diene-2-tosylhydrazone (**52**). Reaction of sodium hydride with **52** yields the corresponding sodium salt (**53**). The sodium salt is thermolyzed in the PE spectrometer to yield 2-diazobicyclo[3.2.0]hepta-3,6-diene (**17**).

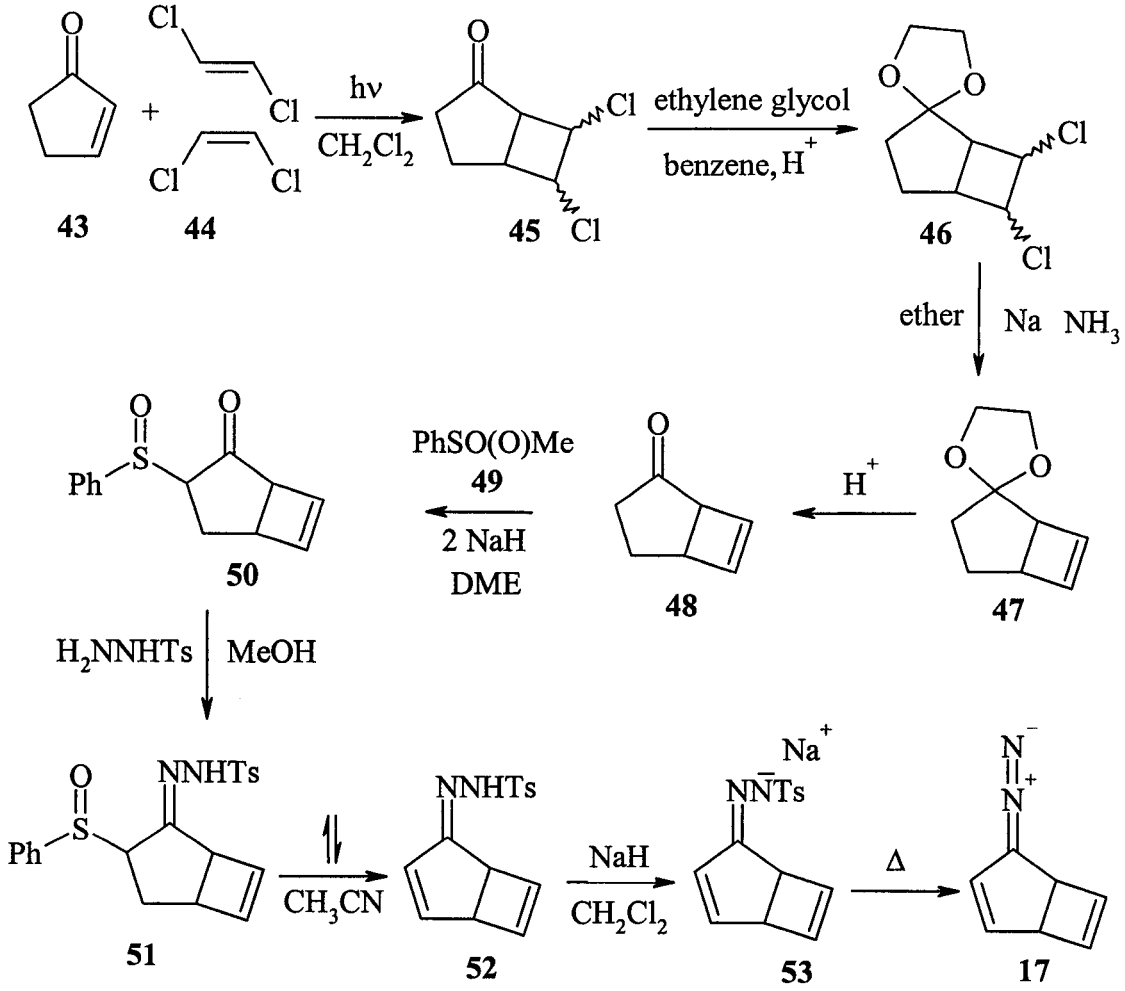

Scheme 5. Outline of the synthetic route to **17**.

3.3.5 Photoelectron spectroscopy and gas phase thermolysis of 17

Thermolysis of **53** in a sample tube attached to the probe of the spectrometer at 100 °C generates 2-diazobicyclo[3.2.0]hepta-3,6-diene.

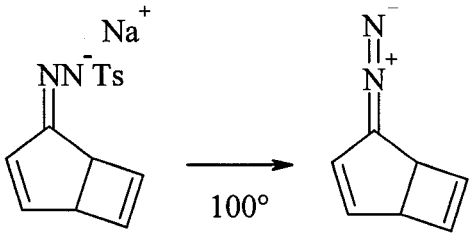

53 **17** [3.6]

The diazo compound exhibits three distinct ionization potential bands at 7.71 eV, 9.55 eV and 10.47 eV, as shown in Figure 20. The calculated Becke3LYP/6-31+G(d) vertical ionization potentials are 7.33 eV, 9.23 eV and 10.31 eV (Table 7).

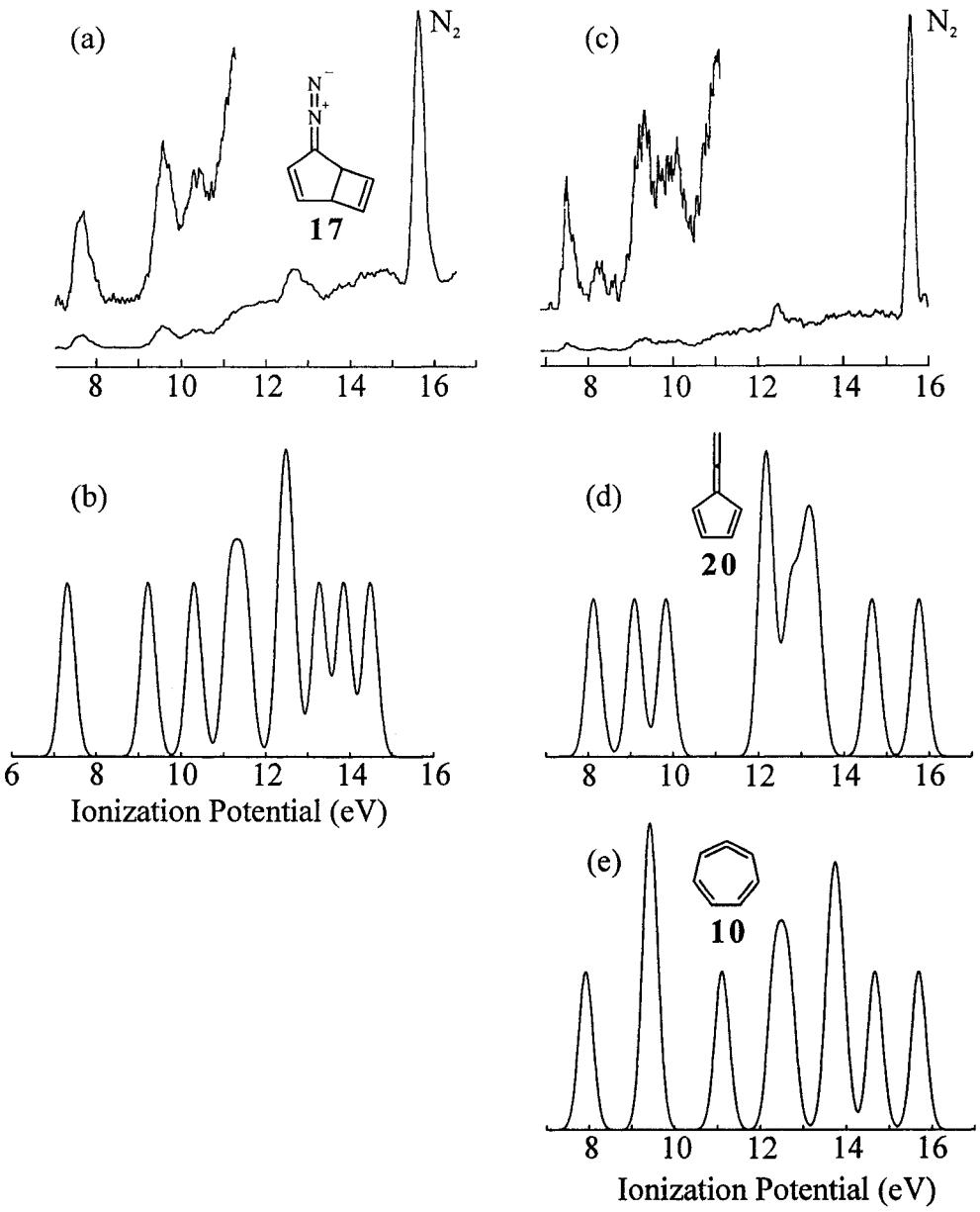

Figure 20. Experimental PE spectra of: (a) **17**, (c) upon thermolysis of **17**, and partial simulated PE spectra of: (b) **17**, (d) **20** and (e) **10**.

Table 7. Experimental, calculated (Becke3LYP/6-31+G(d)) and literature IPs of **17**, **20**, **10**, and spectrum obtained upon thermolysis of **17** (**PY**).

		Ionization Potential				
		eV				
17	Exp.	7.50		9.28	10.12	
	B3LYP	7.44		9.34	10.43	
PY	Exp.	7.54	8.30	9.40	10.16	
10	B3LYP	7.92		9.39	9.48	11.11
20	Lit.[108]		8.29	9.14	10.15	
	B3LYP		8.13	9.10	9.84	

The highest occupied molecular orbital (HOMO) is a π^- orbital with anti-bonding character between the double bonds of the cyclopentene ring and the diazo moiety. The HOMO-1 is a π-MO localized on the C=C double bond in the cyclobutene moiety. The third orbital (HOMO-2) has primarily π bonding character between the double bonds of the cyclopentene ring and the diazo group and is assigned as π^+.

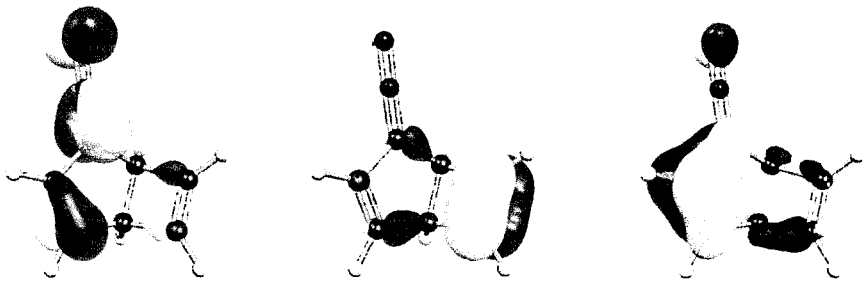

Figure 21. Becke3LYP molecular orbitals of **17** HOMO–HOMO-2.

The thermolysis of **17** with the use of the IR laser in the source chamber of the PE spectrometer was not a simple task. The initial introduction of the heat to the probe rendered no distinct PE spectrum. The spectrum appeared as a flat line with the only visible IP bands being those of nitrogen at 15.6 eV. Lowering the temperature at the tip of the probe by adjusting the power level of the tunable IR laser also proved to be ineffective. Thus, the laser was set at a power which allowed a slightly visible glow of light on the tip of the quartz nozzle in the source chamber of the spectrometer. This was an indication that heat was applied to the tip of the probe. A reasonable spectrum could not be obtained with this setting either. Therefore the temperature at the tip of the nozzle had to be lowered even further. To accomplish this task a beam chopper was employed. A mechanical aluminum rotor with five slits cut into it was placed in front of the laser beam. While the rotor is spinning the intensity of the laser beam is lowered, which in turn lowers the temperature at the tip of the probe. This proved to be an effective way of lowering the laser power and obtaining a thermolysis PE spectrum of **17** (Figure 20c).

The thermolysis spectrum (Figure 20c) shows IP bands with IP values similar to those of **17**. The first IP band in the thermolysis spectrum appears to have the same IP as the first IP of **17**. The second and third IP bands of **17** also appear to be visible in the thermolysis spectrum. There is, however, a difference in the bands appearing in the region between 9 and 10 eV. These two bands are not as well separated as they are in the spectrum of **17**. There also is a new ionization potential band appearing in the thermolysis spectrum at 8.3 eV that is not present in the spectrum of **17**. Although Becke3LYP/6-31+G(d) calculations predict the first IP of **10** to be at 7.92 eV it is

possible that the IP band at 8.3 eV in the thermolysis spectrum of **17** may correspond to the first IP of **10**. This possibility may be accounted for on the basis that Becke3LYP calculations tend to underestimate ionization potentials. This can be seen in the comparison of the first IP of styrene (**37**) which shows a difference between the observed and calculated value of 0.4 eV (Table 4). A difference of 0.25 eV between the experimental and calculated first IP of phenyldiazomethane (**41**) was observed as shown in Table 6. When comparing the calculated first IP of **10** (7.92 eV) with the IP band at 8.3 eV in the thermolysis spectrum of **17** a difference of 0.38 eV is observed. Therefore the possibility that the IP band at 8.3 eV could be due to 1,2,4,6-cycloheptatetraene (**10**) should not be ruled out entirely. It is also possible that the IP band in the region of 10 eV in the thermolysis spectrum of **17** is not part of the PE sepectrum of **10** but rather it is due to the presence of fulvenallene (**20**) in the thermolysis mixture.

It has been shown by Wentrup and coworkers that the thermolysis of phenyldiazomethane (**13**) generates fulvenallene (**20**).[38] Thus the thermolysis spectrum of **17** was compared to a literature PE spectrum of **20**. The PE spectrum of fulvenallene (**20**) reported by Schweig *et al* shows ionization potential bands at 8.29 eV, 9.14 eV, and 10.15 eV.[108] Thus the IP band in the thermolysis spectrum of **17** at 8.3 eV may correspond to **20**. The broad bands in the region of 9 and 10 eV must also incorporate the ionization potentials of fulvenallene. A complete subtraction of the PE spectrum of **17** from the thermolysis spectrum could not be accomplished without generating a negative baseline. However, the presence of the IP band at 7.5 eV in both the PE spectrum of **17** and the thermolysis spectrum suggests that the starting material is still present. A

complete thermolysis of **17** could not be accomplished. Increasing the temperature at the tip of the probe only degraded the quality of the spectrum and the only bands that were visible could be assigned to fulvenallene. Thus the spectrum of **10** could not be recorded.

There also exists another possible C_7H_6 isomer that could contribute to the PE spectrum of the thermolysis. It has been suggested by Wentrup that a bicyclic triene intermediate may be involved in the rearrangement of the C_7H_6 isomers as illustrated in their studies.[38] This isomer, bicyclo[3.2.0]hepta-1,3,6-triene (**18**) has not been isolated, [110,111,112] but its existence on the C_7H_6 potential energy surface has been inferred from the observation of its dimers.[113] Therefore a photoelectron spectroscopic investigation of this compound was undertaken.

3.3.6 Photoelectron spectroscopy of bicyclo[3.2.0]hepta-1,3,6-triene (18)

In order to investigate the C_7H_6 potential energy surface further, a photoelectron spectroscopic study of bicyclo[3.2.0]hepta-1,3,6-triene (**18**) was undertaken. It has been shown by other researchers that attempts to generate **18** in solution resulted in the formation of dimers.[110] Thus a suitable precursor for gas phase studies had to be synthesized. There are two possible precursors which have previously been used to generate **18**. The two precursors are *N,N*-dimethylbicyclo[3.2.0]hepta-3,6-diene-*N*-oxide (**54**) and the analogous methiodide salt (**55**). The *N*-oxide is suitable for gas phase

thermolysis studies and the methiodide salt may be used to generate the dimers in solution.

3.3.7 Synthesis of *N*-oxide 54 and methiodide salt 55

The *N*-oxide **54** was synthesized by reaction of hydrogen peroxide with *N,N*-dimethylbicyclo[3.2.0]hepta-3,6-dien-1-amine (**56**) in methanol. The amine **56** was synthesized in the following manner (eqn. 3.7).

Tropylium bromide (**57**) was synthesized using the procedure of Doering and Knox.[114,115] The bromination of cycloheptatriene (**58**) and subsequent thermolysis under vacuum at 70° C yields tropylium bromide (**57**). Reaction of **57** with dimethylamine gives *N,N*-dimethylcyclohepta-1,3,5-trien-7-amine (**59**). Photolysis of amine **59** with a medium pressure mercury arc lamp yields *N,N*-dimethylbicyclo[3.2.0]hepta-3,6-dien-1-amine (**56**). Treatment of **56** with hydrogen peroxide in methanol gives *N*-oxide (**54**). Alternatively, if amine **56** is treated with excess methyl iodide in ethanol, the methiodide salt (**55**) is obtained (eqn. 3.7).

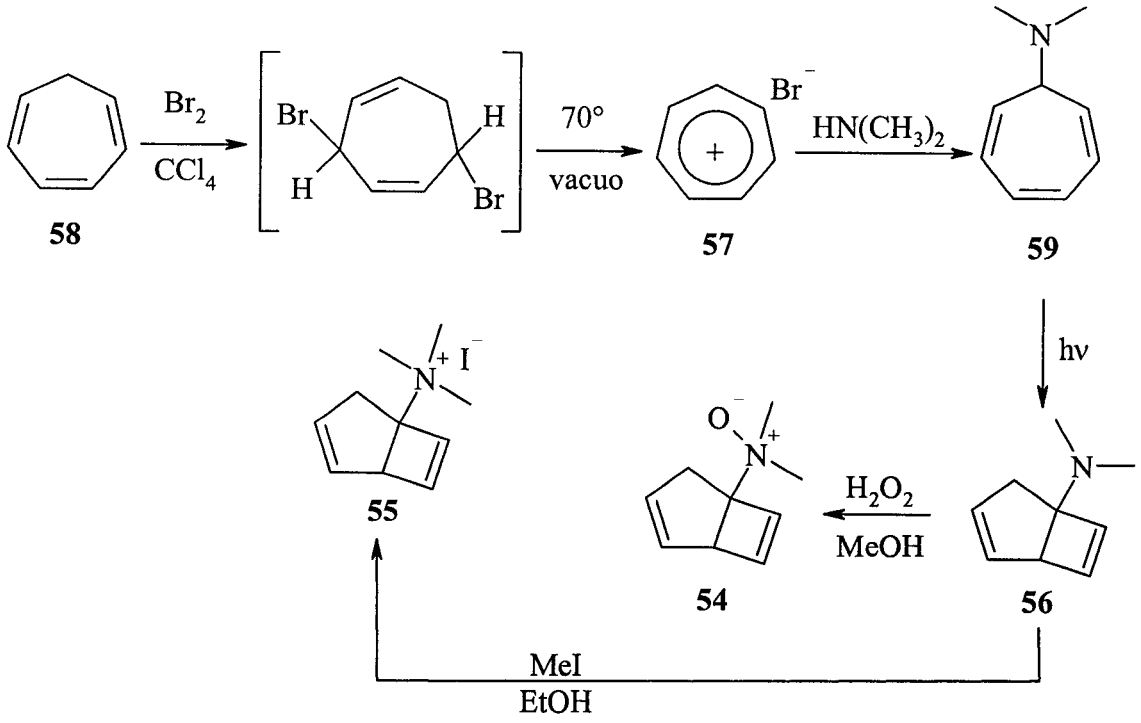
Br2
CCl4
Br
H
H
Br
70°
vacuo
Br
HN(CH3)2
N
58
57
59
hν
N
I
55
O
N
H2O2
MeOH
54
56
MeI
EtOH

[3.7]

3.3.8 Ionization potentials of bicyclo[3.2.0]hepta-1,3,6-diene (18)

The *N*-oxide **54** was thermolyzed in a sample tube attached to the probe of the photoelectron spectrometer at 120°C. The thermolysis spectrum consists of two main IP bands (Figure 22a). The first IP band is observed at 7.23 eV while a second very broad IP band is located between 8.5 and 10 eV. In the thermolysis of **54** two other products are generated in addition to triene **18**: dimethylhydroxyl amine (**60**) and two dimers of **18** (**61**) (Eqn. 3.8). [110]

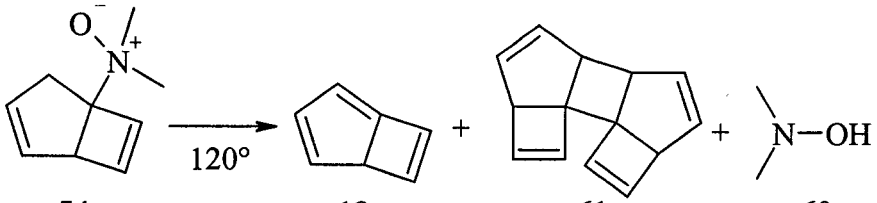

54 **18** **61** **60** [3.8]

In order to elucidate the electronic structure of **18** an authentic PE spectrum of the dimers **61** and dimethylhydroxylamine (**60**) was recorded (Figure 22b,c).

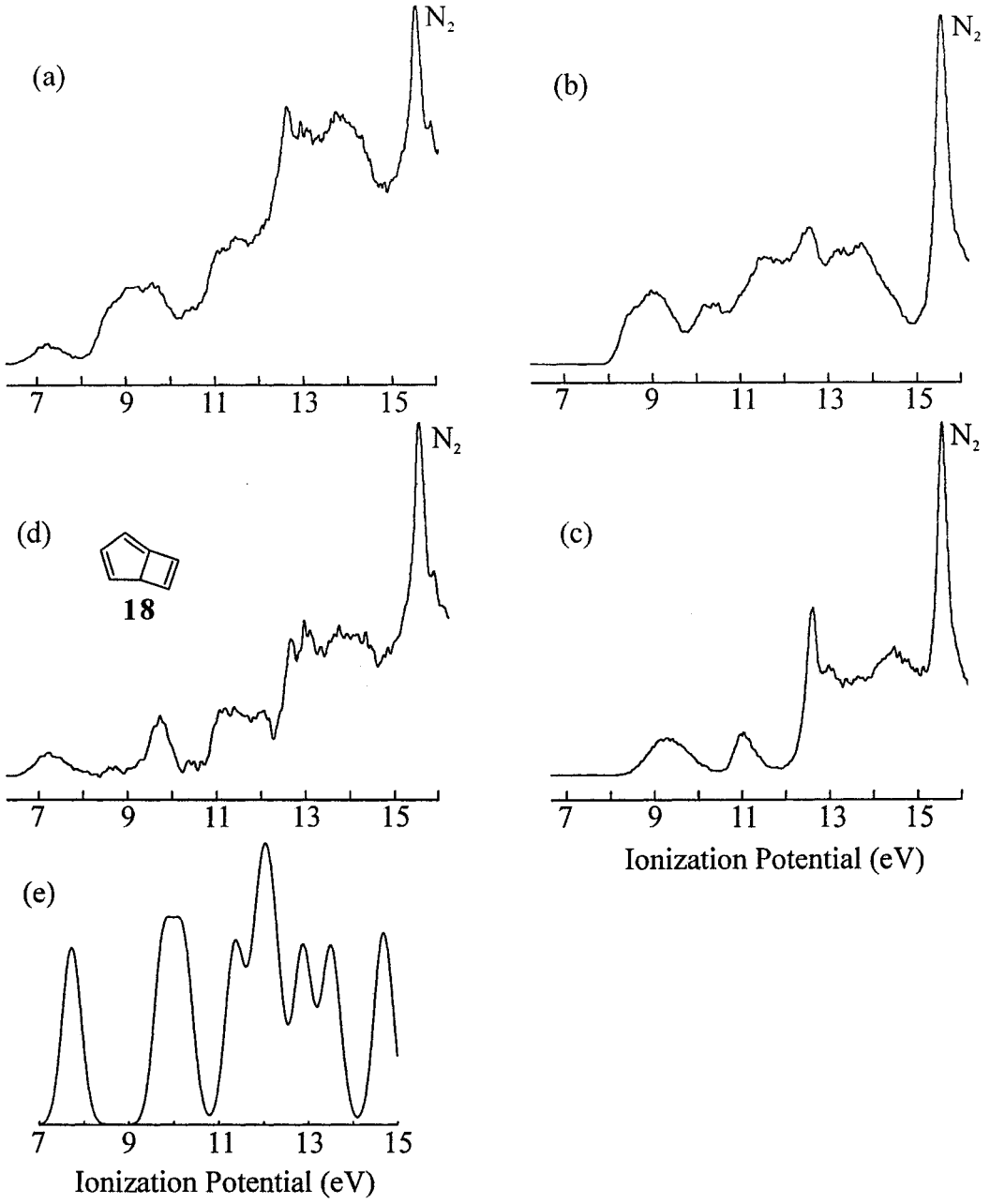

Figure 22. Experimental PE spectra of: (a) upon thermolysis of **54**, (b) **61**, (c) **60**, (d) after subtraction of PE spectra of **60** and **61** from the thermolysis spectrum, (e) simulated partial PE spectrum of **18**.

The dimers were generated as a 1:1 mixture from reaction of potassium *t*-butoxide with the methiodide salt **55**. The dimers are generated as a 50:50 mixture as reported by Bauld,[110] and we confirmed this fact by a GC/MS trace showing two peaks with identical intensity and area. Both peaks showed an $M^{+\bullet}$ ion with m/z 180. The NMR spectrum of the mixture of the two dimers agreed with the NMR data reported by Bauld and coworkers.[110] Two-dimensional NMR spectra (COSY, HSQC and HMBC) of the mixture were too complex to allow unambiguous assignment of the structures of the two dimers. Bauld and coworkers assigned their structures to **61a** and **61b** based on a two step mechanism that initially couples two strained doubly bonded bridge-head carbons, thus relieving strain.[110]

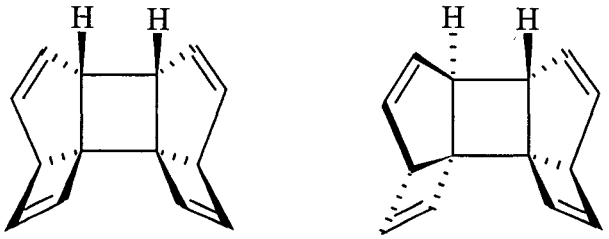

61a **61b**

Figure 23. Structures of dimers **61a** and **61b**.

The photoelectron spectrum of the dimers shows very broad IP bands in the regions from 8 to 9.5 eV and 10 and 11 eV. There is no IP band observed below 8 eV (Figure 22b). This suggests that the PE spectrum obtained upon pyrolysis of **54** contains IPs of the transient triene **18**. The photoelectron spectrum of dimethylhydroxyl amine (**60**) was recorded and revealed that there are also no IP bands below 8 eV in the spectrum of this compound (Figure 22c). The first broad ionization potential band of **60**

is observed in the region between 8.3 and 10.3 eV with vertical ionization potential at 9.3 eV. The second band is narrower than the first and its vertical ionization potential occurs at 11.06 eV. The PE spectra of **61** and **60** were subtracted from the PE spectrum obtained upon thermolysis of **54**, to yield a spectrum showing IP bands at 7.23 eV and at 9.76 eV (Figure 22d). The spectrum is in good agreement with the simulated spectrum of triene **18**. The orbitals which give rise to these ionizations are shown in Figure 24. The experimental and calculated IPs of **18**, **60**, and **61** are listed in Table 8.

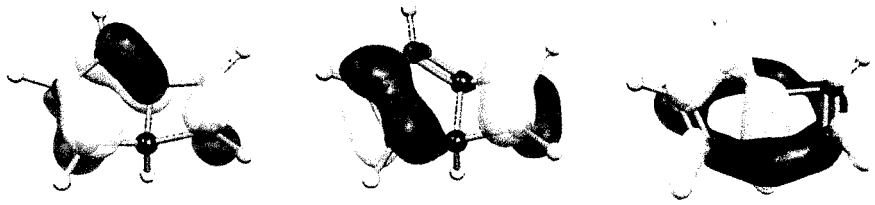

π^- (HOMO) π^+ (HOMO-1) π/σ (HOMO-2)

Figure 24. Becke3LYP molecular orbitals of **18**.

Table 8. Experimental, calculated (Becke3LYP/6-31+G(d)) IPs of **18**, **60**, **61**.

		IP		
		eV		
18	Exp.	7.23	9.76	
	B3LYP	7.73	9.78	10.22
60	Exp.		9.32	11.06
	Lit.[116, 117]		9.18	11.01
	B3LYP		9.1	10.66
61	Exp.		9.04	10.39

A thermolysis of the triene was attempted with the use of the IR laser but showed no differences in the PE spectrum compared to the spectrum obtained during thermolysis of *N*-oxide (**54**). The thermolysis was attempted at several laser power settings but resulted in no change in the PE spectrum. At a very high laser power the spectrum appeared as a base line. In all of these experiments, a heavy carbon deposit formed on the tip of the quartz nozzle. Such deposits reduce the efficiency of laser-induced thermolysis, and it is possible that this factor is responsible for our failure to induce thermal rearrangement of **18** to **20**, the calculated energy barrier for which is 35.9 kcal mol^{-1}.

An attempt was also made to synthesize *N,N*-dimethylcyclohepta-1,3,5-triene-7-amine oxide (**62**). This was done due to the availability of the precursor *N,N*-dimethylcyclohepta-1,3,5-trien-7-amine (**59**) and the possibility that the *N*-oxide of this amine might serve as a viable precursor of 1,2,4,6-cycloheptatetraene (**10**). The reaction of **59** with hydrogen peroxide did not produce the anticipated *N*-oxide (**62**), but rather dimethylformamide and benzene.

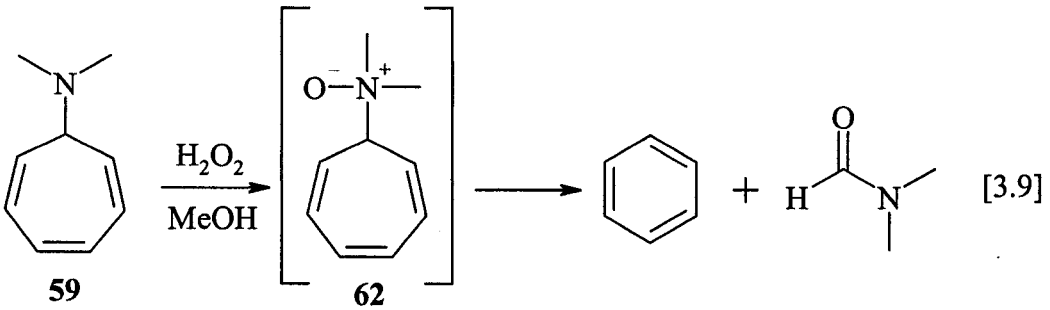

59 **62** [3.9]

It is possible that the *N*-oxide is generated initially, but undergoes dissociation to yield benzene and dimethylformamide through the norcaradiene type intermediate **63** (Eqn.

3.10). Our *ab initio* calculations have shown that the energy barrier for the formation of norcaradiene intermediate of the *N*-oxide is only 6.3 kcal mol^{-1}.

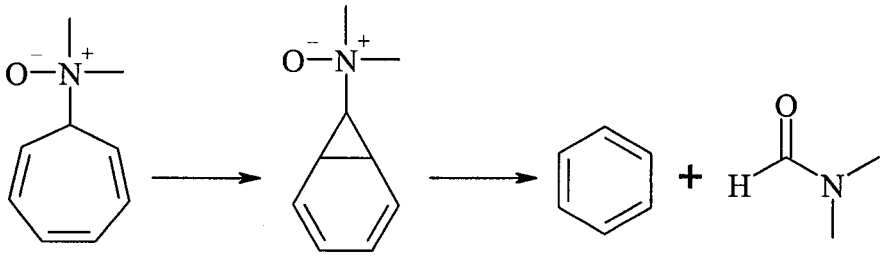

62 **63** [3.10]

3.3.9 The C_7H_6 potential energy surface

In the thermolysis study of **17** it was originally thought that this diazo compound extrudes nitrogen to generate carbene **64**. Chapman and Abelt reported that they did not observe carbene **64** spectrosocopically (ESR) upon thermolysis and photolysis of **17**.[35] The authors reported exclusive observation of **10** in the matrix-isolation IR experiments of **17** but no evidence was found for the formation of bicyclo[3.2.0]hepta-1,3,6-triene **18** (Eqn. 3.11).[35]

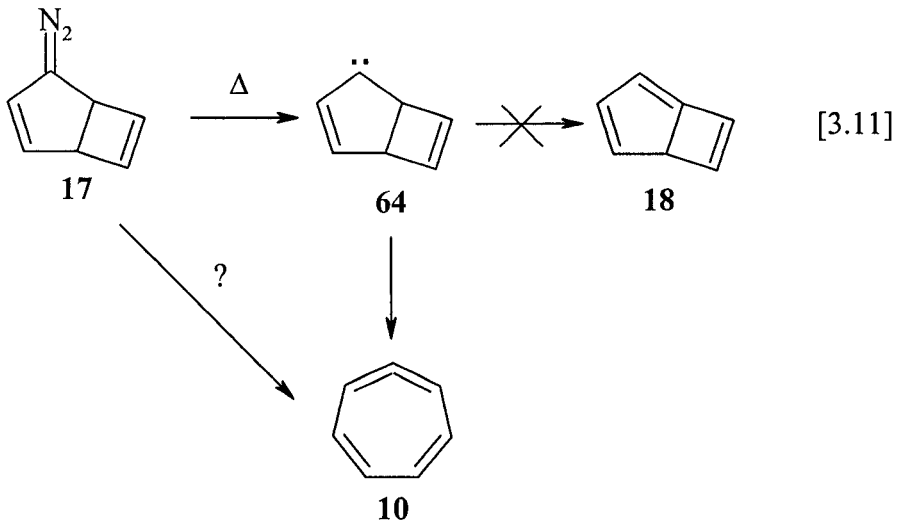

[3.11]

The authors also stated that their study could not answer whether generation of **10** from **17** occurs via carbene **64** or directly from the diazo compound **17**.

Therefore we have computationally investigated the possible paths that may generate **10** from **17**, employing the Becke3LYP/6-31+G(d) level of theory. The possible rearrangement of **17** has not been investigated computationally. A computational study of the possible rearrangements of carbene **64** at a high level of theory (CCSD(T), CASPT2N) has been reported by Patterson and McMahon,[33] while the C_7H_6 potential energy surface has been investigated computationally by Wong and Wentrup, also using high level of theory (G2).[31] Since it is possible that our thermolysis of **17** may have generated fulvenallene (**20**) we also investigated the possible C_7H_6 isomers and their rearrangements at the same level of theory as the rearrangement of **17** (Becke3LYP/6-31+G(d)). The results of our computational study were compared to the results previously reported[31,33] in order to establish whether there are significant discrepancies between Becke3LYP and the results of higher levels of theory.

Cycloheptatetraene (**10**) can be generated from **17** via a mechanism that first involves the cyclobutene ring-opening of **17** to yield 7-diazocyclohepta-1(E),3(Z),5(Z)-triene (**65**) followed by nitrogen extrusion to give **10** (Scheme 6). The Becke3LYP/6-31+G(d) total and relative energies of **17**, **65** and **TS4–TS6** are listed in Table 9.

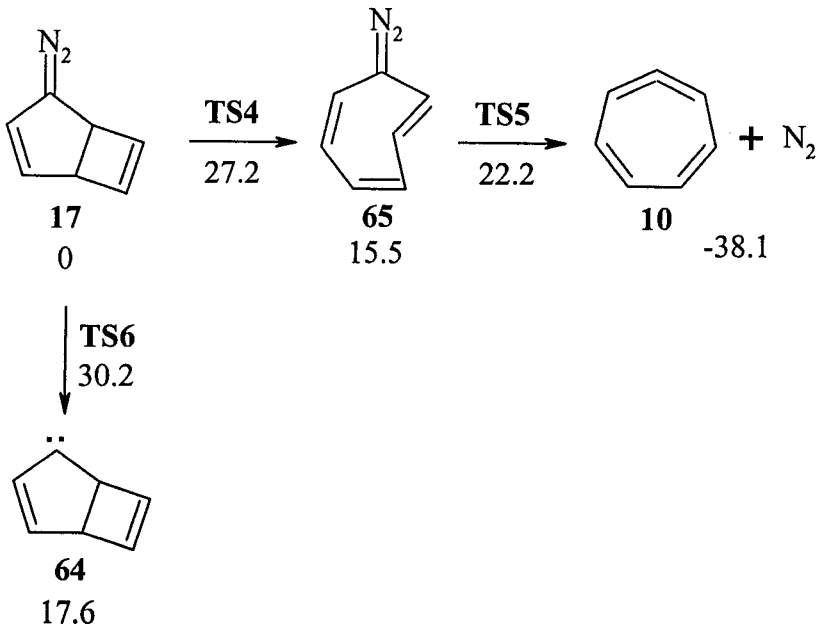

Scheme 6. Thermal rearrangement of **17**. Relative energies shown in kcal mol^{-1}.

Table 9. Becke3LYP/6-31+G(d) total, zero-point-vibrational-energy corrected and relative energies of **17**, **65**, **TS4–TS6**.

	Total Energy	ZPVE correction	Total Energy	Relative Energy
	(hartrees)	(hartrees)	ZPVE corrected	(kcal mol^{-1})
17	-379.728 491	0.113 650	-379.614 841	0.0
65	-379.702 669	0.112 562	-379.590 107	15.5
TS4	-379.681 900	0.110 326	-379.571 574	27.2
TS5	-379.688 724	0.109 236	-379.579 488	22.2
TS6	-379.676 488	0.109 724	-379.566 764	30.2

The transition state (**TS4**) for this rearrangement lies 27 kcal mol^{-1} higher in energy than **17**. The extrusion of nitrogen from **17** via **TS6** has a barrier of 32 kcal mol^{-1}. The difference in energy between the two processes may explain the failure to observe **64** experimentally in previous reports on the thermolysis and photolysis of **17**.[35] Nitrogen extrusion from **65** to generate **10** occurs with an extremely low barrier of 6.7 kcal mol^{-1} and **10** is 53.6 kcal mol^{-1} lower in energy than **65**. Thermal-correction calculations (described in Chapter 1.2.2) for the two processes, the ring-opening of **17** and the nitrogen extrusion from **17**, show no inversion of the energy barriers; the energy barrier for ring-opening was always found to be lower than the energy barrier for nitrogen extrusion as shown in Table 10. **TS4** is lower in energy than **TS6** at all investigated temperatures.

Table 10. Thermally corrected Becke3LYP/6-31+G(d) energy barriers for transformations **TS4**–**TS6**.

	Energy barrier (kcal mol^{-1})			
Temperature °C	**TS6**	**TS4**	**TS4** reverse	**TS5**
25	30.5	27.3	11.5	6.7
100	30.5	27.3	11.4	6.7
200	30.5	27.3	11.3	6.6
300	30.4	27.2	11.2	6.5
400	30.4	27.1	11.0	6.4
500	30.3	27.0	10.9	6.3
600	30.2	26.9	10.7	6.2
700	30.0	26.7	10.6	6.1
800	29.9	26.6	10.4	5.9
900	29.7	26.4	10.3	5.8
1000	29.6	26.2	10.1	5.6

Attempts to locate a transition state of a concerted process that would yield **10** from **17** were unsuccessful. Therefore our calculations indicate that **10** may be the result of a two-step process: a ring-opening of **17** followed by elimination of nitrogen.

It is shown in Eqn 3.11 that if carbene **64** is generated in the thermolysis of **17** it could undergo two possible rearrangements: one to yield bicyclo[3.2.0]hepta-1,3,6-triene (**18**), and one to give 1,2,4,6-cycloheptatetraene (**10**). The Becke3LYP/6-31+G(d) total and relative energies for the processes interconnecting possible C_7H_6 isomers are listed in Table 11. The interconnections of the C_7H_6 isomers are illustrated in Scheme 7.

Table 11. Becke3LYP/6-31+G(d) total, zero point vibratinal energy corrected and relative energies of the C_7H_6 isomers.

	Total Energy (hartrees)	ZPVE correction (hartrees)	Total Energy ZPVE corrected	Relative Energy (kcal mol^{-1})
10	-270.255 046	0.103 603	-270.151 443	0.0
11 (TS15)	-270.224 317	0.103 240	-270.121 077	19.1
13	-270.233 736	0.102 667	-270.131 069	12.8
18	-270.235 145	0.103 581	-270.131 564	12.5
20	-270.273 998	0.102 324	-270.171 674	-12.7
21	-270.229 567	0.102 826	-270.126 741	15.5
64	-270.164 324	0.101 768	-270.062 556	55.8
66	-270.231 767	0.100 559	-270.130 208	13.3
TS7	-270.156 188	0.100 388	-270.055 800	60.0
TS8	-270.120 420	0.097 658	-270.022 762	80.7
TS9	-270.177 816	0.100 680	-270.077 136	46.6
TS10	-270.171 156	0.096 829	-270.074 327	48.4
TS11	-270.187 897	0.099 877	-270.088 020	39.8
TS12	-270.175 501	0.099 428	-270.076 073	47.3
TS13	-270.208 121	0.101 609	-270.106 512	28.2
TS14	-270.226 389	0.101 693	-270.124 696	16.8
N_2	-109.529 779	0.005 592	-109.524 187	---

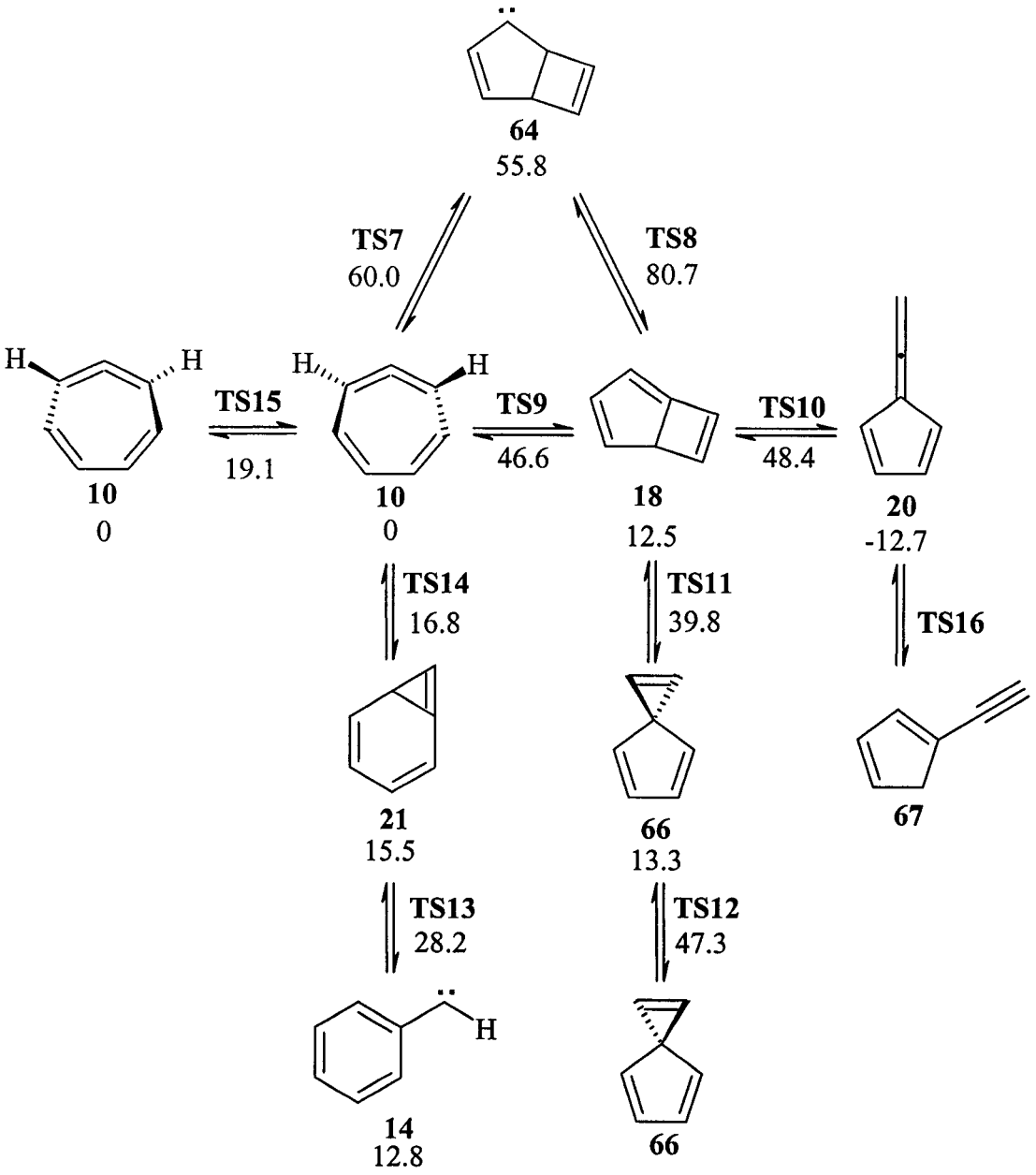

Scheme 7. Possible paths for the thermal rearrangements of **10**. Energy values in kcal mol^{-1}.

Transition state (**TS7**) for the ring-opening of **64** to **10** is only 4.2 kcal mol^{-1} above the energy of carbene **64**. This barrier is in good agreement with the previously reported barrier of 5 kcal mol^{-1} in a high-level calculation of Patterson and McMahon.[33] A much higher barrier of 24.9 kcal mol^{-1} was found for the hydrogen shift (**TS8**) that would generate **18** from **65**. This finding is also in agreement with the result of Patterson and McMahon who have reported this barrier to be 23 kcal mol^{-1}.[33] Therefore calculations indicate that triene **18** will not result directly form carbene **64**.

As shown in Scheme 7 the ring closure of **10** to **18** via transition state **TS9** has a barrier of 46.6 kcal mol^{-1}. Wong and Wentrup reported this barrier to be 55 kcal mol^{-1} at the G2 level of theory.[31] Patterson and McMahon report a value of 44 kcal mol^{-1}.[33] Although there is a difference of 9 kcal mol^{-1} between our result and the reported G2 barrier, it is clear in any case that the barrier is relatively large.

It is also illustrated in Scheme 7 that triene **18** may rearrange to fulvenallene (**20**) via transition state **TS10**. The reported calculations of Wong and Wentrup indicated that this process has a barrier of 51 kcal mol^{-1}.[31] Although the structure of **TS10** was reported, details as to the nature of this transition state were not presented, so it is unclear whether this transition state is that of a concerted process which would involve a concomitant hydrogen shift to give fulvenallene (**20**) or whether there should be another intermediate present which would then rearrange to **20** via a 1,2-hydrogen shift. Our attempts to locate an intermediate equilibrium structure between **18** and **20** were unsuccessful. A transition state structure was located with an energy that was 35.9 kcal mol^{-1} above that of **18**. Inspection of the vibrational mode of the imaginary frequency indicated that this

transition state may be assigned to **TS10**. This transition state has a carbenoid character and shows that the carbenoid center is in plane with the cyclopentadiene ring. Furthermore, the motion of this vibration clearly shows a hydrogen shift to form **20** (Figure 25). Also the carbenoid center shows movement toward the C2 in the cyclopentadiene ring, which confirms that ring opening of **18** occurs in concert with hydrogen shift to yield **20**.

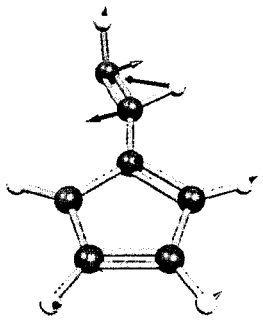

Figure 25. The Becke3LYP geometry of transition state **TS8**. The arrows indicating displacement vectors.

Although there is a difference of 15.1 kcal mol^{-1} between our value and that reported by Wong and Wentrup for this transition state, the structures are similar.

There also exists a transition state **TS11** which connects **18** and **66**. The energy of this transition state structure lies 27.3 kcal mol^{-1} above the energy of **18** which is in agreement with the barrier of 28.4 kcal mol^{-1} reported by Wong and Wentrup at the G2 level of theory.[31] A transition state **TS10** was found for the interconversion of two spiro compounds **66**. The barrier for this process was found to be 33.9 kcal mol^{-1} and is in good agreement with the G2 value of 39.4 kcal mol^{-1}. Therefore it can be seen from our

Becke3LYP and the reported G2 calculations that the rate limiting step in these interconverstions is the generation of **18** from **10**. After this energy barrier is overcome, which may be possible because **10** is generated as a "hot molecule" with a large amount of vibrational energy, the other processes on the C_7H_6 potential energy surface have lower barriers. Thus, it is possible that **18** can rearrange to **66** but since the reverse barrier for the conversion of **66** back to **18** is also low (26.5 kcal mol^{-1}), **18** can rearrange to **20** which has been confirmed by experiments presented in the literature as well as in the PES experiments presented in this thesis. The process of conversion of **20** to **67** which is illustrated in Scheme 7 to occur via transition state **TS16** is ruled out based on the very high energy barrier (80.5 kcal mol^{-1}) reported in the G2 calculations of Wong and Wentrup.[31]

3.3.10 Summary

The thermolysis of phenyldiazoethane has illustrated the utility of the UV photoelectron spectrometer interfaced with a CW CO_2 laser in generating and recording PE spectra of diazo compounds from tosylhydrazone sodium salts. It has also shown that the diazo compound can be successfully thermolyzed in the source chamber of the spectrometer and the PE spectrum of the pyrolysate recorded. The application of *ab initio* calculations to study the possible rearrangements of the intermediates was also confirmed.

A clear spectrum of 1,2,4,6-cycloheptatetraene (**10**) could not be acquired from the thermolysis of phenyldiazomethane (**13**) due to heavy carbonization of the tip of the quartz probe. The thermolysis spectrum was however different from that of the starting material indicating that a thermal reaction had taken place. The thermolysis spectrum could be attributed to a combination of products which may very well include ionization potentials of **10**.

Themolysis of 2-diazobicyclo[3.2.0]hepta-3,6-diene (**17**) has shown ionization potential bands which may be assigned to fulvenallene (**20**). This is in agreement with literature reports stating that **10** rearranges to **20** at high temperatures. The possibility of ionization potential bands from the bicyclo[3.2.0]hepta-1,3,6-triene (**18**) have been ruled out by the themolysis experiment of *N,N*-dimethylbicyclo[3.2.0]hepta-3,6-diene-*N*-oxide (**54**) which has revealed the first two ionization potential bands of this transient. The observation of the IP band at 7.23 eV in the thermolysis spectrum of **54** has illustrated that this transient bicycle[3.2.0]hepta-1,3,6-triene (**18**) is not observable in the thermolysis spectrum of 2-diazobicyclo[3.2.0]hepta-3,6-diene (**17**).

Ab initio calculations of the C_7H_6 potential energy surface have shown similar trends in energy barriers as those reported in the literature by Wong and Wentrup.[31] The computational results confirm the fact that the formation of the triene is the rate limiting step. Furthermore, computations have shown that the barrier for the formation of carbene **64** is higher than the energy barrier for the cyclobutene ring opening of **17**. Thus, **17** ring opens to yield a strained transient intermediate 7-diazocyclohepta-1(E),3(Z),5(Z)-triene (**65**) which readily extrudes nitrogen to give **10**. Generation of **10** is a high energy process

and **10** possessed excess energy (53.6 kcal mol^{-1}) which allows for it to rearrange to **20** as observed in the PES experiments.

Chapter 4

Thermal Ring Expansion of Bicyclic Cyclobutenes

4.1 Background

The electrocyclic ring opening of cyclobutene has been given a lot of attention, from both the photochemical and thermal point of view. The thermal ring opening of cyclobutene is a conrotatory process according to the Woodward-Hoffmann rules.[60,61] Depending on the nature of the substituents at the C3 and C4 position of the cyclobutene, different isomers of the open chain diene are formed. For example, if the substituents on C3 and C4 are *cis* in the cyclobutene, then the product of the ring opening would be an *E,Z* diene. If, on the other hand the substituents on the cyclobutene are *trans*, then the resulting diene is *E,E* or *Z,Z*. The formation of the *E,E* or *Z,Z* diene depends on the direction of rotation of the breaking σ bond of the cyclobutene. A theory of torquoselectivity has been put forth by Houk and coworkers to predict the preferred direction of rotation of the breaking sigma bond based on the nature of the substituents.[66] In general, electron donors preferentially rotate outward while electron acceptors

preferentially rotate inward. These investigations have been performed on monocyclic cyclobutenes which generate an open chain diene upon the thermal ring opening.

The introduction of a second ring, connected to the C3 and C4 positions of the cyclobutene, creates a structural constraint on the possible ways the cyclobutene moiety may undergo thermal ring expansion. The thermal ring-opening of bicyclo[3.2.0]hept-6-ene (**31**) yields *Z,Z*-cyclohepta-1,3-diene and is thought to involve an *E,Z* intermediate,[64] as shown in Eqn. 1.15 in Chapter 1.4.5. Study of the thermal ring-opening of bicyclic cyclobutenes with the use of our unique PE spectrometer may allow the identification of the possible transient *E,Z* diene generated in the thermolysis which will also allow identifying the preferred direction of rotation (torquoselectivity) of the breaking sigma bond in the transition state. This may be accomplished with the use of *ab initio* calculations. The molecules studied in this investigation are bicyclo[3.2.0]hept-6-en-2-one (**48**) and *N,N*-dimethylbicyclo[3.2.0]hepta-3,6-dien-1-amine (**56**). These compounds were chosen since they were made available in the course of the synthesis of the precursors for the compounds in the study described in the previous chapter. The two bicyclic compounds also have two different substituents. An electron withdrawing carbonyl group is present in **48** and an electron donating dimethylamino substituent is present in **56**. This investigation may also illustrate weather the *E,Z* or the *Z,E* or both may be detected and characterized.

4.2 Results and discussion

4.2.1 Synthesis of bicyclo[3.2.0]hept-6-en-2-one (48)

The ketone **48** was synthesized according to Scheme 5, shown Chapter 3.

4.2.2 Photoelectron spectroscopy and thermolysis of 48[118]

The Becke3LYP/6-31+G(d) total energies for optimized equilibrium geometries and radical cations single point calculations of compounds **48** and **68-70** are shown in Table 12. Calculated first vertical ionization potentials were obtained by the calculational method of previously reported in the literature.[9]

Table 12. Becke3LYP/6-31+G(d) total and relative energies of **48**, **68**, **69**, **70**, radical cations (RC) and transition states **Ta** and **Tb**.

	E_T (hartrees)	Relative Energy (kcal mol^{-1})	IP (eV)
48	-346.733 976	0.0	8.73
48–RC	-346.413 253	–	
Ta*	-346.683 808	31.5	
68	-346.705 326	18.0	8.65
68–RC	-346.387 364	–	
69	-346.695 937	23.9	8.75
69–RC	-346.374 501	–	
Tb*	-346.663 182	44.4	
70	-346.763 673	-18.6	8.84
70–RC	-346.438 660	–	

* **Ta** – transition state between **48** and **68**. **Tb** – transition state between **48** and **69**

The experimental and simulated PE spectra of ketone **48** are shown in Figure 26a,b. Although the calculated and experimental IP_vs differ slightly, the agreement in the features of the experimental and simulated spectra is excellent.

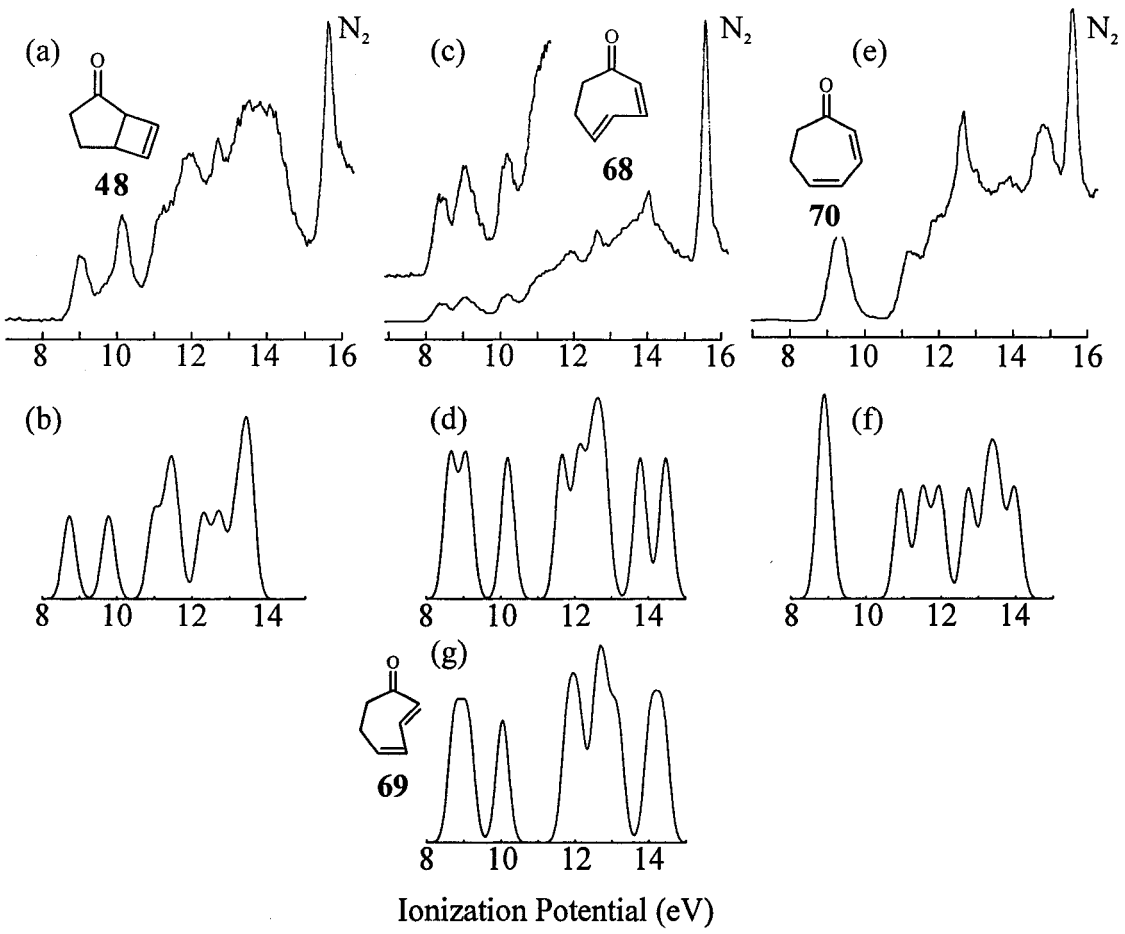

Figure 26. Experimental PE spectra of: (a) **48**, (c) pyrolysis of **48**, (e) **70** and simulated partial PE spectra of: (b) **48**, (d) **68**, (f) **70** and (g) **69**.

The pyrolysis of **48** in the PE spectrometer allowed us to record the PE spectrum of **68** as shown in Figure 26c. The first and the second IP bands of **68** at 8.98 and 10.14 eV are only 0.25 and 0.36 eV higher in energy then the predicted Becke3LYP values as shown in Table 13. This thermal reaction of **48** follows a conrotatory ring opening of the

cyclobutene moiety. A disrotatory ring opening, which is thermally forbidden, would generate cyclohepta-2(*Z*),4(*Z*)-dien-1-one (**70**). We synthesized an authentic sample of **69**[119] and recorded its PE spectrum for comparison as shown in Figure 26e.

Table 13. Experimental and calculated vertical IPs (eV) of **48**, **68**, **69**, and **70**.

48	Becke3LYP	IP_v	8.73	9.78	–
	Exp.	IP_v	8.98	10.14	–
68	Becke3LYP	IP_v	8.65	9.08	10.19
	Exp.	IP_v	8.36	9.06	10.18
69	Becke3LYP	IP_v	8.75	9.10	10.03
	Exp.	IP_v	–	–	–
70	Becke3LYP	IP_v	8.84	8.96	10.93
	Exp.	IP_v	9.36		11.16

Although one could expect two possible products from the conrotatory ring opening, namely dienones **68** or **69**, transition state calculations at Becke3LYP/6-31+G(d) indicate that **68** should be the product. A transition state, which would lead to **70**, could not be located. The simulated PE spectra of **68** and **70** are very distinct. The photoelectron spectrum of the pyrolysate can clearly be assigned to the cyclohepta-2(*Z*),4(*E*)-dien-1-one (**68**) based on the calculated Becke3LYP IPs (Table 13) as well as the simulated spectrum (Figure 26d).

The first and second bands in the PE spectrum of the transient dienone **68** are separated by 0.7 eV, while the second and third bands are separated by 1.1 eV. The three IP bands in **68** are observed at 8.36, 9.06, and 10.18 eV while the predicted Becke3LYP IPs are at 8.65, 9.08, and 10.19 eV. The difference between the first experimental and calculated IP_v is only 0.29 eV, while the second and third IP_vs show a difference of 0.02 and 0.01 eV, confirming an excellent correlation between experiment and theory. An excellent correlation is also observed between the experimental and simulated spectra of

70, which are shown in Figure 26e and 26f. A single large IP band is observed in the experimental spectrum as predicted in the simulated spectrum at 9 eV.

At the Becke3LYP/6-31+G(d) level the conrotatory ring opening of **48** has a barrier of 31.5 kcal $mole^{-1}$. The transition state was confirmed by a frequency calculation, which had one negative eigenvalue with a single negative frequency. Visualization of this vibrational mode showed that the newly forming double bond at position C4 in the product is the *trans* double bond. This thermal reaction, in principle, could lead to two different products, where both would be the result of a conrotatory ring opening. In one case, there is a transition state that leads to **68**. The transition state that would link **48** and **69** was also found at the Becke3LYP/6-31+G(d) level of theory with the barrier being 44.4 kcal $mole^{-1}$. Therefore it is clear that the PE spectrum observed upon the pyrolysis of **48** is that of **68**. The computational evidence shows that it is unlikely that **69** is generated in the thermal rearrangement of **48**. Experimental and computational evidence shows that **70** is not generated in the rearrangement of **48**. The difference of 12.9 kcal $mole^{-1}$ in the activation energy between the two processes clearly indicates that the rearrangement of **48** to **68** is favored. The calculations also predict that **68** is 5.9 kcal mol^{-1} more stable thermodynamically than **69**. The calculated total and relative energies of **48**, and **68–70** , radical cations (RC) and transition states **TSa** and **TSb** are shown in Table 12. The possible rearrangement of **48** is illustrated in Scheme 8.

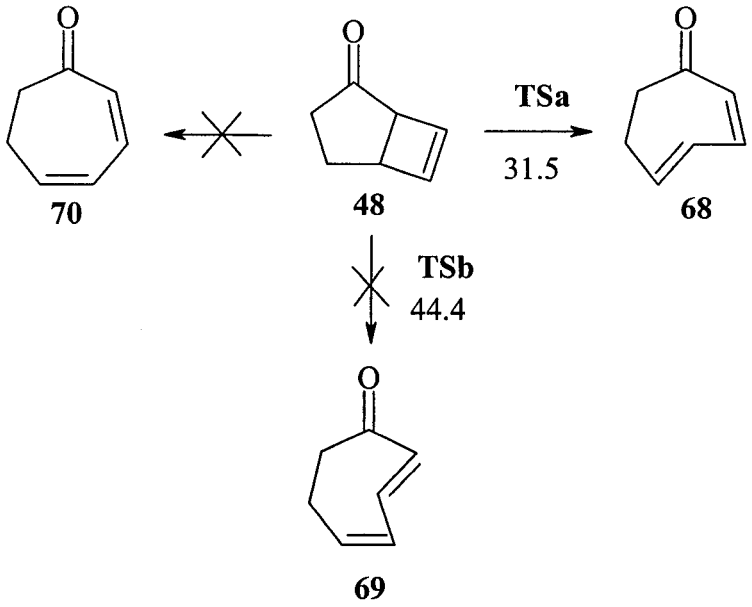

Scheme 8. Thermal rearrangement of **48**.

Our pyrolysis experiments on **48** have shown that this bicyclic enone undergoes a thermal ring opening that obeys the Woodward-Hoffmann rules and follows the conrotatory path. This is the first report of the transient dienone **68** and its photoelectron spectrum. That the pyrolysate was not **70** was confirmed by recording an authentic PE spectrum of **70**. This is also the first report of the PE spectrum of this compound. The possibility of **69** as the product of the pyrolysis was eliminated based on transition state calculations, which have shown that the transition state that links **48** and **69** is 12.9 kcal mol^{-1} higher in energy then the transition state linking **48** and **68**. Therefore bicyclo[3.2.0]hept-6-en-2-one (**48**),[120,121] when pyrolysed, undergoes a ring opening to the transient dienone, cyclohepta-2(*Z*),4(*E*)-dien-1-one (**68**), and not **69** or **70**.

4.2.3 Synthesis of *N,N*-dimethylbicyclo[3.2.0]hepta-3,6-dien-1-amine (56)

The amine **56** was synthesized according to the procedure described in Chapter 3.3.7 and illustrated in Equation 3.7.

4.2.4 Thermolysis and PE spectroscopy of *N,N*-dimethybicyclo[3.2.0]hepta-3,6-dien-1-amine (56)

The total energies and predicted first vertical ionization potential of **56** is shown in Table 14.

Table 14. Total energies and predicted first vertical ionization potentials of **56, 71–73.**

	Number of electrons	Becke3LYP/6-31+G(d)	
		E_T (hartrees)	IP_v (eV)
56	*N*	-405.449 623	7.71
	N–1	-405.166 255	
71	*N*	-405.437 626	6.52
	N–1	-405.198 103	
73	*N*	-405.416 460	7.19
	N–1	-405.152 349	
72	*N*	-405.498 283	6.94
	N–1	-405.243 082	

The photoelectron spectrum of **56** shows two distinct, broad ionization potential (IP) bands with vertical ionization potentials at 8.0 eV and 9.1 eV as shown in Figure 27a. This is the first report of the PE spectrum of this compound.

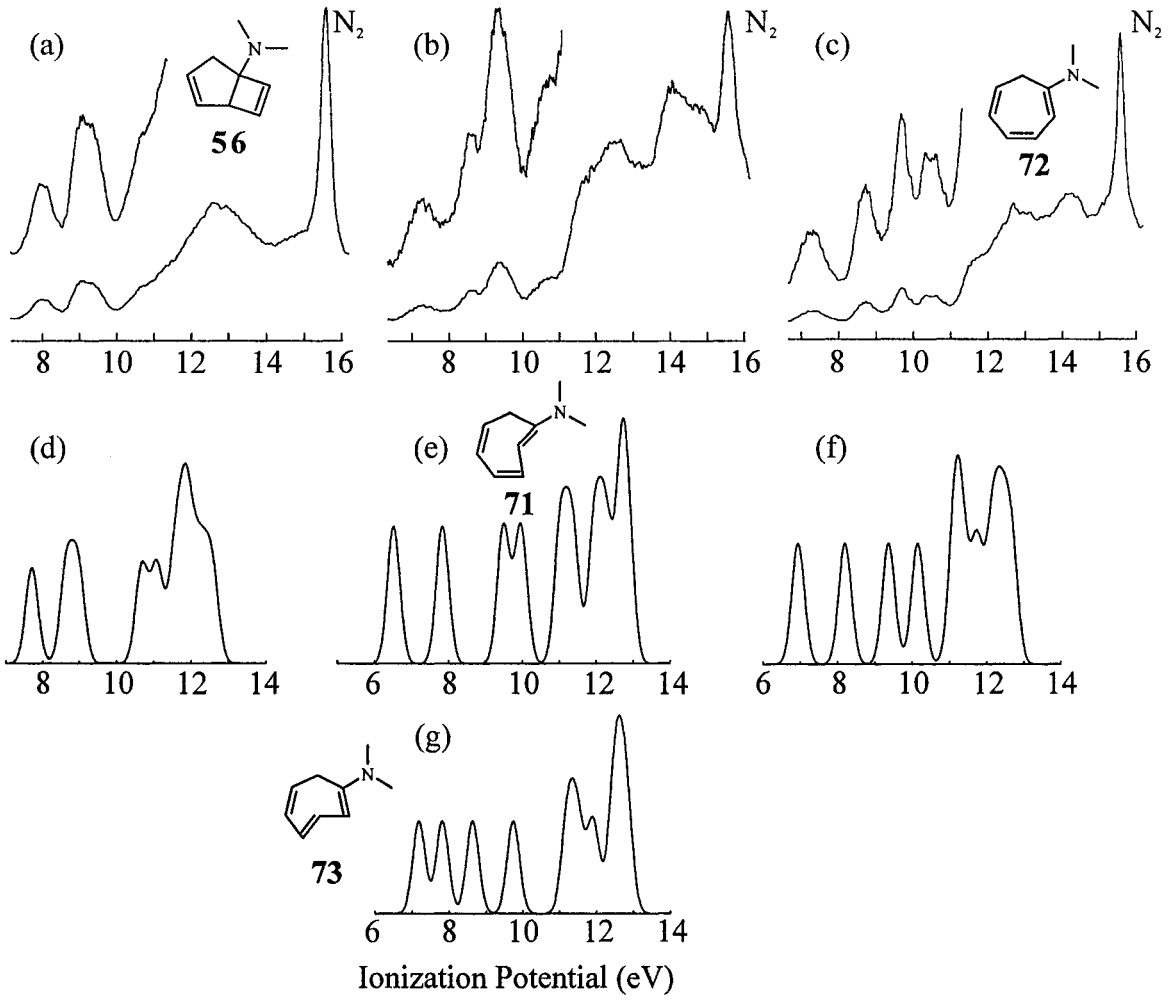

Figure 27. Experimental PE spectra of: (a) **56**, (b) pyrolysate of **56**, (c) **72**, and simulated partial PE spectra of (d) **56**, (e) **71**, (f) **72** and (g) **73**.

The first IP arises from the ionization from the highest occupied molecular orbital (HOMO) which is mainly the lone pair of nitrogen with a contribution from the bridging σ bond and is illustrated as $n_N(\sigma)$ in Figure 28. The experimental and calculated IPs are listed in Table 15. The predicted Becke first IP is lower than the experimentally observed IP by 0.29 eV. A similar difference between the predicted and experimental IP is observed in the second band. This broad band is an overlap of two IPs. The predicted IPs occur at 8.65 eV and 8.97 eV. These vertical ionization potentials correspond to the ionizations from the HOMO-1 and HOMO-2 which both have π character (Figure 28). Taking the average between these two calculated IPs and comparing this value to the observed IP yields a difference of 0.29 eV.

Table 15. Experimental and calculated B3LYP/6-31+G(d) IPs of **56, 71–73.**

		Ionization Potential (eV)			
56	Exp.	8.0	9.1		---
	B3LYP	7.71	8.65	8.97	10.68
PY[a]	Exp.	7.3	8.7	9.4	10.4
71	Exp.	---	---	---	---
	B3LYP	6.52	7.84	9.49	9.96
73	Exp.	---	---	---	---
	B3LYP	7.19	7.82	8.64	9.74
72	Exp.	7.3	8.7	9.7	10.4
	B3LYP	6.94	8.20	9.37	10.15

[a] Obtained upon thermolysis of **56**

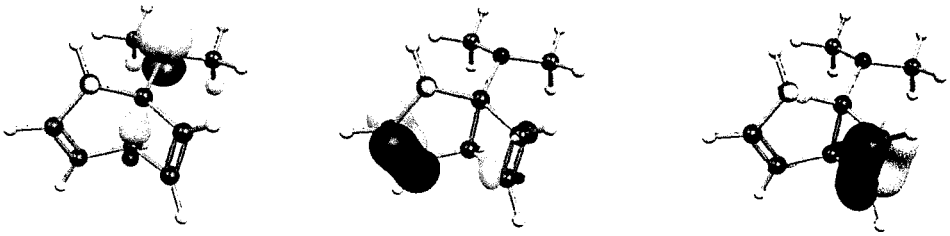

$n_N(\sigma)$ (HOMO) π (HOMO-1) π (HOMO-2)

Figure 28. Becke3LYP molecular orbitals of **56**.

The simulated PE spectrum of **56** (Figure 27d) correlates well with the experimental spectrum (Figure 27a). The simulation shows two broad bands which are similar in shape and intensity to the broad IP bands observed experimentally. Upon thermolysis of **56** the PE spectrum undergoes a complete change. A new broad IP band is now visible at 7.3 eV. A second broad band now appears at 8.7 eV, and the third and fourth IP bands appear at 9.4 and 10.4 eV respectively (Figure 27b). The calculated first ionization potential of **71** is predicted to be 6.52 eV which is not seen in the PE spectrum obtained upon the pyrolysis **56** when the spectrum was scanned between 6–16 eV. The low IP is expected because the HOMO is mainly localized on the *trans* double bond which reduces the conjugation of the double bonds in the cycloheptatriene ring (Figure 29). A comparison of calculated first IP's and total energies and energies of the radical cations are shown in Table 14. The difference between the calculated first IP of **71** and the first experimentally observed IP of the pyrolysate is 0.78 eV. Similarly, the difference between the second computed IP and the second experimental IP is 0.86 eV. These differences between the theoretical and experimental ionization potential are too large to allow for the assignment of the pyrolysis spectrum to **71**.

We have also synthesized an authentic sample of *N,N*-dimethylcyclohepta-1(*Z*),3(*Z*),5(*Z*)-trien-1-amine (**72**) according to the procedure of Ter Borg[122], and recorded its spectrum for comparison (Figure 27c). It is apparent that the PE spectra of the pyrolysate and **72** show significant similarity. The PE spectrum of **72** shows four distinct IP bands at 7.3 eV, 8.7 eV, 9.7 eV and 10.4 eV. The differences between the experimental and calculated IPs are 0.36 eV, 0.50 eV, 0.33 eV and 0.25 eV. A simulation of the PE spectrum of **72**, correlates very well with the experimental observation showing four distinct IP bands (Figure 27f).

The IPs of **72** may be assigned to the Becke MOs as shown in Figure 29. The four IPs correspond to the orbitals HOMO–HOMO-3. The first MO has antibonding character between the nitrogen lone pair and the π of the adjecent C1–C2 double bond and is denoted as $n_N\pi^-$. HOMO-1, which is denoted as $n_N\pi$, also exhibits orbital mixing between the nitrogen lone pair and the π system of the cycloheptatriene. In HOMO-3 the nitrogen lone pair mix with the adjacent double bond with a bonding character and it is shown as $n_N\pi^+$ in Figure 29. The fourth MO (HOMO-3) has a π bonding character with all three double bonds in the cycloheptatriene ring and no contribution from the nitrogen of the dimethylamino substituent. Figure 29 also shows a comparison between the MOs of **71** and **72** and their ionization potentials. The HOMO of **71** is also a $n_N\pi^-$ MO but with a considerably larger π orbital coefficient on the strained trans double bond than is observed in the first MO of **72**. HOMO-1 of **71** has π rather than $n_N\pi$ character as it is observed in **72** thus exhibits no orbital mixing between the nitrogen lone pair and the cycloheptatriene ring. HOMO-2 of **71** also has $n_N\pi^+$ character as it is seen in **72**, but with

the twisted strained double bond in **71**, the bonding orbital coefficients are localized around the C1-N bond, whereas in **72** the bonding orbital coefficients in HOMO-2 incorporate N–C1–C2. Lastly, HOMO-3 in **71** has bonding π character between C3–C4–C5–C6 and there is no contribution from the *trans* double bond in this MO. In contrast, HOMO-3 of **72** includes all three double bonds (Figure 29).

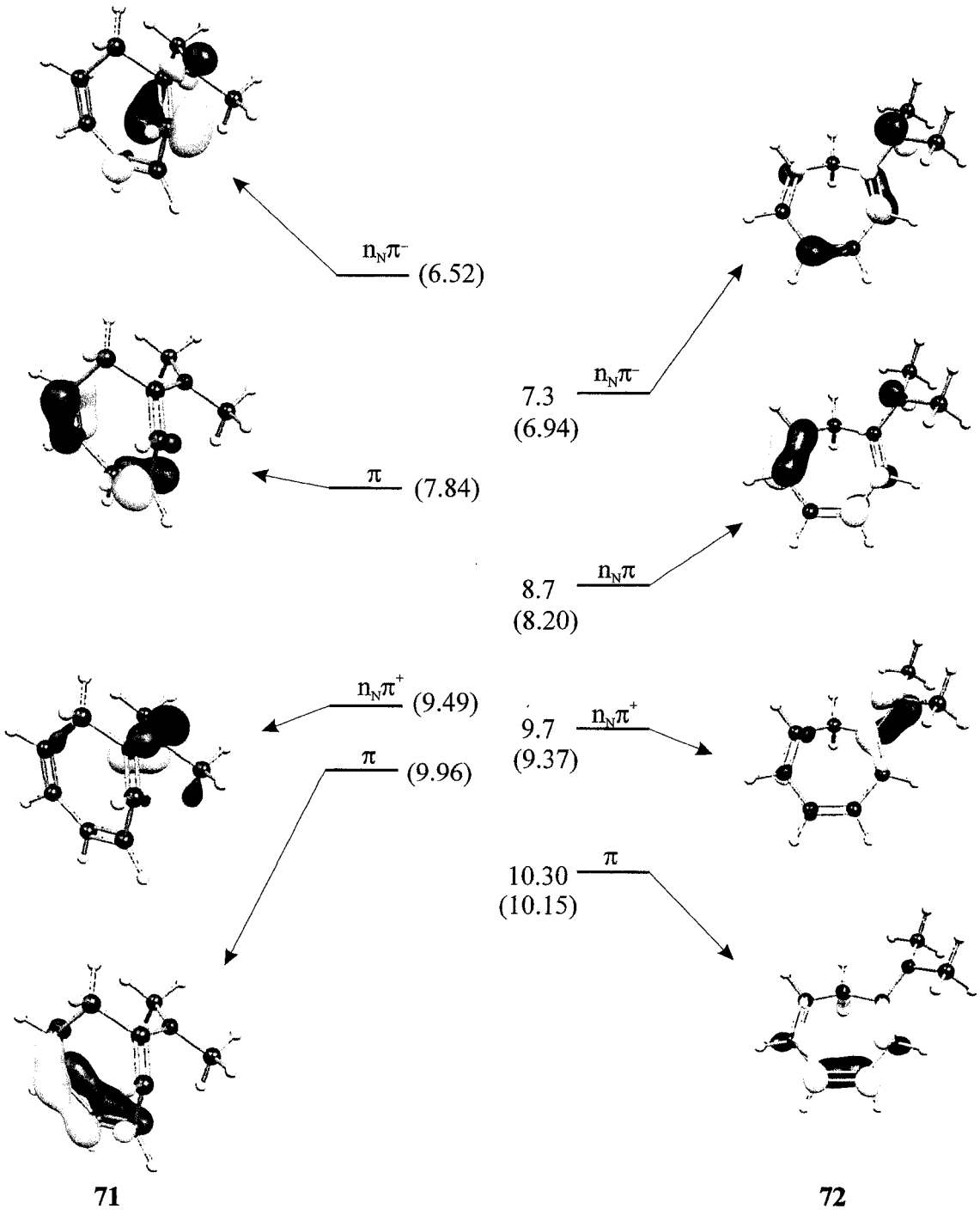

Figure 29. Becke3LYP MOs (HOMO–HOMO-3) for **71** and **72** with assignment of ionization potentials. Values in brackets are the calculated IPs.

The broad band observed in the thermolysis spectrum of **56** at 9.4 eV does correspond to the third IP band of **72**. A spectrum obtained from the pyrolysis of *N,N*-dimethylcyclohepta-1,3,5-trien-7-amine (**59**) also exhibits broadened third IP band (Figure 30); **59** yields **72** via a 1,5-hydrogen shift.[122]

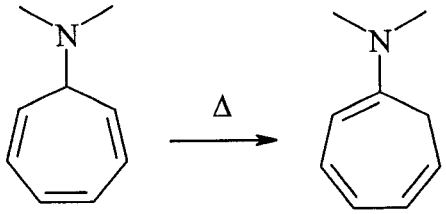

59 **72** [4.1]

The thermolysis PE spectra of **72** and **59** show significant similarity and are shown in Figure 30. Calculations show that *N,N*-dimethylcyclohepta-1,3,5-trien-1-amine (**72**) can exist in two conformations. One, where the lone pair of the nitrogen of the dimethylamino group points in a direction opposite to the C7 methylene group (Figure 31, **72a**), and one where the dimethylamino lone pair points in the same direction as the C7 methylene group (Figure 31, **72b**). The B3LYP energy barrier for the rotation of the dimethylamino group was found to be 8.3 kcal mol^{-1}. Similarly, heating **72** under the pyrolysis conditions yields a spectrum with a broadened third IP band. The predicted first four B3LYP IPs of **72a** are: 6.87 eV, 8.31 eV, 9.47 eV, 10.21 eV. The predicted first four B3LYP IPs of **72b** are: 6.94 eV, 8.21 eV, 9.38, eV, 10.16 eV; the rotation of the dimethylamino group has the largest impact on the third IP band. The calculations predict that the second and third IP bands are affected by the rotation of the dimethylamino group which seems to be in accord with experiment.

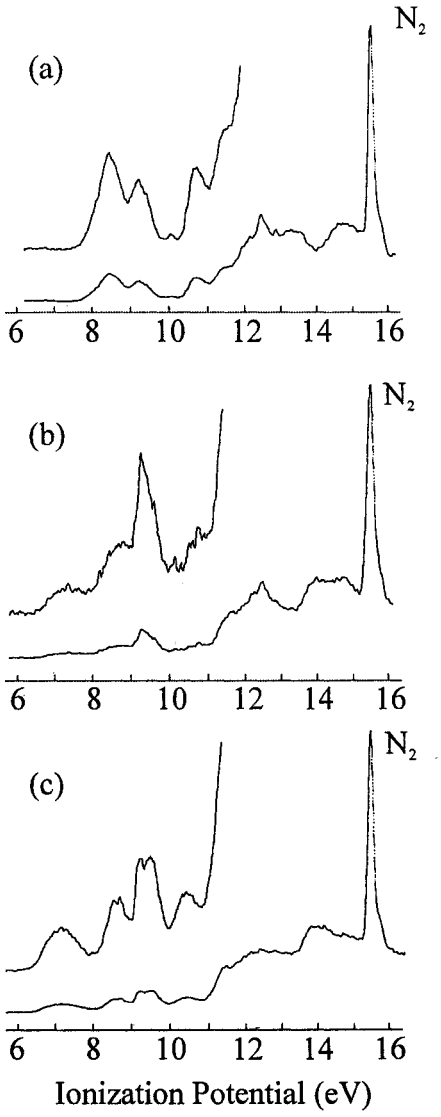

Figure 30. PE spectra of: (a) **59**, (b) thermolysis of **59** and (c) thermolysis of **72**.

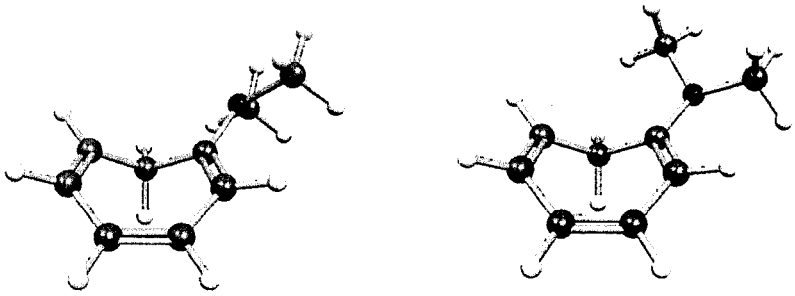

72a **72b**

Figure 31. Becke3LYP equilibrium geometries of rotational isomers **72a** and **72b**.

The isomerization of **56** to **72** was confirmed by an NMR experiment. An NMR spectrum of **56** in $CDCl_3$ was recorded and the sample was allowed to stand at room temperature (25°C) in the dark for 24 hours. Another NMR spectrum was then recorded showing the appearance of signals with resonances corresponding to **72**. Leaving the sample at room temperature for five days shows the decrease in the intensity of the signals from **56** and increase in intensity of the signals of **72** in the ration of 1:1. The NMR spectra were compared to the NMR spectrum of authentic **72** confirming that the new signals are those of **72**.

4.2.5 Computational investigation of the thermal rearrangement of 56

The Becke3LYP/6-31+G(d) total, zero-point-energy corrected and relative energies of **56**, **71-77** and the transition states are shown in Table 16.

Table 16. Total, ZPVE correction and relative energies (ZPVE corrected).

	Total Energy B3LYP/6-31+G(d)	ZPVE correction B3LYP/6-31+G(d)	Relative Energy (kcal mol^{-1})
56	-405.449 623	0.200 566	0.0
71	-405.437 626	0.200 423	7.4
73	-405.416 460	0.199 689	20.3
72	-405.498 283	0.201 878	-29.7
TSa	-405.413 277	0.198 522	21.5
TSb	-405.400 939	0.197 151	28.4
TSc	-405.428 237	0.199 062	5.0*
74	-212.572 560	0.125 833	---
75	-271.457 492	0.126 879	0.0
76	-271.444 528	0.125 863	7.5
77	-233.410 529	0.118 863	---
77a	-233.395 029	0.118 197	2.9
77b	-233.400 300	0.118 851	0.0

* Energy barrier for the isomerization of **71** to **72** with respect to **71**.

The observation that thermolysis of **56** gives a spectrum that can be assigned to **72** would suggest that the thermal electrocyclic reaction follows the forbidden disrotatory path. A transition state calculation on the ring opening of **56** to yield **71** (**TSa**) indicates that the energy barrier for this process is 21.5 kcal mol^{-1}. The computed, zero-point-energy corrected barrier (**TSb**) for the ring opening to **73** is 28.4 kcal mol^{-1}. The

forbidden disrotatory transition state that would directly link **56** and **72** could not be located. Since **71** was not observed upon the thermolysis of **56** we located the transition state for the isomerisation of the *trans* double bond in **71** to the cis isomer. This transition state (**TSc**) lies only 5.0 kcal mol^{-1} above the energy of **73**. The possible rearrangement of **56** is illustrated in Scheme 9.

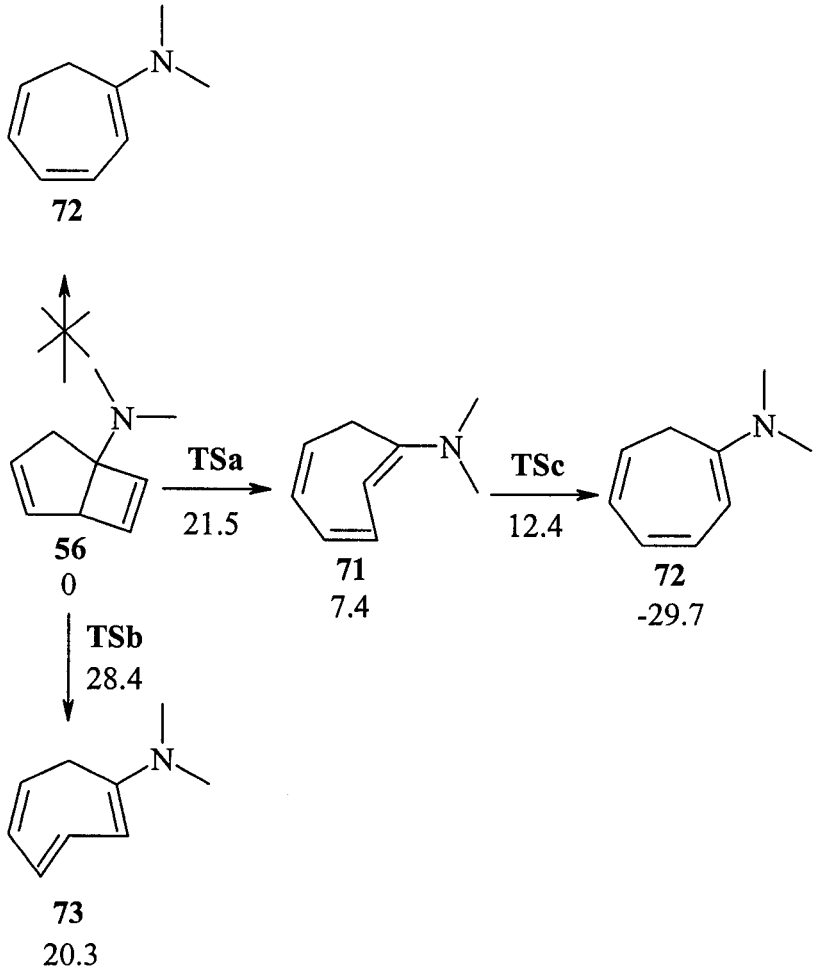

Scheme 9. The thermal rearrangement of **56**. Relative energies in kcal mol^{-1}.

The strained geometry of **71** allows for a resonance interaction between the lone pair of nitrogen of the dimethylamino group and the *trans* C1–C2 double bond in the cycloheptatriene ring. In the case of **56**, the dimethylamino group is pyramidalized with a dihedral angle of 28.2° between C1–C8–C9–N of the dimethylamine. In the case of **71** the dimethylamino group is pyramidalized with a dihedral angle of only 9.3°. This planarization allows for delocalization of the electrons from nitrogen over the π-bond of the adjacent *trans* C1-C2 double bond, which lowers the barrier making it possible for this *trans* double bond to isomerize to the *cis* conformation. The driving force for the process is the release of strain energy of 37.1 kcal mol^{-1} which generates **72** with all *cis* double bonds, allowing for a complete conjugation of the cyclic π system, as seen in HOMO-3 of **72** and not in **71** (Figure 29). Triene **72** is 29.7 kcal mol^{-1} lower in energy than **56** and 37.1 kcal mol^{-1} lower in energy than **71**. Therefore **56** initially undergoes a thermal conrotatory ring opening to yield **71**, followed by isomerization of the *trans* double bond in **71** to the *cis* double bond to yield **72**, as shown by *ab initio* calculations. The total and relative energies of the four compounds and the transition states are listed in Table 16.

According to the principal of torquoselectivity, electron donors preferentially favor the formation of a *trans* double bond to which the electron donating group is attached while electron acceptors yield a *cis* double bond when both substituents are in the *cis* position on the starting cyclobutene. Thus the electron donating group rotates outward upon breaking of the sigma bond in the cyclobutene moiety, while an electron acceptor substituent rotates inward.[66] In the case of the conrotatory ring opening in **56** we

acceptor substituent rotates inward.[66] In the case of the conrotatory ring opening in **56** we found that the *inward – outward* rotation terminology does not apply in the same way as described by Houk.[66] The constrained geometry of the bicyclic system does not allow for the rotation of the substituents at the bridgehead carbons of the breaking σ bond. The bridgehead carbons C1 and C4 move away from each other in the transition state as shown by the displacement vectors illustrated in Figure 32c, while the substituent undergoes planarization through the movement of the C1–N bond. The dimethylamino group shows marginal movement inward rather that outward, which is contrary to the theoretical predictions that donors preferentially rotate outward.

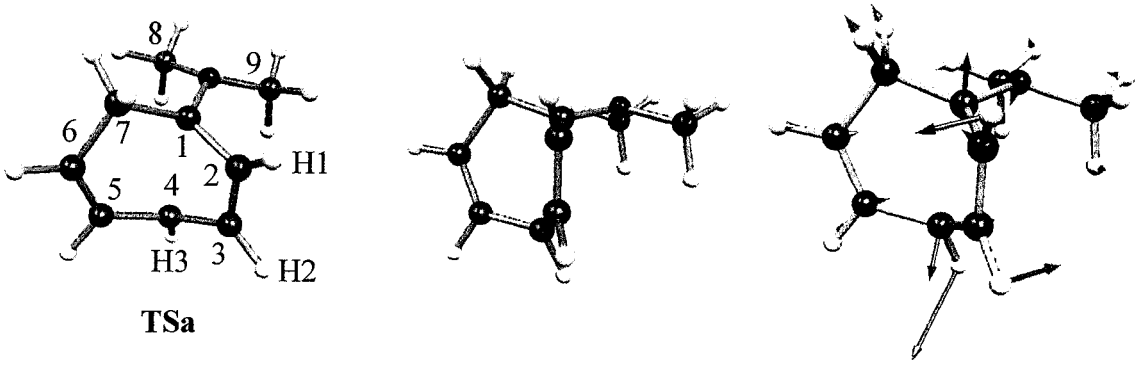

Figure 32. Becke3LYP molecular geometries of **TSa**: (a) front view with number assignments, (b) view along C2–C1 bond, and (c) displacement vectors corresponding to the vibration of the negative frequency.

The hydrogen at the C4 position in **56** is evidently rotating outward while C5 shows no apparent movement. It is still in accord with the theory that the electron donating groups generate a *trans* double bond in the final product of the ring opening, in cases where the substituents on the cyclobutene ring of the starting material are *cis*.

compared between **56** and **71** as shown in Table 19. Also the C1–C2 single bond in **56** becomes shorter by 0.136 Å in **71**. Although this bond shortens as it becomes a strained *trans* double bond in **71**, it is 0.015 Å longer than the corresponding C1–C2 *cis* double bond of **72**. Therefore, because of the strain in the 7-membered ring in **71** introduced by the elongated *trans* double bond between C1–C2, **71** undergoes a *trans-cis* isomerization to yield **72**. Since there is a break in the conjugation of the π system introduced by the *trans* bond between C3–C4 in **73**, all double bonds are shorter that those in **71** and **72** as shown in Table 17.

Table 17. Selected Becke3LYP/6-31+G(d) bond lengths (Å) and dihedral angles for **56**, **TSa**, **71–74**.

	56	**TSa**	**71**	**72**	**73**	**74**
N–C1	1.460	1.374	1.370	1.393	1.412	1.388
C1–C2	1.525	1.484	1.389	1.374	1.342	1.348
C2–C3	1.340	1.353	1.461	1.437	1.472	
C3–C4	1.529	1.462	1.367	1.373	1.330	
C4–C5	1.504	1.472	1.478	1.441	1.476	
C5–C6	1.341	1.351	1.362	1.355	1.329	
C6–C7	1.510	1.513	1.530	1.506	1.538	
C7–C1	1.559	1.505	1.498	1.523	1.555	
C1–C4	1.613	2.254	2.781	3.143	2.814	
C1–C8–C9–N	28.2	20.3	9.3	18.4	22.6	19.7*
N–C1–C2–H1	60.8	94.6	156.9	13.3	8.7	
H2–C3–C4–H3	67.8	33.8	7.0	0.2	175.9	

* dihedral angle between C1, carbons of the two methyl groups of the amine and the nitrogen atom

A calculation of *N,N*-dimethyl-*N*-vinylamine (**74**) shows that the amine is pyramidalized with the dihedral angle of 19.7° between C1, the two methyl groups of the amine and the nitrogen. The C1–N bond of **74** is slightly shorter than in **72** and the C1–C2 double bond is also shorter than in **72** and **71** by 0.026 Å and 0.041 Å respectively, but it is only slightly longer than in **73**. This indicates that the conjugation plays a significant role in determining the bond lengths in these molecules.

The thermal conrotatory ring opening of **56** yields **71** and not **73** because **71** has two coplanar double bonds which extend the conjugation. In **73** this conjugation is reduced by the *trans* double bond between C3–C4. Our calculations on the unsubstituted cycloheptatriene indicate a difference in energy of 8.1 kcal mol^{-1} between cyclohepta-1(*E*),3(*Z*),5(*Z*)-triene (**75**) and cyclohepta-1(*Z*),3(*E*),5(*Z*)-triene (**76**), **75** being lower in energy than **76** (Figure 33).

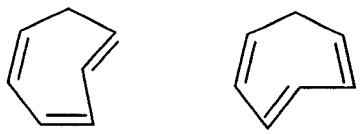

75 **76**

Figure 33. Cyclohepta-1(*E*),3(*Z*),5(*Z*)-triene (**75**) and cyclohepta-1(*Z*),3(*E*),5(*Z*)-triene (**76**).

A calculation on 1,3,5-hexatriene (**77**) also shows a considerable difference in energy between two hexatrienes which have constrained dihedral angles to resemble those of **75** and **76** (Figure 34).

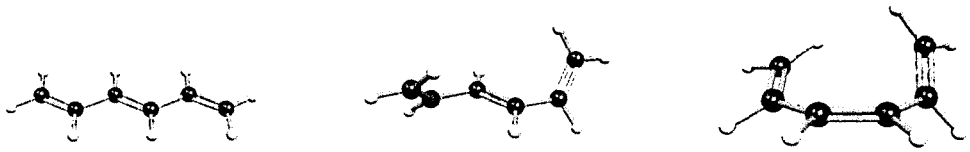

77 **77a** **77b**

Figure 34. Becke3LYP optimized geometries of hexatrienes **77**, **77a**, and **77b**.

In hexatriene **77a** the dihedral angles between C1–C2–C3–C4 and C3–C4–C5–C6 have been constrained to 57° to resemble **76**. Similarly in hexatriene **77b**, the dihedral angle between C1–C2–C3–C4 has also been constrained to 57° to resemble **75**. The difference in energy between the two hexatrienes was found to be 3.3 kcal mol^{-1}. The total and relative energies are listed in Table 16. The conjugation of the double bonds in **77b** is reduced thus increasing the energy. The energy of the system is higher in a case where none of the double bonds are coplanar as in **76** and **73** and it is lower in a case where at least two of the double bonds are conjugated and coplanar as in **75** and **71**. Therefore the formation of **71** is favored over **73** since in **71** the conjugation is preserved between two double bonds whereas in **73** there is a complete break in the conjugation of the π system.

4.2.6 Summary

The thermal ring expansion of **48** and **56** both follow the thermally allowed conrotatory path. Transient strained dienone **68** has been observed with photoelectron spectroscopy. In the case of the thermal ring expansion of **56** transient **71** was not observed directly. Calculations indicate that **71** is a transient intermediate with its barrier for isomerization to **72** being 5.9 kcal mol^{-1}. *Ab initio* calculations of the energy barriers for the two possible conrotatory modes predicted the formation of **68** to be 12.9 kcal mol^{-1} more favorable than the formation of **69**. Similarly, calculation of the energy barriers for the two possible conrotatory ring openings of **56** predicted the formation of **71** to be 7.7 kcal mol^{-1} more favorable than the formation of **73**.

Chapter 5

Photoelectron Spectroscopy of 7-Substituted Cycloheptatrienes

5.1 Background

Ter Borg and coworkers have studied the thermal behavior of 7-substituted cycloheptatrienes. [96,123,124] In their studies the authors found that upon thermal isomerization the equilibrium composition of mono-substituted cycloheptatrienes varies considerably with the nature of the substituent. For example, in the thermal isomerization of 7-dimethylaminocycloheptatriene, 1-dimethylaminocycloheptatriene is the sole product with none of the 3-, 2-, or 7- isomers being present, while the thermal behavior of 7-methylcycloheptatriene shows the equilibrium composition to be: 1-methyl (57%), 3-methyl (24%), 2-methyl (17%), and 7-methyl (2%).[96] Transannular 1-5 shifts of hydrogen were responsible for the isomerization. Similarly it was found that 7-D-cycloheptatriene undergoes photochemical [1,7]-H migration. Bicyclo[3.2.0]hepta-2,6-diene was also detected along with the cycloheptatriene isomers.[94] 7-Methoxycycloheptatriene has been shown to isomerize thermally as well as photochemically to the 1-isomer in the vapour phase, which upon further photolysis isomerizes to 1-methoxybicyclo[3.2.0]hepta-3,6-diene.[125]

Cycloheptatrienes substituted at the 7-position can exist in the *axial* and the *equatorial* conformations as shown in Figure 35. We have undertaken a photoelectron spectroscopic study of cycloheptatriene (**58**), 7-methylthiocycloheptatriene (**78**), 7-methoxycycloheptatriene (**79**), 7-dimethylaminocycloheptatriene (**59**), and 7-methylcycloheptatriene (**80**) in order to investigate whether it is possible to use PE spectroscopy to gain information on the conformational properties of these compounds. The photoelectron spectra of these compounds have not yet been reported. A computational study of 7-methylcycloheptatriene indicated that this isomer should exist preferentially in the *axial* conformation,[99] while our preliminary calculation has indicated otherwise. This has prompted us to investigate several 7- substituted cycloheptatrienes experimentally and computationally.

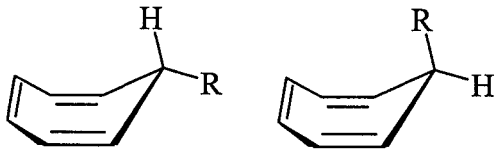

equatorial axial

R: OMe, SMe, $N(CH_3)_2$, CH_3, H

Figure 35. Schematic view of *equatorial* and *axial* isomers of cycloheptatriene.

5.2 Results

5.2.1 Synthesis of 7-substituted cycloheptatrienes

Cycloheptatrienes **59**, **78–80** were synthesized from tropylium bromide (**57**), the synthesis of which was given in Chapter 3.3.7 (eqn. 3.7). Cycloheptatriene (**58**) is a commercially available compound and was distilled prior to experiments. A reaction of **57** with sodium thiomethoxide, sodium methoxide, dimethylamine, and methyllithium has yielded the respective cycloheptatrienes as illustrated in Equation 5.1.

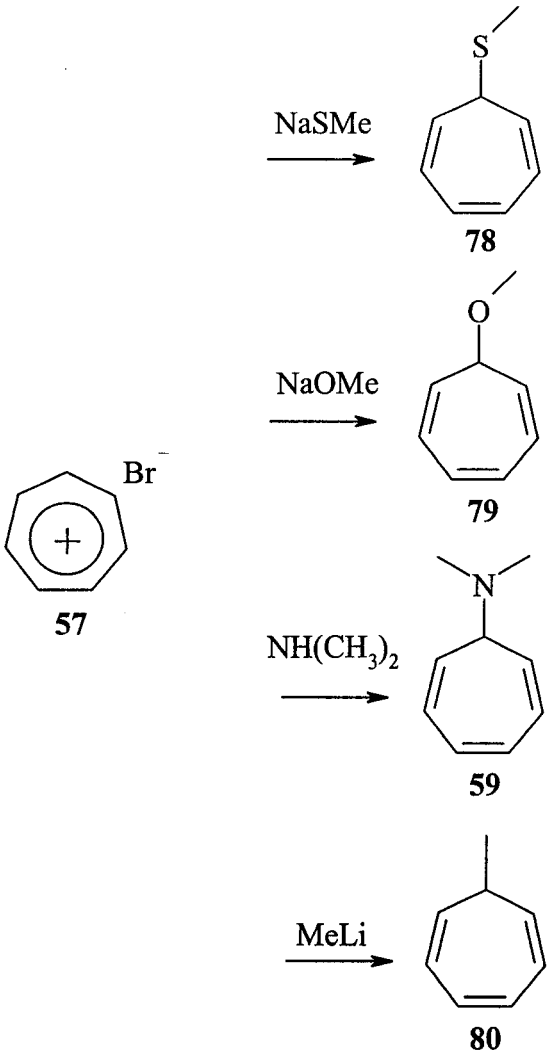

[5.1]

5.2.2 Photoelectron spectra of 7-substituted cycloheptatrienes

The Becke3LYP/6-31+G(d) total energies for optimized equilibrium geometries and radical cation single point calculations of compounds **58, 59 78–89** are shown in Table 18.

Table 18. Total energies E_T (hartrees) of 7-substituted cycloheptatrienes **58**, **59**, **78–80** (N electrons) and their radical cations[a] ($N-1$ electrons) and derived first vertical ionization potentials IP_v (eV)

	Substituent	Number of electrons	Becke3LYP/6-31+G(d)	
			E_T	IP_v
58	H	N	-271.521 961	8.12
		$N-1$	-271.223 426	
78e[b]	SMe	N	-709.020 628	8.09
		$N-1$	-708.723 337	
78a[c]	SMe	N	-709.022 476	7.73
		$N-1$	-708.738 418	
79e	OMe	N	-386.043 106	8.23
		$N-1$	-385.740 485	
79a	OMe	N	-386.040 779	8.21
		$N-1$	-385.739 220	
59e	NMe_2	N	-405.484 745	7.96
		$N-1$	-405.192 022	
59a	NMe_2	N	-405.481 941	7.65
		$N-1$	-405.200 904	
80e	Me	N	-310.838 050	8.09
		$N-1$	-310.540 637	
80a	Me	N	-310.835 282	7.93
		$N-1$	-310.543 848	

[a] Single point energy calculations on the optimized molecule (N electrons) geometries.
[b] **e** – equatorial
[c] **a** – axial

The experimental and simulated photoelectron spectra of **58** and **78** are shown in Figure 36. The PE spectra of **59**, **79** and **80** are shown in Figure 37 and the simulated partial PE spectra are also shown in Figure 37.

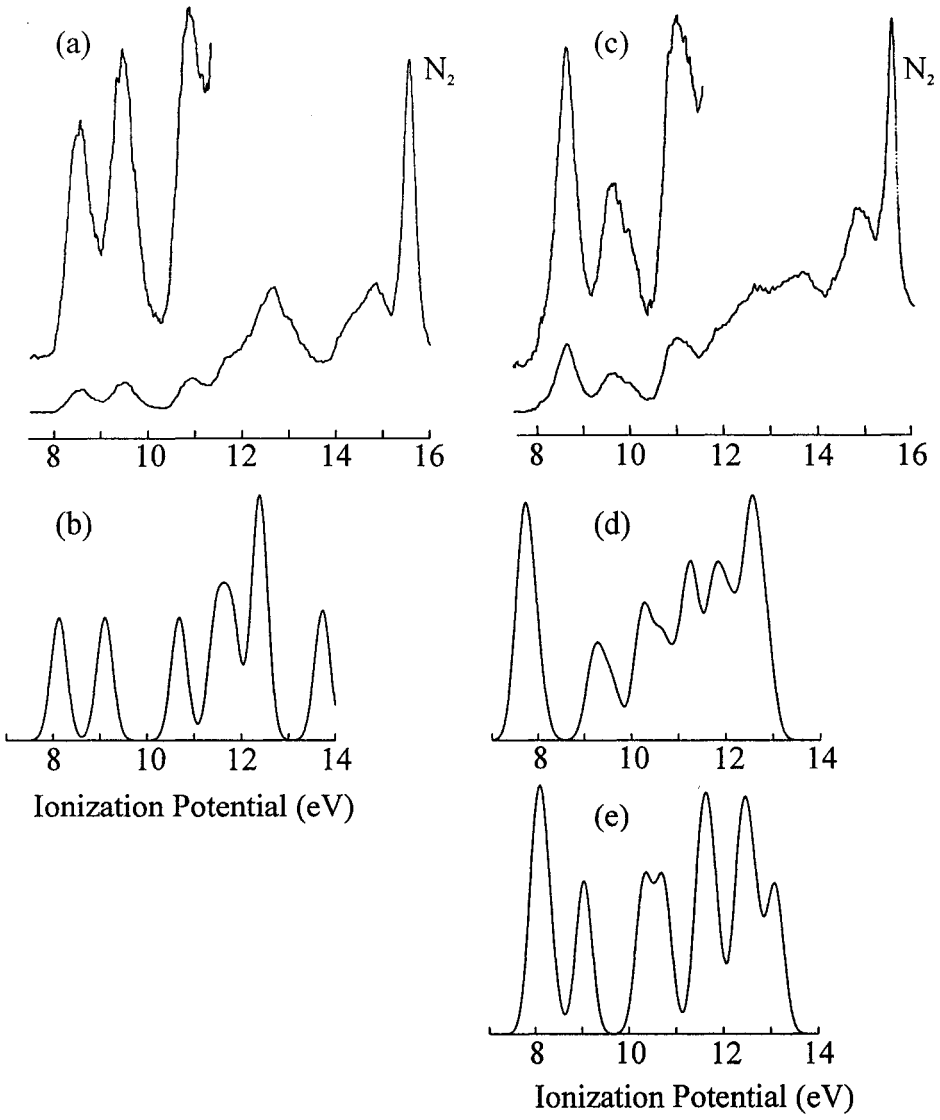

Figure 36. Experimental PE spectra of: (a) **58**, (c) **78** and simulated partial PE spectra of: (b) **58**, (d) *axial* **78** and (e) *equatorial* **78**.

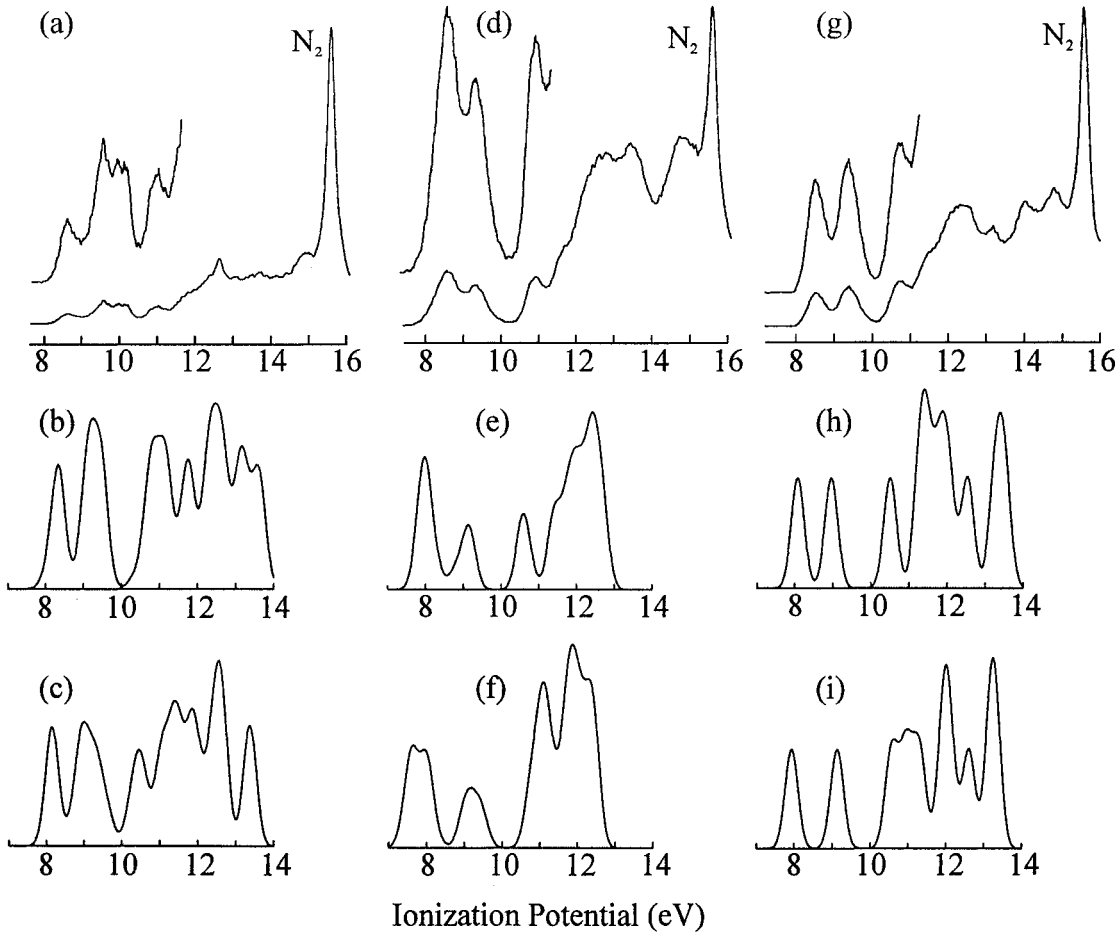

Figure 37. Experimental PE spectra of: (a) **79**, (d) **59**, (g) **80** and simulated partial PE spectra of: (b) *equatorial* **79**, (c) *axial* **79**, (e) *equatorial* **59**, (f) *axial* **59**, (h) *equatorial* **80**, (i) *axial* **80**.

The experimental and calculated vertical ionization potentials and orbital energies of compounds **58**, **59**, and **78–80** are shown in Table 19.

Table 19. Experimental and calculated vertical ionization potentials IP (eV) of cycloheptatrienes **58**, **59**, **78–80**.

58	Becke3LYP	IP_v	8.1	9.1	10.7	11.5	11.8
	Exp.	IP_v	8.6	9.5	10.9		
78	Becke3LYP	IP_v[a]	7.7	8.1	9.7	10.5	11.1
	Exp.	IP_v	------8.7[b]------		9.7	------11.1------	
79	Becke3LYP	IP_v	8.2	9.0	9.4	10.7	11.1
	Exp.	IP_v	8.6	9.6	10.0	11.1	
59	Becke3LYP	IP_v	8.0	8.1	8.8	10.6	11.3
	Exp.	IP_v	------8.6[b]------		9.4	10.9	
80	Becke3LYP	IP_v	8.1	9.0	10.5	11.3	
	Exp.	IP_v	8.5	9.4	10.8		

[a] Calculated IPs for the *axial* isomer.
[b] Consists of two overlapping bands.

The calculated vertical ionization potentials for compounds **79**, **59**, and **80** are of the *equatorial* isomers. The ionization potentials of compound **78** are compared to the calculated vertical ionization potentials for its *axial* isomer.

5.2.3 Calculated conformational properties of 7-substituted cycloheptatrienes

The most stable conformation in the CHT isomers **59**, **79**, and **80** is the *equatorial* conformation where the substituent is situated opposite of the ring rather than over the ring as in the *axial* conformation as shown in Figure 37.

Glidewell[99] performed a computational study on 7-methylcycloheptatriene (**80**) using the MNDO method and has reported the *axial* isomer to be 1.8 kcal mol^{-1} more stable then the *equatorial* isomer, contrary to our results. Becke3LYP/6-31+G(d) calculations place the *axial* isomer 1.7 kcal mol^{-1} higher in energy than the *equatorial* isomer. Donovan and White carried out semiempirical, *ab initio*, and DFT calculations on 7-methoxycycloheptatriene (**79**) finding that the *equatorial* conformation is favored by 1.2 kcal mol^{-1} at Becke3LYP/6-31G(d).[100] Our calculations agree with those of Donovan and White and predict the *equatorial* isomer of **79** to be 1.5 kcal mol^{-1} lower in energy then the *axial* isomer.

In the case of cycloheptatriene (**58**), the *equatorial* and *axial* conformational isomers are indistinguishable. The Becke potential energy surface for the *equatorial*-cycloheptatrienes **78**, **79**, and **80**, obtained by varying the dihedral angle between H-7 and the substituent group, revealed that the gauche conformation is lowest in energy in the three cycloheptatrienes as shown in Table 20. It is also the lowest energy conformation in the case of the *axial* isomers with the exception of **78** where the anti conformation is favored. The Newman projections for the corresponding cycloheptatrienes are shown in Figure 38.

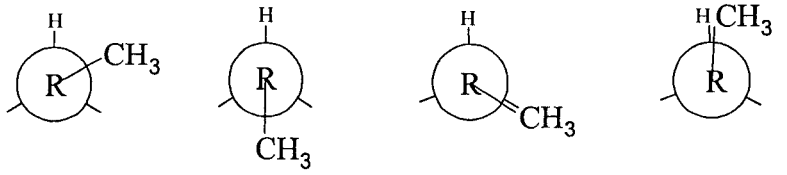

gauche anti eclipsed (0°) eclipsed (120°)

R = O, S

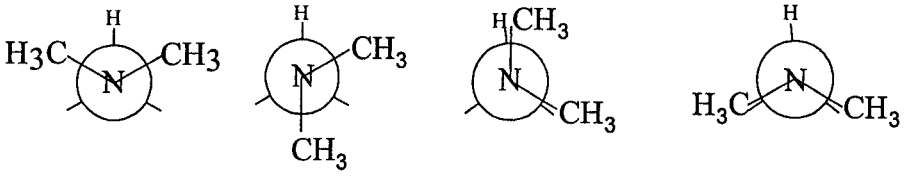

gauche anti eclipsed (0°) eclipsed (120°)

Figure 38. Newman projections for cycloheptatrienes.

Table 20. Becke3LYP/6-31+G(d) total energies E_T (hartrees) and relative energies RE (kcal mol^{-1}) of conformational isomers of **59**, **78**, and **79** as a function of angle.

		Gauche	Anti	Eclipsed (0°)	Eclipsed (120°)
78e	E_T	-709.020 628	-709.019 463	-709.018 633	-709.014 300
	RE	0	0.7	1.3	4.0
78a	E_T	-709.020 213	-709.022 476	-709.014 999	-709.018 597
	RE	1.4	0	4.7	2.4
79e	E_T	-386.043 106	-386.037 906	-386.023 171	-386.033 959
	RE	0	3.3	12.5	5.7
79a	E_T	-386.040 779	-386.039 789	-386.0378 16	-386.033 281
	RE	0	0.6	1.9	4.7
59e	E_T	-405.484 744	-405.482 763	-405.477 537	-405.468 419
	RE	0	1.2	4.5	10.2
59a	E_T	-405.481 941	-405.4809949	N/A*	-405.469 322
	RE	0	0.6		7.9

* The eclipsed (0°) conformation of **59a** could not be optimized.

Cycloheptatrienes **59**, **78–80** experience *axial* and *equatorial* isomerism. The Becke total energies, relative energies and energy barrier for three interconversions of the conformers are shown in Tables 21. All compounds are predicted to have the *equatorial* conformer lowest in energy, with the exception of **78**, which is lowest in energy in the *axial* conformation.

Table 21. Total (hartrees) and relative (kcal/mol) energies of the *equatorial* and *axial* cycloheptatriene isomers **59**, **78–80**, calculated at the Becke3LYP/6-31+G(d) level of theory.

	E_T	Relative Energy
	(hartrees)	(kcal mol^{-1})
78e	-709.020 628	1.2
TS78	-709.014 588	4.9
78a	-709.022 476	0
79e	-386.043 106	0
TS79	-386.034 776	5.2
79a	-386.040 779	1.5
59e	-405.484 745	0
TS59	Could not be found	
59a	-405.481 941	1.8
80e	-310.838 050	0
TS80	-310.828 007	6.3
80a	-310.835 282	1.7

5.2.4 Discussion

The photoelectron spectra of cycloheptatrienes **59**, **79**, and **80** indicate that these compounds exist predominantly in the *equatorial* conformation which is supported by calculations (Table 21). The comparison of the experimental and simulated spectra of the respective *equatorial* isomers helps in making the distinction between the *axial* and *equatorial* isomers. The simulated PE spectra of the *axial* isomers differ significantly from the experimental spectra. The 7-methylthiocycloheptatriene (**78**) shows a PE spectrum which is mainly that of the *axial* isomer. This is also supported by the calculations, which predict the *axial* isomer to be 1.2 kcal mol^{-1} lower in energy than the *equatorial* isomer thus accounting for 85-90 percent of the *axial* isomer at equilibrium.[126] The simulated spectrum of **78a** is in good agreement with experimental spectrum while the simulated spectrum of **78e** differs significantly from the experimental spectrum.

The fact that the PE spectra of **59**, **79** and **80** are mainly those of the *equatorial* isomers and the PE spectrum of **78** is mainly that of the *axial* isomer is supported by calculations. Calculations of the transition states for the isomerization of the *axial* and *equatorial* isomers show that the barrier for the isomerization of 7-methoxycycloheptatriene **79e** to **79a** is 5.2 kcal mol^{-1}. The free-energy-corrected energy difference between **79e** and **79a** was found to be 1.7 kcal mol^{-1} in favor of the *equatorial* isomer. This supports the observation that the PE spectrum of **79** is largely that of the *equatorial* isomer. The reverse is seen in the case of **78**. The energy barrier for the isomerization of 7-methylthiocycloheptatriene **78e** to **78a** is 3.7 kcal mol^{-1}, and the free-

energy-corrected energy difference between **78a** and **78e** was found to be 1.2 kcal mol^{-1} in favor of the *axial* isomer. The PE spectrum in this case is largely that of the *axial* isomer (Figure 36). The transition state calculations illustrate the ease of conversion of the *equatorial* and *axial* isomers. The energy barrier for the conversion of **79e** to **79a** is 1.5 kcal mol^{-1} higher then the energy barrier for the conversion of **78e** to **78a**.

The bond length between the sulfur and C7 in **78** is 1.9 Å (Becke3LYP) which is longer then the bond lengths between O-C7 in **79** (1.4 Å), N-C7 in **59** (1.5 Å), and CH_3-C7 in **80** (1.5 Å). The bond length between S-C7 in the *equatorial* **78** is 0.1 Å shorter than in *axial* **78**. This longer bond between the sulfur atom and the cycloheptatriene ring in *axial* **78** allows for the planarization of the cycloheptatriene ring in **78**, making it possible to accommodate the methylthio group over the CHT ring. It has also been reported in the literature that 7-$Si(CH_3)_3C_7H_7$ is more stable in the *axial* conformation.[99] The *axial* conformation has also been observed in 7-$Ph_3SnC_7H_7$.[127]

5.2.5 Summary

The photoelectron spectra of cycloheptatrienes **58**, **59**, **78**, **79**, and **80** were recorded and interpreted with the use of calculations at the Becke3LYP level of theory. Simulated PE spectra of the *axial* and *equatorial* isomers of all compounds have shown that the PE spectra of compounds **59**, **79** and **80** are those of the *equatorial* isomers and are in good agreement with the experiment. The simulation has also shown that the PE spectrum of **78** is mainly that of the *axial* isomer. The photoelectron spectroscopy

combined with Becke3LYP calculations was used to gain information about the highest occupied molecular orbitals and the composition of the first ionization potential bands in the cycloheptatrienes.

Chapter 6

Conclusions

Several conclusions can be made base on the results presented in this thesis.

The thermolysis and photoelectron spectroscopic study of phenyldiazoethane (**35**) has confirmed the validity of the experiments. With the use of the IR laser **35** was thermolized to yield the only observable product styrene (**37**). The PE spectra of both **35** and **37** were assigned based on literature as well as calculated values. This experiment has also confirmed that Becke3LYP/6-31+G(d) calculations, used to predict ionization potentials give results that are in good agreement with experimental values.

Photoelectron spectroscopy and thermolysis of precursors to 1,2,4,6-cycloheptatetraene (**10**) have confirmed that this transient rearranges to fulvenallene at high temperatures. Although a clear PE spectrum of cycloheptatetraene could not be recorded, the ionization potential bands observed in the thermolysis PE spectra may correspond to IP bands of **10**. Calculations of vertical ionization potentials of the precursors, possible thermolysis products and cycloheptatetraene suggest that cycloheptatetraene should exhibit ionization potentials in the same regions as those of the precursors as well as the other possible product, fulvenallene. Bicyclo[3.2.0]hepta-1,3,6-triene has previously been implicated as an intermediate involved in the thermal

rearrangement of **10**.[38,31,33] The photoelectron spectrum of this triene was obtained after subtraction of spectra of the byproducts generated upon thermolysis of the precursor *N*-oxide (**54**). The ionization potential bands that were revealed in this experiment were compared to the calculated IPs of the triene showing remarkable correlations. Comparison of the IP bands of the triene to the IP bands observed in the thermolysis spectrum of **17** have shown that the transient triene (**18**) was not observable in the photoelectron spectroscopic studies of cycloheptatetraene under our experimental conditions.

The use of photoelectron spectroscopy to study the thermal cyclobutene ring opening of bicyclic cyclobutenes has illustrated its ability to identify the strained transient products of the thermal cyclobutene ring opening as in the case of bicyclo[3.2.0]hept-6-en-2-one (**48**) which yielded cyclohepta-2(*Z*),4(*E*)-dien-1-one (**68**). In the case of *N,N*-dimethylbicyclo[3.2.0]hepta-3,6-dien-1-amine, the transient *E,Z,Z* product was not observed. This intermediate underwent a *trans-cis* isomerization, which was confirmed by *ab initio* calculation to have a low energy barrier.

The photoelectron study of 7-substituted cycloheptatrienes has shown that all but one of the cycloheptatrienes prefer the conformation in which the substituent is in the *equatorial* position. 7-Methylthiocycloheptatriene was found to prefer the conformation where the methylthio substituent is in the *axial* position. The finding has been confirmed by simulated PE spectra and by *ab initio* calculations which also predict the *axial*-7-methylthiocycloheptatriene to be lowest in energy.

Therefore it has been illustrated that UV photoelectron spectroscopy combined with *ab initio* MO calculations is an excellent tool for the study of transient species generated directly in the source chamber of the spectrometer. It has also proved to be useful in the study of stable molecules probing their conformational properties.

Chapter 7

Experimental

7.1 General

UV photoelectron spectra were recorded on a photoelectron spectrometer interfaced with a CW CO_2 laser and calibrated using the IP band of N_2 which is seen at 15.6 eV in all experimental spectra.[105] The linearity of the spectral scale was calibrated using the two lowest IP bands of methyl iodide at 9.54 eV and 10.16 eV prior to the experiments. The PE spectra were recorded at pressures between 2×10^{-3} and 6×10^{-3} torr. Depending on the volatility of a sample the sample compartment was either cooled or heated. Pyrolysis of experiments were accomplished using a CW CO_2 laser focused on a tip of a quartz nozzle of the probe directly in the source chamber of the PE spectrometer. The laser is used as a directed heat source which provides a 2-3 mm hot zone that is 10 mm away from the ionization zone.

^{1}H and ^{13}C NMR spectra were recorded on a Bruker AV200 NMR spectrometer using deuterated chloroform, dichloromethane, dimethylsulfoxide, or methanol solutions

and are reported in parts per million downfield from tetramethylsilane using residual hydrogenated solvent resonances as the internal standard.

7.2 Computational resources

Initial molecular geometries were generated using HyperChem 5.1[128] at a semi-empirical level of theory. *Ab initio* calculation have been performed on IBM RS/6000 model 39H, 350, SGI Octane (dual processor), and 1.9 GHz dual processor Intel machine under Linux with Gaussian 94 and Gaussian 98.[129,130] All equilibrium geometries and transition states were optimized at the Becke3LYP/6-31+G(d) level of theory. Transition states were verified by a single negative frequency and a single negative eigenvalue. Illustrations of optimized molecular geometries, molecular orbitals, and transition state vibrations were created using a molecular visualization package Molekel 4.1.[131] Simulated partial PE spectra were calculated using Fortran program PESPEC.[14]

7.3 Commercial Reagents

Dichloromethane, hexanes, methanol, acetonitrile, petroleum ether, pentane were used as received. Diethyl ether, benzene and dimethoxyethane were distilled over sodium prior to use. Acetophenone and benzaldehyde were used as received. 2-Cyclopentene-1-one and cycloheptatriene were distilled prior to experiments. A *cis–trans* mixture of 1,2-dichloroethylene, potassium *tert*-butoxide, sodium hydride, methyllithium, methyl iodide,

lead (IV) acetate, ethylene glycol, *p*-toluenesulfonehydrazide and diphenyldisulfide were all used as received from Aldrich.

7.4 Preparation of Compounds

7.4.1 Phenyldiazomethane (13)

A solution of benzaldehyde (3 g, 0.028 mol) in methanol (35 mL) was stirred with *p*-toluenesulfonhydrazide (4 g, 0.022 mol) at room temperature for two hours under nitrogen. The solution was then allowed to crystallize in a refrigerator overnight. The needle-like colorless crystals were then collected and dried. A solution of benzaldehyde tosylhydrazone (0.5 g, 0.002 mol) in dichloromethane (15 mL) was treated with sodium hydride (0.09 g). The solution was stirred at room temperature for 2 hours. Upon addition of petroleum ether (100 mL), precipitation occurred and the precipitate was collected by vacuum filtration. Phenyldiazomethene was generated in the PE spectrometer by pyrolysis of the sodium salt. Phenyldiazoethane (**35**) was prepared in the same manner as **13**. The diazo compounds were identified by PE spectroscopy and data were compared to literature.[106] IP (eV): 7.88, 9.36, 10.16.

7.4.2 2-Diazobicyclo[3.2.0]hepta-3,6-diene (17)[35]

7.4.2.1 Bicyclo[3.2.0]hept-6-en-2-one (48)

A solution of cyclopent-2-en-1-one (25 g, 0.305 mol), and a mixture of cis- and trans-1,2-dichloroethylene (115 mL) in dichloromethane (350 mL) was degassed with nitrogen for 1 hour. The solution was stirred and irradiated with a Hanovia medium pressure mercury arc lamp fitted with a pyrex filter with a constant follow of dry nitrogen over 22 hours. After removal of solvent 40 mL of isomeric products was collected. Distillation of the brown oil yielded a pale yellow oil.

A solution of isomeric dichloroketones (11.5 g,) in benzene (250 mL) was stirred with ethylene glycol (7g) and a catalytic amount of sulfuric acid at reflux temperature for 24 hours with constant removal of water with the use of a Dean–Stark trap. After this time the solution was allowed to come to room temperature and was washed with 2 x 100 mL of 5% $NaHCO_3$. The benzene layer was then washed with water and dried with anhydrous $MgSO_4$. After filtration of the solution the benzene was removed under vacuum and the product was distilled to give 13g of the acetal. The acetal (**46**) (13g) was dissolved in dry diethyl ether (150 mL) and the solution was added to 400 mL of liquid ammonia. To this stirred solution sodium metal was added in small pieces until the blue color persisted for 30 minutes. Ammonium chloride was then added to quench the reaction. The solution was then allowed to come to room temperature and the ammonia was allowed to evaporate. Water was then added (200 mL) and the mixture was stirred

for 1 hour. The solution was then extracted with diethyl ether (2 x 200 mL) and the ethereal extracts were then stirred with 100 mL of 1.5M HCl at room temperature overnight. The mixture was then separated and the aqueous layer was washed with 200 mL of ether. The organic extracts were combined and washed with 5% sodium bicarbonate (2 x 100 mL) and with water (2 x 200 mL). After the organic extracts were dried with anhydrous calcium chloride, the solution was filtered and the solvent was removed. Distillation of the residue afforded 3g of pure **48,** which was identified base on reported data.[120,132] ^{1}H NMR ($CDCl_3$) δ: 6.30 (d, 1H), 6.09 (d, 1H), 3.45 (m, 1H), 3.16 (s, 1H), 2.90 (m, 1H), 2.16 (m, 1H), 1.88 (m, 2H). ^{13}C NMR ($CDCl_3$) δ: 217.2, 143.3, 136.6, 54.4, 44.5, 34.4, 21.7.

7.4.2.2 Methyl benzenesulfinate (**49**)

Methyl benzenesufinate was prepared according to the procedure by Field and Lock.[109]

To a solution of diphenyldisulfide in 225 mL chloroform and 225 mL methanol at reflux lead (IV) acetate (55.4 g) in 200 mL of chloroform was add over 1 hour. Four such additions of lead (IV) acetate were done over 4 hours. The solution was then allowed to reflux for additional 12 hours. Chloroform (1L) was removed by distillation. The mixture was allowed to come to room temperature and 130 mL of distilled water was added to destroy any excess lead tetraacetate. The solution was then filtered through a Celite coated filter paper. The chloroform layer was washed with distilled water until the

washings were free of lead ions as tested by placement of a drop of the washings into an aqueous solution of sodium sulfide. The lack of appearance of a dark coloration of the sodium sulfide solution indicated that the washings were free of lead ions. The chloroform layer was then dried with anhydrous $MgSO_4$ and filtered. Removal of the solvent on a rotary evaporator resulted in a pale yellow liquid which was then placed under vacuum over night. Distillation afforded 20.1g of a pale yellow liquid which becomes colorless upon standing. The purity of **49** was checked by NMR. ^{1}H NMR ($CDCl_3$) δ: 7.67 (m 2H), 7.51 (m, 2H), 3.43 (s, 3H). ^{13}C NMR ($CDCl_3$) δ: 143.7, 132.1, 128.9, 125.2, 49.4

7.4.2.3 3-(Phenylsulfinyl)bicyclo[3.2.0]hept-6-en-2-one (**50**)[35]

A solution of ketone (**48**) (2 g) in dry DME (10 mL) was added to a slurry of NaH (2.3g), methyl benzenesulfinate (3.0 g) and DME which were heated at reflux under nitrogen. After the addition reflux was continued for additional 10 minutes and the reaction mixture was allowed to come to room temperature. Residual NaH was quenched by addition of ethanol (10 mL). The solution was then dissolved in 5% NaOH (100 mL) and extracted with diethyl ether (2 x 100 mL). The aqueous layer was acidified to pH 0 and was extracted with diethyl ether (2 x 100 mL). The combined ethereal extracts were washed with saturated sodium bicarbonate and dried with anhydrous Na_2SO_4. Filtration and removal of the solvent afforded 3.5 g of crude product which used without further purification. The product was identified based on the following spectral data with was

compared to literature.[35] ^{1}H NMR ($CDCl_3$) δ 7.45-7.55 (m, 5H), 6.26 (d, 1H), 6.05 (d, 1H), 3.95 (dd, 1H), 3.46 (m, 2H), 2.48-2.67 (m, 2H), 1.51 (dd, 1H).

7.4.2.4 3-(Phenylsulfinyl)bicyclo[3.2.0]hept-6-en-2-one tosylhydrazone (**51**)

A solution of crude (**50**) (3.5 g), *p*-toluenesulfonhydrazide (2.4 g) in 20 mL of methanol was stirred at room temperature under nitrogen for 24 hours. The solution was then cooled in an ice bath and the precipitate was collected by vacuum filtration and was washed with cold 95% ethanol. The product was then dried in air for 3 hours affording 2 g of white solid. The tosylhydrazone (**51**) was identified based on the following spectral data which agreed with that previously reported in the literature.[35] MP. 160°C. ^{1}H NMR (CD_2Cl_2) δ 7.91 (m, 2H) 7.11-7.62 (m, 7H) 6.04 (m, 1H) 5.10-5.26 (m, 1H) 2.48-2.56 (m, 1H) 2.51 (s, 3H), 2.30 (m, 1H), 1.90-2.10 (m, 2H).

7.4.2.5 Bicyclo[3.2.0]hepta-3,6-dien-2-one tosylhydrazone (**52**)

A solution of **51** in 60 mL acetonitrile was heated at reflux under nitrogen until the reaction mixture has just become clear (~ 3 hours). The solvent was then removed using a rotary evaporator and the residue was dissolved in a minimum amount of dichloromethane and was placed in a freezer over night for crystallization. The precipitated material was isolated using a centrifuge. The solid was dried in vacuo giving unreacted starting material which was identified by NMR. The mother liquor was

concentrated on a rotary evaporator and placed in a freezer to allow further crystallization. The precipitate was collected using a centrifuge and was dried under vacuum. The compund **52** was identified base on the following spectral data which agree with that previously reported in the literature.[35] MP. 155°C. ^{1}H NMR ($CDCl_3$) δ 7.87 (d, 2H), 7.50 (br s, 1H), 7.31 (d, 2H), 6.62 (dd, 1H), 6.33 (d, 1H), 6.17 (d, 1H), 6.16 (d, 1H), 3.94 (d, 1H), 3.84 (d, 1H), 2.42 (s, 3H).

7.4.2.6 Bicyclo[3.2.0]hepta-3,6-dien-2-one tosylhydrazone sodium salt (**53**)

A solution of tosylhydrazone (**52**) (0.35 g) in 10 mL dichloromethane was added all at once to a NaH (0.08 g) under nitrogen. The solution was allowed to stir for 2.5 hours. After dilution with petroleum ether (150 mL) a beige solid precipitated and was collected by vacuum filtration affording 0.37 g of the sodium salt **53** which was dried under vacuum. Pyrolysis of the salt in a sample tube attached to the PE spectrometer allowed to record the PE spectrum of **17**.

7.4.3 Tropylim Bromide (57)[114,115]

A solution of 1,3,5-cycloheptatriene (24.2 g, 0.263 mol) in dichloromethane (200 mL) was placed in a round bottom flask cooled in a dry ice / acetone bath. A solution of bromine (15 mL) in dichloromethane (120 mL) was added dropwise. After the addition, the reaction mixture was allowed to come to room temperature. Removal of solvent

resulted in a dark brown oil which was heated with stirring under vacuum in a round bottom flask fitted with a downward distillation apparatus at a temperature of 70 °C over night. The dark solid residue was grinded in with mortar and pestle under dichloromethane and was filterd filtered. Tropylium Bromide was collected as a pale green solid.

7.4.4 *N,N*-Dimethylcyclohepta-1,3,5-trien-7-amine (59)

N,N-dimethylcyclohepta-1,3,5-triene-7-amine (**59**) was synthesized according to a procedure by Doering and Knox.[114]

A solution of tropylium bromide (**57**) (5.8 g) in 35 mL of distilled water was treated with 20% dimethylamine in water (40 mL). Immediately upon addition a light brown oil separated. The solution was extracted with pentane (2 x 20 mL). The combined organic extracts were dried with anhydrous $MgSO_4$. Filtration and removal of solvent resulted in 3.5 g of yellow oil. Purity of product **59** was confirmed by NMR.

^{1}H NMR ($CDCl_3$) δ 1.86 (t, 1 H), 2.37 (s, 6 H), 5.45 (m, 2 H), 6.17 (m, 2 H), 6.71 (m, 2 H). ^{13}C ($CDCl_3$) δ 43.2, 65.6, 122.8, 123.5, 130.6.

7.4.5 *N,N*-dimethylbicyclo[3.2.0]hepta-3,6-dien-1-amine (56)[91,125]

A solution of **59** (2 g) in 1 L of hexanes (Omnisolve) was degassed for 1 hour with nitrogen and photolyzed with medium pressure mercury arc lamp of 6.5 hours. The

solution was then filtered to remove precipitated polymeric material and the solvent was removed using a rotary evaporator affording 1.6 g of amine **56**. The product was checked by NMR and was used in PE spectroscopic experiments without further purification. ^{1}H NMR ($CDCl_3$) δ 6.31 (br s, 2H), 5.74 (m, 2H), 3.48 (m, 1H), 2.25 (s, 6H), 2.23-2.28 (m, 2H)

7.4.6 *N,N*-Dimethylbicyclo[3.2.0]hepta-3,6-dien-1-amine oxide (54)[110]

A solution of tertiary amine (**56**) (1 g) in 30 mL of methanol was treated with 30% hydrogen peroxide (2 g).[133] The solution was stirred over night at room temperature under nitrogen. Excess hydrogen peroxide was quenched with palladium on charcoal. The solution was filtered and the solvent removed on a rotary evaporator. The sample was dried under vacuum. The N-oxide was identified by NMR in dueterated methanol. ^{1}H NMR (CD_3OD) δ 6.55 (d, 2H), 6.26 (d, 2H), 5.83 (br s, 2H), 3.95 (br s, 1H), 3.36 (s, 3H), 3.33 (s, 3H).

7.4.7 *N,N*-Dimethylcyclohepta-1,3,5-trien-1-amine (71)[96]

A neat sample of (**59**) (4 g) was heated at 100°C with stirring for 20 hours. The resulting dark brown oil was distilled using a bulb to bulb distillation apparatus affording 2.4 g of orange liquid. The amine **63** was identified by NMR. ^{1}H NMR ($CDCl_3$) δ 6.44

(dd, 1H), 6.21 (dd, 1H), 6.06 (dd, 1H), 5.21 (dd, 2H), 2.83 (s, 6H), 2.50 (d, 2H). ^{13}C NMR ($CDCl_3$) δ 30.2, 40.7, 99.1, 113.2, 120.0, 127.9, 130.6, 143.0.

7.4.8 7-(methylthio)cyclohepta-1,3,5-triene (78)

To a solution of 2 g. (0.01 mole) of tropylium bromide (**57**) in 10 mL of methanol a solution of 0.7 g (0.01 mole) of sodiumthiomethoxide in 30 ml. methanol was added. The solution was allowed to stir for 0.5 hours. Excess sodiumthiomethoxide was quenched with 50 mL of water. The resulting solution was extracted with diethylether (3 x 30 ml.) which was dried with magnesium sulfate. Removal of solvent produced 7-(methylthio)cyclohepta-1,3,5-triene. ^1H NMR ($CDCl_3$) δ 2.08 (s, 3 H), 3.43 (t, 1 H), 5.47 (m, 2 H), 6.21 (m, 2 H), 6.50 (m, 2 H). ^{13}C ($CDCl_3$) δ 13.4, 44.0, 124.6, 126.7, 131.1.

7.4.9 7-Methoxycycloheptatriene (79)

A solution of 2 g (0.01 mole) of tropylium bromide in 10 mL of methanol was added to a solution of sodium methoxide in methanol (1.5 g Na in 20 mL MeOH). The mixture was stirred for 45 minutes, and filtered to remove precipitated sodium bromide. Removal of solvent afforded yellow oil, which was washed with water and extracted with diethylether (3 x 10 ml.) and dried with anhydrous $MgSO_4$. ^1H NMR ($CDCl_3$) δ 3.41 (s, 3 H), 3.41 (t, 1 H), 5.51 (m, 2 H), 6.18 (m, 2 H), 6.67 (m, 2 H). ^{13}C ($CDCl_3$) δ 56.5, 77.9, 123.2, 125.4, 131.1.

7.4.10 7-Methylcycloheptatriene (80)

To a vigorously stirred suspension of 2 g. (0.01 mol) of tropylium bromide (**57**) in dry diethylether, a 1.4 M solution of methyllithium in diethylether was added dropwize (100% excess). Exothermic reaction took place upon addition of methyllithium and reflux was observed. The reaction mixture was allowed to stir for additional 30 minutes, 20 mL of 2N HCl was added with care, the mixture was separated and washed twice with 10 mL portions of 2N NaOH, and three 15 mL portions of water. The ethereal layer was dried with anhydrous $CaCl_2$. Removal of solvent afforded 0.15 g (14%) of **79**. ^{1}H NMR ($CDCl_3$) δ 1.34 (d, 3 H), δ 1.64 (m, 1 H), δ 5.12 (m, 2 H), δ 6.13 (m, 2 H), δ 6.63 (m, 2 H). ^{13}C NMR ($CDCl_3$) δ 19.1, 33.5, 124.4, 128.2, 131.1.

7.4.11 Cyclohepta-2,4-dien-1-one (70)[119]

Cyclohepta-3,5-dienone which was prepared by a procedures of Hine[119] and Schuster[134] was added dropwise as a 90% solution in dichloromethane to a rapidly stirred FSO_3H (10 mL) at –78°C. After addition the solution was warmed to room temperature and was allowed to stir for additional 4 hours. The acid solution was added dropwise to a rapidly stirred suspension of $NaHCO_3$ (20 g) in water (50 mL) which was kept between –5 to 0 °. The solution was then extracted with ether and the collected solid was also washed with ether. Combined ethereal extracts were washed with water until neutral and were dried over $MgSO_4$. Removal of ether using a rotary evaporator yielded orange oil

which was distilled using a bulb to bulb apparatus. The compound was identified based on the following spectral data. ^{1}H NMR ($CDCl_3$) δ 6.42-6.60 (m, 2H), 6.01-6.13 (m, 2H), 2.58-2.64 (m, 2H), 2.31-2.41 (m, 2H).

7.4.12 Dimers (61)

A solution of *N,N*-dimethylbicyclo[3.2.0]hepta-3,6-dien-1-amine (**56**) (1.3 g) in absolute ethanol was treated with excess methyliodide (3 mL). The reaction was allowed to stir overnight at room temperature. The solvent was then removed resulting in a dark brown precipitate. The methiodide salt (0.9 g) was dissolved in DMSO and was treated with potassium tert-butoxide (0.3 g). After two hour the reaction mixture was diluted with water and extracted with pentane. The pentane extracts were dried with $MgSO_4$ and after filtration the solvent was removed. The resulting brown oily residue was confirmed to be a 50:50 mixture of dimers by GC/MS trace showing two peaks with retention times of 17.7 and 18.3 minutes both having m/e 180. The dimers were also identified base on reported data.[110] Dimer (A) ^{1}H NMR ($CDCl_3$) δ 6.43 (d, 2H), 6.14 (d, 2H), 5.92-5.90 (m, 4H), 3.63 (s, 2H), 2.73 (s, 2H). ^{13}C NMR ($CDCl_3$) δ 144.4, 137.8, 135.9, 134.0, 63.7, 58.7, 53.5. Dimer (B) ^{1}H NMR ($CDCl_3$) δ 6.32 (d, 4H), 5.89 (d, 2H), 5.69 (d 2H), 3.67 (s, 2H), 3.39 (s, 2H). ^{13}C NMR ($CDCl_3$) δ 142.9, 139.6, 134.97, 134.93, 62.4, 59.9, 50.6.

References

1 J. W. Rabalais. "*Principles of Ultraviolet Photoelectron Spectroscopy*"; Wiley, Toronto, 1977.

2 N. H. Werstiuk, C. D. Roy, J. Ma. *Can. J. Chem.* 1994, **72**, 2537.

3 N. H. Werstiuk, C. D. Roy, J. Ma. *Can. J. Chem.* 1995, **73**, 146.

4 W. J. Hehre, L. Radom, P. v. R. Schleyer, J. A. Pople, *Ab Initio Molecular Orbital Theory*; John Wiley & Sons; New York, 1986.

5 A. D. Becke. *J. Chem. Phys.* 1993, **98**, 5648.

6 C. Lee, W. Yang, R. G. Parr. *Phys. Rev. B* 1988, **37**, 785.

7 J. B. Foresman, E. Frish. *"Exploring Chemistry with Electronic Structure Methods"* 2nd ed., Gaussian, Inc., Pittsburgh, PA. 1993.

8 T. A. Koopmans. *Physica* 1934, **1**, 104.

9 H. M. Muchall, N. H. Werstiuk, B. Choudhury. *Can. J. Chem.* 1998, **76**, 221.

10 H. M. Muchall, N. H. Werstiuk, B. Choudhury, J. Ma, J. Warkentin, J. P. Pezacki. *Can. J. Chem.* 1998, **76**, 238.

11 N. H. Werstiuk, H. M. Muchall, J. Ma, M. T. H. Liu. *Can. J. Chem.* 1998, **76**, 1162.

12 H. M. Muchall, P. Rademacher. *J. Mol. Struc.* 1997, **435**, 157.

13 H. M. Muchall, N. H. Werstiuk, J. L. Pitters, M. S. Workentin. *Tetrahedron* 1999, **55**, 3767.

14 N. H. Werstiuk, G. Timmins, J. Ma, T. A. Wildman. *Can. J. Chem.* 1992, **70**, 1971.

15 *"Webster's Encyclopedic Unabridged Dictionary of the English Language"* Gramercy Books, 1989, New Jersey.

16 W. Kirmse. *"Carbene Chemistry"* 2nd ed., Academic Press; New York, 1971.

17 T. H. Lowry, K. S. Richardson. *"Mechanism and Theory in Organic Chemistry"* 3rd ed., Harper and Collins Publishers; New York, 1987.

18 J. Hine. *J. Am. Chem. Soc.* 1950, **72**, 2438.

19 J. Hine, A. M. Dowell, Jr. *J. Am. Chem. Soc.* 1954, **76**, 2699.

20 J. Hine, A. M. Dowell, Jr., J. E. Singley, Jr. *J. Am. Chem. Soc.* 1956, **78**, 479.

21 H. E. Simmons, T. L. Cairns, S. A. Vladuchick, C. M. Hoiness. *Org. Reactions* 1973, **20**, 1.

22 W. J. Baron, M. R. DeCamp, M. E. Hendrick, M. Jones, Jr., R. H. Levin, M. B. Sohn. *"Carbenes"* Vol. 1, M. Jones, R. A. Moss, Eds., Wiley: New York, 1973, p. 1.

23 S. Braslavsky, J. Heicklen. *Chem. Rev.* 1977, **77**, 473.

24 R. H. Shapiro. *Org. Reactions* 1976, **23**, 405.

25 A. J. Arduengo III, H. Bock, H. Chen, M. Denk, D. A. Dixon, J. C. Green, W. A. Herrmann, N. L. Jones, M. Wagner, R. West. *J. Am. Chem. Soc.* 1994, **116**, 6641.

26 R. P. Johnson. *Chem. Rev.* 1989, **89**, 1111.

27 (a) A. E. Favorski. *J. Gen. Chem. USSR (Eng. Transl.)* 1936, **6**, 720. (b) A. E. Favorski. *Bull. Soc. Chim. Fr.* 1936, **5**, 1727.

28 N. A. Domnin. *J. Gen. Chem.USSR (Engl. Transl.)* 1945, **15**, 461. ibid. 1940, **10**, 1939.

29 W. J. Ball, S. R. Landor. *Proc. Chem. Soc., London* 1961, 143. *J. Chem. Soc.* 1962, 2298.

30 R. J. McMahon, C. J. Abelt, O. L. Chapman, J. W. Johnson, C. L. Kreil, J-P. LeRoux, A. M. Mooring, P. R. West. *J. Am. Chem. Soc.* 1987, **109**, 2456.

31 M. W. Wong, C. Wentrup. *J. Org. Chem.* 1996, **61**, 7022.

32 S. Matzinger, T. Bally, E. V. Patterson, R. J. McMahon. *J. Am. Chem. Soc.* 1996, **118**, 1535.

33 E. V. Patterson, R. J. McMahon. *J. Org. Chem.* 1997, **62**, 4398.

34 P. R. West, O. L. Chapman, J-P. LeRoux. *J. Am. Chem. Soc.* 1982, **104**, 1779.

35 O. L. Chapman, C. J. Abelt. *J. Org. Chem.* 1987, **52**, 1218.

36 R. C. Joines, A. B. Turner, W. M. Jones. *J. Am. Chem. Soc.* 1969, **91**, 7754.

37 C. Wentrup, K. Wilczek. *Helv. Chim. Acta* 1970, **53**, 1459.

38 C. Wentrup, E. Wentrup-Byrne, P. Müller. *Chem. Comm.* 1977, 210.

39 W. D. Crow, M. N. Paddon-Row. *J. Am. Chem. Soc.* 1972, **94**, 4746.

40 W. J. Baron, M. Jones, Jr., P. P. Gaspar. *J. Am. Chem. Soc.* 1970, **92**, 4739.

41 W. E. Billups, L. E. Reed, E. W. Casserly, L. P. Lin. *J. Org. Chem.* 1981, **46**, 1326.

42 W. E. Billups, L. E. Reed. *Tetrahedron Lett.* 1977, 2239.

43 P. C. Miller, P. P. Gaspar. *J. Org. Chem.* 1991, **56**, 5101.

44 O. L. Chapman, R. J. McMahon, P. R. West. *J. Am. Chem. Soc.* 1984, **106**, 7973.

45 P. R. West, A. M. Mooring, R. J. McMahon, O. L. Chapman. *J. Org. Chem.* 1986, **51**, 1316.

46 J. E. Chateauneuf, K. A. Horn, T. G. Savino. *J. Am. Chem. Soc.* 1988, **110**, 539.

47 S. W. Albrecht, R. J. McMahon. *J. Am. Chem. Soc.* 1993, **115**, 855.

48 Y. Xie, P. R. Schreiner, P. v. R. Schleyer, H. F. Schaefer III. *J. Am. Chem. Soc.* 1997, **119**, 1370.

49 P. A. Bonvallet, R. J. McMahon. *J. Am. Chem. Soc.* 2000, **121**, 10496.

50 S. Matzinger, T. Bally. *J. Phys. Chem. A* 2000, **104**, 3544.

51 R. Warmuth, M. A. Marvel. *Angew. Chem. Int. Ed.* 2000, **39**, 1117.

52 R. Warmuth, M. A. Marvel. *Chem. Eur. J.* 2001, **7**, 1209.

53 L. Radom, H. F. Schaefer III, M. A. Vincent. *Nouv. J. Chim.* 1980, **4**, 411.

54 M. Z. Kassaee, M. R. Nimlos, K. E. Downie, E. E. Waali. *Tetrahedron* 1984

55 C. L. Janssen, H. F. Schaefer III. *J. Am. Chem. Soc.* 1987, **109**, 5030.

56 C. M. Geise, C. M. Hadad. *J. Org. Chem.* 2002, **67**, 2532.

57 F. A. Carey, R. J. Sundberg. *"Advanced Organic Chemistry, Part A: Structure and Mechanisms"*, 3rd ed. Plenum Press; New York, 1990.

58 R. Huisgen. *Angew. Chem. Int. Ed. Engl.* 1968, **7**, 321.

59 I. Fleming. *"Frontier Orbitals and Organic Chemical Reactions"*, John Wiley & Sons, Ltd.; New York, 1976.

60 R. B. Woodward, R. Hoffmann. *J. Am. Chem. Soc.* 1965, 87, 395.

61 R. B. Woodward, R. Hoffmann. "*The Conservation of Orbital Symmetry*"; *Angew. Chem. Int. Ed. Engl.* 1969, **8**, 781.

62 R. Srinivasan. *J. Am. Chem. Soc.* 1969, **91**, 7557.

63 R. E. K. Winter. *Tetrahedron Lett.* 1965, 1207.

64 G. R. Branton, H. M. Frey, R. F. Skinner. *Trans. Faraday Soc.* 1966, **62**, 1546.

65 H. M. Frey. *Trans. Faraday Soc.* 1962, **58**, 957.

66 W. R. Dolbier Jr., H. Koroniak, K. N. Houk, C. Sheu. *Acc. Chem. Res.* 1996, **29**, 471.

67 W. R. Dolbier Jr., H. Koroniak, D. J. Burton, A. R. Bailey, G. S. Shaw, S. W. Hansen. *J. Am. Chem. Soc.* 1984, **106**, 1871.

68 W. Kirmse, N. G. Rondan, K. N. Houk. *J. Am. Chem. Soc.* 1984, **106**, 7989.

69 N. G. Rondan, K. N. Houk. *J. Am. Chem. Soc.* 1985, **107**, 2099.

70 K. Rudolf, D. C. Spellmeyer, K. N. Houk. *J. Org. Chem.* 1987, **52**, 3708.

71 K. N. Houk, D. C. Spellmeyer, C. W. Jefford, C. G. Rimbault, Y. Wang, R. D. Miller. *J. Org. Chem.* 1988, **53**, 2125.

72 K. Nakamura, K. N. Houk. *Heterocycles* 1993, **35**, 631.

73 E. A. Kallel, K. N. Houk. *J. Org. Chem.* 1989 **54**, 6606.

74 D. A. Smith, C. W. Ulmer. *J. Org. Chem.* 1993, **58**, 4118.

75 D. A. Smith, C. W. Ulmer. *J. Org. Chem.* 1991, **56**, 4444.

76 D. A. Smith, E. W. Ulmer. *Tetrahedron Lett.* 1991, **32**, 752.

77 J. D. Evanseck, B. E. Thomas, K. H. Houk. *J. Org. Chem.* 1995, **60**, 7134.

78 B. E. Thomas, J. D. Evanseck, K. N. Houk. *J. Am. Chem. Soc.* 1993, **115**, 4165.

79 S. Niwayama, E. A. Kallel, C. Sheu, K. H. Houk. *J. Org. Chem.* 1996, **61**, 2517.

80 P. Radlick, W. Fenical. *Tetrahedron Lett.* 1967,4901.

81 R. Criegee, D. Seebach, R. E. Winter, B. Borretzen, H. A. Burne. *Chem.Ber.* 1965, **98**, 2339.

82 G. R. Branton, H. M. Frey, D. C. Montague, I. D. R. Stevens. *Trans. Faraday Soc.* 1966, **62**, 659.

83 J. Bramham, C. J. Samuel. *J. Chem. Soc., Chem. Comm.* 1989, 29.

84 J. S. McConaghy, J. J. Bloomfield. *Tetrahedron Lett.* 1969, 3719.

85 J. J. Bloomfield, J. S. McConaghy, A. G. Hortmann. *Tetrahedron Lett.* 1969, 3723.

86 Y. Inoue, S. Hagiwara, Y. Daino, T. Hakushi. *J. Chem. Soc., Chem. Commun.* 1985, 1307.

87 H. M Muchall, N. H. Werstiuk, J. Ma, T. T. Tidwell, K. Sung. *Can. J. Chem.* 1997, **75**, 1851.

88 R. S. Brown, F. S. Jorgensen. *"Conformational Analysis by Photoelectron Spectroscopy"*, in *Electron Spectroscopy: Theory, Techniques and Applications* vol. 5, eds. C. R. Brundle, A. D. Baker, Academic Press, New York, 1984, pp. 1-115.

89 A. Ladenburg. *Liebigs Ann. Chem.* 1883, **217**, 74.

90 Y. Inadomi, K. Morihashi, O. Kikuchi. *J. Mol. Struc.* 1998, **428**, 143.

91 A. P. Ter Borg, E. Razenberg, H. Kloosterziel. *Chem. Comm.* 1967, 1210.

92 W. R. Roth. *Angew. Chem.* 1963, **75**, 921.

93 W. von E. Doering, P. P. Gaspar. *J. Am. Chem. Soc.* 1963, **85**, 3043.

94 A. P. Ter Borg, H. Kloosterziel. *Rec. Trav. Chim.* 1965, **84**, 241.

95 W. G. Dauben, R. L. Cargill. *Tetrahedron* 1961, **12**, 186.

96 A. P. Ter Borg, E. Razenberg, H. Kloosterziel. *Rec. Trav. Chim.* 1965, **84**, 1230.

97 M. Traetteberg. *J. Am. Chem. Soc.* 1964, **86**, 4265.

98 S. S. Butcher. *J. Chem. Phys.* 1965, **42**, 1833.

99 C. Glidewell. *J. Organomet. Chem.* 1984, **266**, 25.

100 W. H. Donovan, W. E. White. *J. Org. Chem.* 1996, **61**, 969.

101 M Rubin. *J. Am. Chem. Soc.* 1981, **103**, 7791.

102 F. R. Jensen, L. A. Smith. *J. Am. Chem. Soc.* 1964, **86**, 956.

103 F. A. L. Anet. *J. Am. Chem. Soc.* 1964, **86**, 548.

104 E. I. Freedberg, M. Kopelvenich, F. A. L. Anet. *J. Phys. Org. Chem.* 2001, **14**, 625.

105 N. H. Werstiuk, D. N. Butler, and E. Shahid. *Can. J. Chem.* **65**, 760, (1986).

106 A. S. Vorob'ev, I. I. Furlei, Yu. Z. Ekov, A. M. Nazarov, G. A. Yamilova, U. M. Dzhemilev, and V. A. Dokiechev. *Russ. Chem. Bull.* **42**, 281, 1993.

107 K. Kimura, S. Katsumata, Y. Achiba, T. Yamazaki, S. Iwata. "*Handbook of HeI Photoelectron Spectra of Fundamental Organic Molecules.*" Japan Scientific Societies Press, Tokyo, 1981.

108 C. Muller, A. Schweig, W. Thiel, W. Grahn, R. G. Bergman, K. P. C. Vollhardt. *J. Am. Chem. Soc.* 1979, **101**, 5579.

109 L. Field, J. M. Locke. "*Organic Synthesis*", ed. H. E. Baumgarten, Wiley, New York, 1973; collect. Vol. V, pp. 723.

110 N. L. Bauld, C. E. Dahl, Y. S. Rim. *J. Am. Chem. Soc.* 1969, **91**, 2787.

111 R. Breslow, W. Washburn, R. G. Bergman. *J. Am. Chem. Soc.* 1969, **91**, 196.

112 R. Breslow, W. Washburn. *J. Am. Chem. Soc.* 1970, **92**, 428.

113 W. M. Jones, W. T. Brown. *J. Org. Chem.* 1979, **44**, 3090.

114 W. von E. Doering, L. H. Knox. *J. Am. Chem. Soc.* 1957, **79**, 352.

115 W. von E. Doering, L. H. Knox. *J. Am. Chem. Soc.* 1954, **76**, 3203.

116 P. Rademacher and B. Freckmann. *J. Elect. Spect. Rel. Phen.* 1980,**19**, 251.

117 W. Schafer, A. Schweig. *Angew. Chem. Inter. Ed.* 1972, **11**, 836.

118 T. Bajorek, N. H. Werstiuk. *Chem. Comm.* 2002, 648.

119 K. E. Hine, R. F. Childs. *J. Am. Chem. Soc.* 1973, **95**, 3289.

120 T. Svensson. *Chemica Scripta* 1973, **3**, 171.

121 C. G. Souten, F. E. Barton Jr., J. R. Burges, P. R. Story, J. F. Garst. *Chem. Comm.* 1969, 78.

122 A. P. Ter Borg, E. Razenberg and H. Kloosterziel. *Rec. Trav. Chim.* 1966, **85**, 774.

123 A.P. ter Borg, H. Kloosterziel. *Rec. Trav. Chim.* 1963, **82**, 741.

124 A.P. ter Borg, H. Kloosterziel. *Rec. Trav. Chim.* 1965 **84**, 245.

125 O.L. Chapman and G.W. Borden. *Proc. Chem. Soc.* 1963, 221.

126 E. L. Eliel. *"Stereochemistry of carbon compounds"*. McGraw-Hill Book Company, Inc., New York, 1962, back cover.

127 J. E. Weindenborner, R. B. Larrabee, A. L. Bednowitz. *J. Am. Chem. Soc.* 1972, **94**, 4140.

128 HyperChem(TM), Hypercube, Inc., 1115 NW 4th Street, Gainesville, Florida 32601, USA.

129 M. J. Frisch, G. W. Trucks, H. B. Schlegel, G. E. Scuseria, M. A. Robb, J. R. Cheeseman, V. G. Zakrzewski, J. A. Montgomery, Jr., R. E. Stratmann, J. C. Burant, S. Dapprich, J. M. Millam, A. D. Daniels, K. N. Kudin, M. C. Strain, O. Farkas, J. Tomasi, V. Barone, M. Cossi, R. Cammi, B. Mennucci, C. Pomelli, C. Adamo, S. Clifford, J. Ochterski, G. A. Petersson, P. Y. Ayala, Q. Cui, K. Morokuma, D. K. Malick, A. D. Rabuck, K. Raghavachari, J. B. Foresman, J. Cioslowski, J. V. Ortiz, A. G. Baboul, B. B. Stefanov, G. Liu, A. Liashenko, P.

Piskorz, I. Komaromi, R. Gomperts, R. L. Martin, D. J. Fox, T. Keith, M. A. Al-Laham, C. Y. Peng, A. Nanayakkara, M. Challacombe, P. M. W. Gill, B. Johnson, W. Chen, M. W. Wong, J. L. Andres, C. Gonzalez, M. Head-Gordon, E. S. Replogle, and J. A. Pople. Gaussian 98, Revision A.9, Gaussian, Inc., Pittsburgh PA, 1998.

130 M.J. Frisch, G.W. Trucks, H.B. Schlegel, P.M. W. Gill, B.G. Johnson, M.A. Robb, J.R. Cheeseman, T. Keith, G.A. Petersson, J.A. Montgomery, K. Raghavachari, M.A. Al-Laham, V.G. Zakrzewski, J.V. Ortiz, J.B. Foresman, C.Y. Peng, P.Y. Ayala, W. Chen, M.W. Wong, J.L. Andres, E.S. Replogle, R. Gomperts, R.L. Martin, D.J. Fox, J.S. Binkley, D.J. Defrees, J. Baker, J.P. Stewart, M. Head-Gordon, C. Gonzalez, and J.A. Pople. Gaussian 94, Revision B.3, Gaussian, Inc., Pittsburgh PA, 1995.

131 (a) MOLEKEL 4.3, P. Flükiger, H. P. Lüthi, S Portmann, J. Weber, Swiss Center for Scientific Computing, Manno (Switzerland), 2000-2002. (b) S. Portmann and H. P. Luthi. MOLEKEL: An Interactive Molecular Graphics Tool. *Chimia* 2000, **54**, 766.

132 W. Kirmse, S. Schoen, R. Siegfried. *Chem. Ber.* 1990, **123**, 411.

133 A. C. Cope, E. Ciganek. *"Organic Synthesis"*, ed. N. Rabjohn, Wiley, New York, 1963, Collect, Vol, IV, p. 612.

134 D. I. Schuster, B. R. Sckolnick, F. T. H. Lee. *J. Am. Chem. Soc.* 1968, **90**, 1300.